VOL. XVI (I)
Special Issue
Jan.-June 2023

ISSN: 2454-5430

ANVESHA THE HORIZON

(Half Yearly Peer-Reviewed Journal)

Special Issue
A Proceeding on
"Basic Analytical Technique: X-Ray Diffraction and Transmission Electron Microscopy for the Crystallographic and Medical Applications"

KISAN POST GRADUATE COLLEGE, BAHRAICH
(Autonomous)
Affiliated to: Dr. Rammanohar Lohia Avadh University, Ayodhya
Uttar Pradesh, 224001 India.

Editorial Board

Advisory Board

1. **Prof. Pratibha Goyal (Vice-Chancellor)**
   Dr. Rammanohar Lohia Avadh University, Ayodhya.
2. **Prof. A.D.N. Bajpayi (Vice-Chancellor)**
   Rani Durgavati University, Jabalpur.
3. **Prof. O.P.S. Negi (Vice-Chancellor)**
   Uttarakhand Open University, Haldwani, Uttarakhand.
4. **Prof. S.N. Shukla (Vice-Chancellor)**
   Pt. Ravishankar Shukla University (PRSU), Raipur
5. **Prof. Balak Das (Rtd.)**
   Department of Physics, Lucknow University, Lucknow.
6. **Prof. Ramji Pathak**
   Department of Physics, D.A.V. P. G. College, Lucknow.
7. **Prof. Vidyanand Singh**
   Indian Reference Material Division, National Physical Laboratory, New Delhi.
8. **Prof. Rajbir Singh**
   Department of Economics, Kisan Post Graduate College, Bahraich.
9. **Prof. Sameer Sinha**
   Department of Physics, Ganpat Sahai P.G. College, Sultanpur.
10. **Prof. Rajeev Tripathi**
    Principal, D.A.V. P. G. College, Lucknow.
11. **Prof. Janardan Pandey**
    Principal, Department of Physics, M.L.K. P.G. College, Balrampur.
12. **Prof. Shivam Srivastava**
    Principal, MMM P. G. College, Kalakankar, Pratapgarh.
13. **Prof. Vikas Dubey**
    Principal, Government P. G. College, Kunidhar, Manila, Almora, Uttarakhand.
14. **Prof. Ashish Saxena**
    Department of Applied Physics, Nehru Memorial Shiv Narayan Das Mahavidyalaya, Budaun.
15. **Prof. Lalit Kumar Dwivedi**
    Department of Physics, KNI Sultanpur.
16. **Prof. Bal Chandra Yadav**
    Department of Physical Science, BBA University, Lucknow.
17. **Prof. Surya Bhan Rawat**
    Department of Sociology, Kisan Post Graduate College, Bahraich.
18. **Dr. Isht Vibhu**
    Department of Physics, Y.D. P.G. College, Lakhimpur Kheri.
19. **Dr. Vishalakshi Singh**
    Department of Physics, Government P.G. College, Saidabad, Prayagraj.

Index

Organizing Secretary Message

As a **Organizing Secretary,** It is my privilege and honor to welcome you all to the **"National Seminar on Basic Analytical Technique: X-Ray Diffraction and Transmission Electron Microscopy for the Crystallographic and Medical Applications"** organized by the Department of Physics, Kisan P. G. College, Bahraich, Uttar Pradesh on 27th, 28th March 2023.

I am also feeling delightful to share our thought about the fundamental technique used for eliminating the fingerprint of the crystallographic information i.e. X-ray Diffraction (XRD) and Transmission Electron Microscopy (TEM). XRD is the most basic and easiest tool to gather the crystallographic information of the crystalline materials followed by the refinement of the XRD data using suitable software with the help of standard data collected from different crystallographic database available in the market. XRD is mostly applicable for all the crystalline structures having even very complex structures like proteins but it can be verified from the simulated XRD data using density functional theory calculation.

Although, it is an indirect technique which does not give the direct image of the planes or atoms containing particular crystal but it gives only the diffraction pattern. After the deep analysis of these diffraction patterns, we can collect the information about the crystals such as lattice parameters, orientation of the planes, angle between the crystallographic axes etc. However, TEM is very sophisticated technique used to eliminate the same crystallographic information as obtained from the XRD technique. TEM technique is operated in the dark and bright mode both depending upon the type of specimen under investigation. From this technique, we can collect the information about the sample from their core because high energetic electrons can penetrate the sample and each selected area can be scanned by the electron beam. This technique provides the direct image of the crystallographic planes, their orientations, spacing between them, different grains etc. By combining these two techniques, we can crosscheck the validity of the data obtained from any one of these two techniques. All the physical properties are strongly linked with the crystal structure of any materials.

Therefore, it is necessary to evaluate the crystal structure of the system first and correlate it with their physical property. It is well known that most of the materials are found to be a well-defined structure to gain the more stability which is the nature the universe, and which encourage us to study much about structure of the materials. I hope that this article will provide a useful content to the readers to encourage towards the research in their concerned field and enhance their knowledge in the different field. Different aspects of the data analysis are also contained in the book.

Dr. Bal Govind
(Organizing Secretary)
NSBAT-2023

Convenor Message

As a **Convenor,** It is my privilege and honor to welcome you all to the **"National Seminar on Basic Analytical Technique: X-Ray Diffraction and Transmission Electron Microscopy for the Crystallographic and Medical Applications"** organized by the Department of Physics,Kisan P. G. College, Bahraich, Uttar Pradesh on 27th, 28th March 2023. I am also privileged toshed light on the pivotal role of X-ray Diffraction (XRD) and Transmission Electron Microscopy(TEM) in advancing both crystallographic studies and medical research. These analyticaltechniques have revolutionized our understanding of matter at the atomic and molecular levels,shaping numerous fields including material science, pharmaceuticals, and structural biology. X-rayDiffraction having the ability to elucidate the arrangement of atoms within a crystal latticestands as a cornerstone technique in Crystallography. From determining crystal structures tostudying phase transitions, its applications are vast and profound in material science. XRDfacilitates the design of novel materials with tailored properties, driving innovations inelectronics, catalysis and energy storage. Moreover, its significance extends to pharmaceuticals,where precise structural information aids in drug design and formulation, enhancing therapeuticefficacy and safety.

Transmission Electron Microscopy, on the other hand, offers unparalleled resolution, allowing researchers to visualize individual atoms and defects within materials. With TEM, we delve into the intricate world of nono-material's, exploring their morphology, composition and electronic properties. In medicine, TEM plays a pivotal role in understanding cellular structures, disease mechanism and drug delivery system at the nano-scale. From diagnosing disease to developing targeted therapies, TEM empowers medical researchers with invaluable insight into the complex interplay between biomolecules and nanomaterials. The synergy between X-ray Diffraction and Transmission Electron Microscopy epitomizes the interdisciplinary nature of modern science. By combining these techniques, researchers can correlate microscopic properties with atomic-scale structures, unraveling the fundamental principles governing matter behavior.

As we navigate the frontier of science and medicine, let us recognize the indispensable contributions of X-ray Diffraction and Transmission Electron Microscopy. Through their lens, we gain a deeper understanding of the world around us, unveiling mysteries and unlocking potentials that were once beyond imagination. Let us continue to harness the power of these analytical techniques to drive innovation, inspire discovery and ultimately, improve the human condition.

Mr. Kishun Bir
(Convenor)
NSBAT-2023

Effect of Size dependent elastic properties of transition nano metal compounds

Abhishek Gautam*[1] and Dharm Veer Singh[1]

[1]Agra College Agra, U.P., India 282002
Corresponding Author's E-mail: gautamclassesagra6@gmail.com

Abstract- Current applications of transition metal nanoferrites thermal decay of ammonium perchlorate and ignition of solid composite have been reviewed. In present investigation, powder samples of Nif, Mnf, Cof, CuF and CdF ferrites nano partials. Transition metal nanoferrites, investigate by various methods, were make unused of as catalyst in thermal decay of ammonium perchlorate and ignition. Particle sizes of nanoferrites are dependent on transition metal and the verius method used. The series of definite shapes for nanoferrites have been remark, from spherical to nanotubes and nanorods. Morphology of nanoparticles, ratios of deferent taype atoms, specific surface area, etc., can considerably influence the catalytic activity of nanoferrites applications include the use of mainly cobalt, nickel, copper, zinc, manganese, cadmium nanoferrites, as well as their commend -metal ignition. We also, investigate those peak values of permeability and porosity increasing each other, and therefore entry length increases proportional increasing porosity with all deferent parameters kept constant. A plot of peak dielectric constant versus porosity and tangent loss versus porosity revealed. Comparative between dielectric constant v/s porosity as all function. Dielectric loss (tanδ) vs porosity as a function as a all function.
Keywords: Dielectric constant, tangent loss (tanδ), porosity, particle size analysis.

Introduction-Nanoparticles have a big specific surface area, properties are control by surfaces preferably than bulk. The particular surface area is frequently as a basic unit for the particle properties of nanoparticles. In which, methodologies and object to be considered for scanning particle size from particular surface area is going to be discussed. On half of this section is going to be necessary for measuring particle size dissemination from specific surface area. In the last half, pore size distribution is going to be evaluated as an application of the measurement of specific surface area. Nif, Mnf, Cof, CuF and CdF ferrites nano particles are one of the most adaptable magnetic ferrites nano materials for general use, which have many application both low and high frequency devices and take part in a useful role in deferent type technological applications such as micro wave devices, high speed digital tape power transformers in electronics, read/write heads

for,etc. other then of their high resistivity, low dielectric losses, high Curie temperature, mechanical solidity and chemical firmness [1-6]. Significant to access thoroughly the influence of particle shapes and particle size distribution for calculating particle size from specific surface area. in which selecting area, using electron microscopic watching or other particle size calculation are preferable in merger with the calculation of specific surface area.

Complete investigation of these calculation would enable to approximate sensible and meaningful particle size. Through the past decades, the design, composition and characterization of ferromagnetic nano particle such as NiF, MnF, CoF, CuF and CdF sized scale have been very high interest [7–12]. Magnetic nanoparticles have a unique physical properties and high capability for applications in various areas of high-density perpendicular at height angles according, ferro fluid color imaging, Ferro fluids, very high frequency near about

(350 MHz–3GHz) devices, magnetic freezing and drugtransporter for site-specific drug delivery [13–17]. For occurrence, manganese ruby spinal ferrite $MnFe_2O_4$ nana particles could confused for contrast improvement agents in magnetic sonority imaging technology [18–22].

The authority of the unused stress in the ferroelectric thin films is at present topic and many large researchers are diligently piloting the connected studies on the unused stress in ferroelectric thin films. the dielectric and ferroelectric properties such as Electrical properties are think about to be intrinsic independent of the shape and size of the ferro nonmaterial such as NiF, MnF, CoF, CuF and CdF., these physical properties of the ferro nanomaterials can be frequently the particle size is below some tens of nanometers by the size effect [23-25].

The transition nanoferrites materials air permeability is one of the most important properties of fabric ferrites nanomterial materials that ensure their comfort. For many such as NiF, MnF, CoF, CuF and CdF materials for technical applications. The air permeability fabric depends on many parameters of fabric. In this study, we attempted to establish a theoretical model for the porosity and prognosticated the permeability of interlace fabrics. A theoretical model was created to prognosticated the total porosity and the permeability of a fabric structure turn on the geometrical parameters such as pore size, theoretical values of air permeability were obtained very close to the experimental values.[26] Presented the synthesis of nanometer cobalt ferrite as NiF, MnF, CoF, CuF and CdF by release thermal method and its characterization by XRD and TEM.

In this paper we have studied metal nano compound (NiF, MnF, CoF, CuF and CdF) in detail by means of various experimental probes such as neutron diffraction, magnetization, optical, and

magneto-transport measurements. We have used the standard particle size of (NiF, MnF, CoF, CuF and CdF) estimated from XRD and TEM is given in [27]. The dielectric constant and loss calculations were also performed to support the experimental results.

Method and Calculation-

When y = 0; k = 0, at this situation, start the no-slip condition which means that there is literally no motion at the point on contact of the fluid with the inner surface.

$$Y = \frac{a}{2} \qquad \text{.....(1)}$$

Thus

$$k_{max} = \frac{\phi}{2}\left(a\left(\frac{a}{2}\right) - \left(\frac{a}{2}\right)^2\right), \quad k_{max} = \frac{\phi}{2}\left(\frac{a^2}{2} - \frac{a^2}{2}\right) \qquad \text{.....(2)}$$

$$k_{max} = \phi\frac{a^2}{8}, \qquad \text{.....(3)}$$

Where a is the radius of the pipe

$$K = \emptyset\frac{a^2}{8} \qquad \text{.....(4)}$$

This is in agreement with where *Á* is the porosity of the medium. Thickness *a*, the permeability *k* is not uniform throughout the cross-section of °ow.

$$\bar{K} = \phi\frac{r^2}{8} \qquad \text{.....(5)}$$

Which is the average value for k for a system comprising of a bundle of capillary tubes of the same radii and length? R is the radius of each capillary tube. If a porous system is conceived to be a bundle of capillary tubes, then it can be shown that the permeability of the medium depends on the pore-size distribution and porosity. A flow network of tubes would be similar to layers of different permeability's in parallel such that the average permeability could be calculated by adaption.

$$\bar{k} = \frac{\sum_{j=1}^{n} k_j h_j}{\sum_{j=1}^{n} h_j} \qquad \text{.....(6)}$$

$$\bar{k} = \frac{\sum_{j=1}^{m} k_j A_j}{\sum_{j=1}^{m} A_j} \qquad \text{.....(7)}$$

Where k_j is the permeability of one capillary tube and A_j is the area of flow represented by a bundle of tubes of permeability k_j J Permittivity of the vacuum

Dielectric constant-

The compound dielectric constant k be made up a real part k' which appear for the storage and an imaginary part k" which represents the loss. The following notations are used for the compound dielectric constant mutually

$\kappa = \kappa^* = \varepsilon_r = \varepsilon_r^*$ ……...(8)

where $\varepsilon = \varepsilon^* = \varepsilon_0\varepsilon_r$ is the absolute permittivity (or permittivity), ε_r is the relative permittivity

$\epsilon_0 = \frac{1}{36\pi} 10^{-9} F/M$ ……..(9)

Permittivity describes the interaction of a material with an electric field E and is a complex quantity

$\frac{\varepsilon}{\varepsilon_0} = \varepsilon_r = \varepsilon_r - j\varepsilon_r''$ …….(10)

Dielectric constant (K) is parallel to relative permittivity (ε_r) or the completely permittivity (ε) relative to the permittivity of free space (ε_o). The real part of permittivity (ε_r) is a gauge of how much energy from an external electric field is stored in a material. The made-up part of permittivity (ε_r) is called the loss factor and is a measure of how dissipative or lossy a material is to an external electric field. The imaginary part of permittivity (ε_r) is continually greater than zero and frequently much smaller than (ε_r). The loss factor includes the effects of both dielectric loss and conductivity.

$\varepsilon_r = \frac{\varepsilon_S}{\varepsilon_0}$ …….(11)

Total porosity is defined as the fraction of the bulk rock volume V that is not occupied by solid matter. If = V – Vs, we can write the porosity as:

$\emptyset = \frac{V_B - V_S}{V_B}$ …….(12)

The porosity can be expressed either as a fraction or as a percentage. Two out of the three terms are required to calculate porosity

Result and Discussion-

In summary, the real size depended dielectric constant and tangential loss. The Dielectric constant variable with respect to Ferro magnetic nano particle size so dielectric constant the increasing

point. Represented the theoretical work by table and figures, figures (1-5) represent relation between porosity and dielectric constant, the dielectric constant direct proportional to porosity.

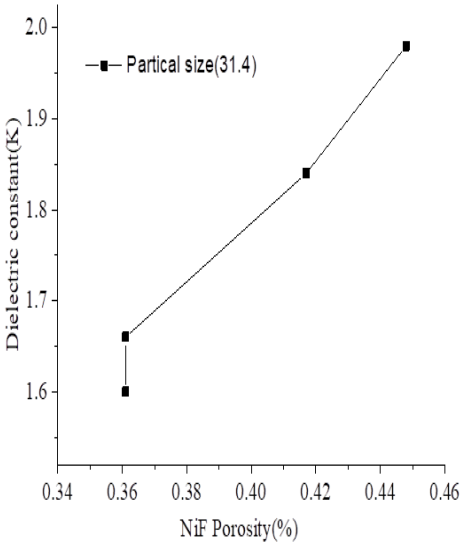

Figure 1. Dielectric constant vs porosity as a function of NiF.

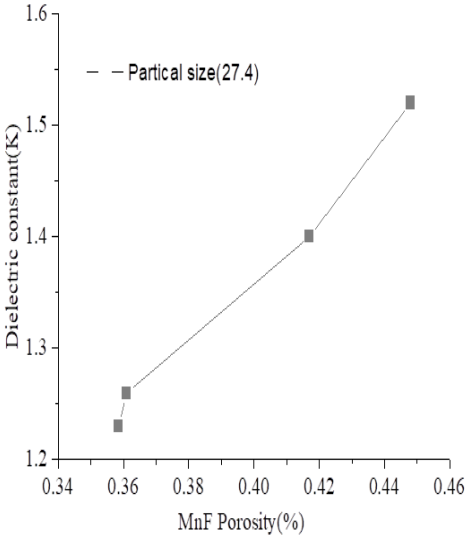

Figure 2. Dielectric constant vs porosity as a function of MnF.

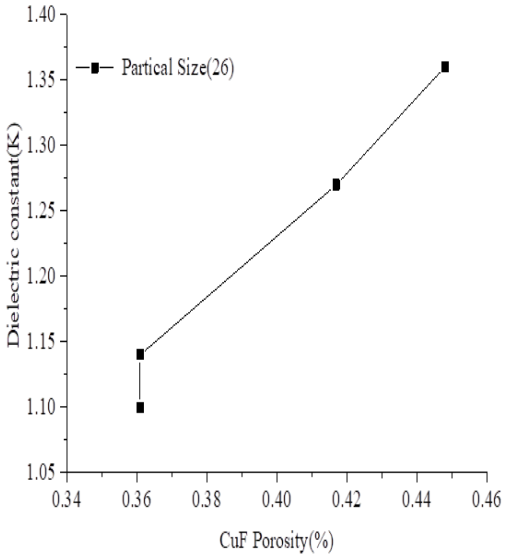

Figure 3. Dielectric constant vs porosity as a function of CuF.

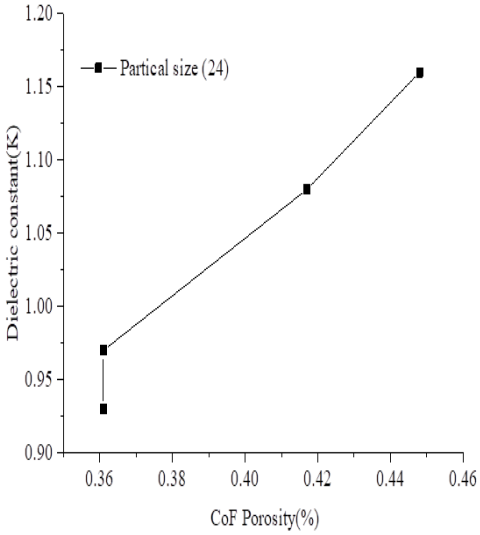

Figure 4. Dielectric constant vs porosity as a function of CoF

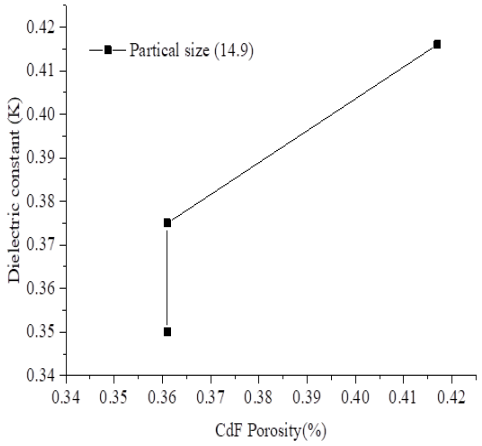

Figure 5. Dielectric constant vs porosity as a function of CdF.

The ferromagnetic nano particle size is increasedment then dielectric constant is increasedment. The figures 6 to 10 are represent relation between porosity and tangential loss (tanδ). Draw the graph horizontally porosity and vertical (tanδ). The loss (tanδ) and porosity is directly propertical each other the porosity NiF, MnF, CuF, CoF, CdF, incresedment ordered so find the dielectric constant then incresedment ordered.

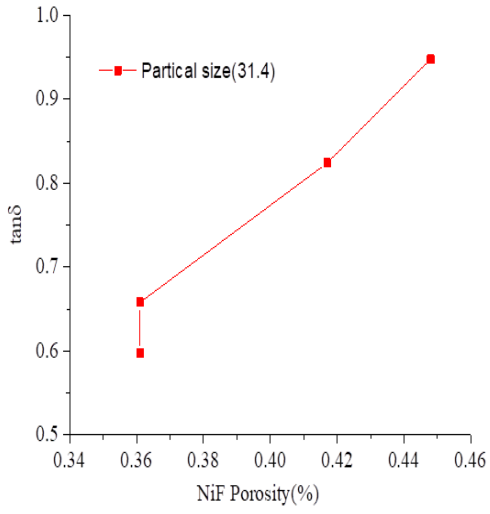

Figure 6. Dielectric loss (tanδ) vs porosity function of MnF.

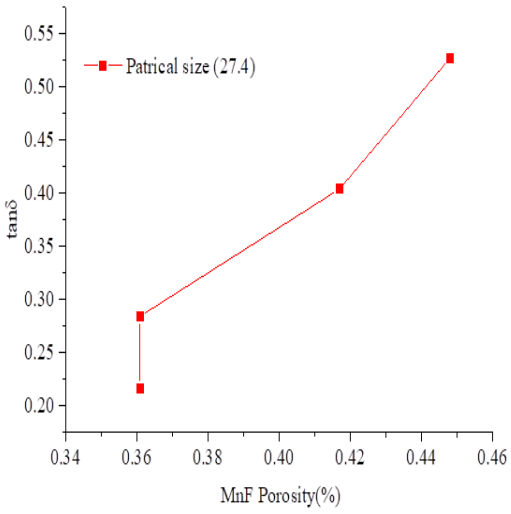

Figure 7. Dielectric loss (tanδ) vs porosity as a as a function of NiF.

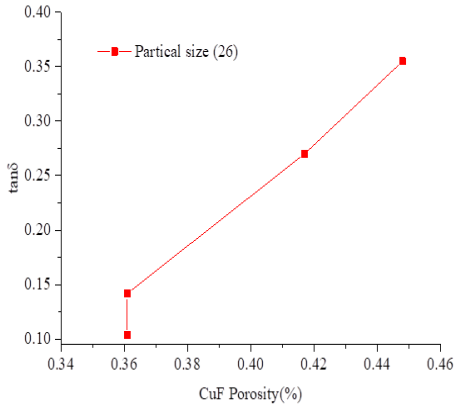

Figure 8. Dielectric loss (tanδ) vs porosity as a function of CuF.

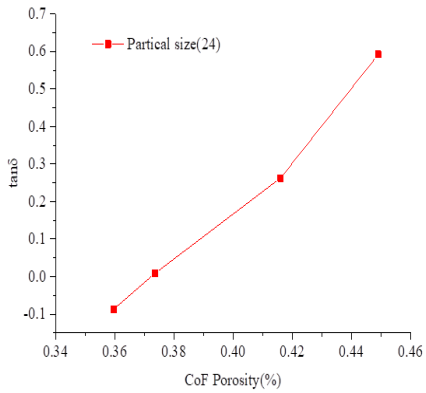

Figure 9. Dielectric loss (tanδ) vs porosity as a function of CoF.

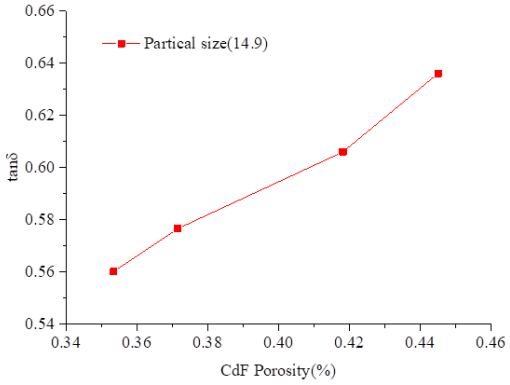

Figure 10. Dielectric loss (tanδ) vs porosity as a function of CdF.

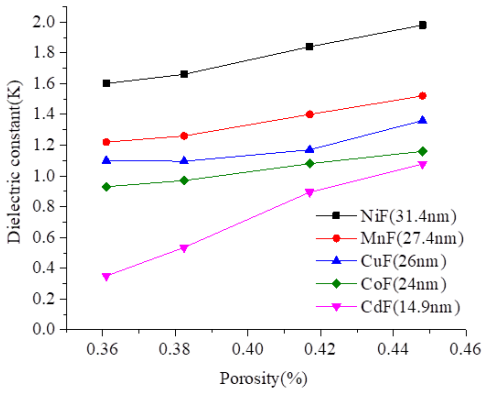

Figure 11. Comparative between dielectric constant vs porosity function.

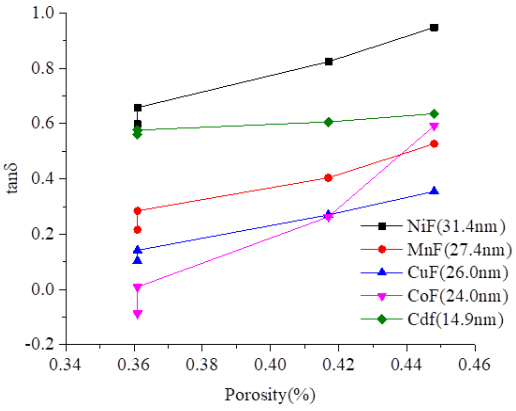

Figure 12. Dielectric loss (tanδ) vs porosity as a function as a all function.

The figures 11 and 12 in which represent common comparison dielectric constant v/s porosity ferromagnetic nano particle NiF, MnF, CuF, CoF, CdF . The Ferromagnetic nano particle size is low so graphical line is tangential ordered, the Ferro magnetic nano particle size is very high then graphical line is horizontally for me.

Defend in which table 1 to 5 the ferromagnetic nano particle such as NiF, MnF, CuF, CoF, CdF particle size analyzed with dielectric constant and tangent loss (tanδ) respect to porosity theoretical calculation as show in table 1 to 5. The Dielectric constant directly proportional to tangent loss (tanδ).

Table 1. Particle size analysis with dielectric constant and tangent loss (tanδ).

Sample	**Particle size (31.4nm)**		
	Porosity (%)	**Dielectric constant(k)**	**Tangent loss (tanδ)**
NiF	0.361	1.60	0.5980
	0.361	1.66	0.6580
	0.417	1.84	0.8240
	0.448	1.98	0.9480

Table 2. Particle size analysis with dielectric constant and tangent loss (tanδ).

Sample	**Particle size (27.4nm)**		
	Porosity (%)	**Dielectric constant (k)**	**Tangent loss (tanδ)**
MnF	0.361	1.22	0.2162
	0.361	1.26	0.2845
	0.417	1.40	0.404
	0.448	1.52	0.527

Table 3. Particle size analysis with dielectric constant and tangent loss (tanδ).

Sample	**Particle size (26.nm)**		
	Porosity (%)	**Dielectric constant (k)**	**Tangent loss (tanδ)**
CuF	0.361	1.10	0.1034
	0.361	1.14	0.142
	0.417	1.27	0.270
	0.448	1.36	0.355

Table 4. Particle size analysis with dielectric constant and tangent loss (tanδ).

Sample	**Particle size (24.nm)**		
	Porosity (%)	**Dielectric constant(k)**	**Tangent loss (tanδ)**
CoF	0.361	.93	0.6042
	0.361	.97	-0.0682
	0.417	1.08	-0.0320
	0.448	1.16	0.1519

Table 5. Particle size analysis with dielectric constant and tangent loss (tanδ).

Sample	**Particle size (14.9nm)**		
	Porosity (%)	**Dielectric constant(k)**	**Tangent loss (tanδ)**
CdF	0.361	0.35	0.644
	0.361	0.375	0.6272
	0.417	0.416	0.5630
	0.448	0..447	0.5538

The justified result of dielectric constant tangent loss with respect porosity ferromagnetic nano particle such as NiF, MnF, CuF, CoF, FdF, have been compared with experimental and theoretical data and substantial agreements can be observed with experimental data.

Conclusions-

The highest value of dielectric constant permeability which correspond with the point at which transition ferromagnetic nano particle such as NiF, MnF, CuF, CoF, FdF, length is highest varies with tangent loss (tanδ) and porosity of the room temperature. less the porosity at a room temperature then presents the small value tangent loss and dielectric constant of the transition ferromagnetic nano particle. Specially, for porous medium with porosities 0.361, 0.375, 0.417, 0.448 and 0.467.The positive nano particle in this ferromagnetic material arises due to Lorentz force. The dielectric constant and loss calculations accounting for porosity correlations of the ferromagnetic nano particle porosity of metals reproduces the ferromagnetic ordering and effective partial size.

Reference-

1. Nowak, J. J., Robertazzi, R. P., Sun, J. Z., Hu, G., Park, J. H., Lee, J., ... & Worledge, D. C. (2016). Dependence of voltage and size on write error rates in spin-transfer torque magnetic random-access memory. *IEEE Magnetics Letters*, *7*, 1-4.
2. Slonczewski, J. C. (1996). Current-drivenexcitation of magnetic multilayers. *Journal of Magnetism and Magnetic Materials*, *159*(1-2), L1-L7.
3. Iusipova, I. (2018). Critical switching characteristics of three-layered spin valve for different materials and alloys with uniaxial anisotropy. In *EPJ Web of Conferences* (Vol. 185, p. 01012). EDP Sciences.
4. Masuda, H., Higashitani, K., & Yoshida, H. (2006). *Powder technology: handling and operations, process instrumentation, and working hazards*. CRC Press.
5. Suzuki, M. (2018). 1.3 PARTICLE SHAPE. *Nanoparticle Technology Handbook*, 10.
6. Gregg, S. J., & Sing,K. S. W. (1982). Adsorption,surface area and porosity. Academic Press, London. *Adsorption surface area and porosity. 2nd ed. Academic Press, London.*
7. Kondo, S., Ishikawa, T., & Abe, I. (1991). Kyuchaku no kagaku. *Maruzen, Tokyo*, *104*.
8. Barrett, E. P., Joyner, L. G., & Halenda, P. P. (1951). The determination of pore volume and area distributions in porous substances. I. Computations from nitrogen isotherms. *Journal of the American Chemical society*, *73*(1), 373-380.
9. Pierce, C. (1953). Computation of pore sizes from physical adsorption data. *The Journal of Physical Chemistry*, *57*(2), 149-152.

10. Igarashi, H., & Okazaki, K. (1977). Effects of porosity and grain size on the magnetic properties of NiZn ferrite. *Journal of the American Ceramic Society*, *60*(1-2), 51-54.

11. Kulikowski, J. (1984). Soft magnetic ferrites—development or stagnation?. *Journal of Magnetism and Magnetic Materials*, *41*(1-3), 56-62.

12. Ravindranathan, P., & Patil, K. C. (1987). Novel solid solution precursor method for the preparation of ultrafine Ni-Zn ferrites. *Journal of Materials Science*, *22*, 3261-3264.

13. Slick, P. I. (1980). Ch. 3 in" Ferromagnetic Materials", Vol. 2, North Holl. *Pub. Co*. 182.

14. Martinez, B., Obradors, X., Balcells, L., Rouanet, A., & Monty, C. (1998). Low temperature surface spin-glass transition in γ-Fe 2 O 3 nanoparticles. *Physical Review Letters*, *80*(1), 181.

15. Martinez, B., Obradors, X., Balcells, L., Rouanet, A., & Monty, C. (1998). Low temperature surface spin-glass transition in γ-Fe 2 O 3 nanoparticles. *Physical Review Letters*, *80*(1), 181.

16. Martinez, B., Obradors, X., Balcells, L., Rouanet, A., & Monty, C. (1998). Low temperature surface spin-glass transition in γ-Fe 2 O 3 nanoparticles. *Physical Review Letters*, *80*(1), 181.

17. Awschalom, D. D., & DiVincenzo, D. P. (1995). Complex dynamics of mesoscopic magnets. *Physics Today*, *48*(4), 43-48.

18. Liu, C., & Zhang, Z. J. (2001). Size-dependent superparamagnetic properties of Mn spinel ferrite nanoparticles synthesized from reverse micelles. *Chemistry of Materials*, *13*(6), 2092-2096.

19. Tang, Z. X., Sorensen, C. M., Klabunde, K. J., & Hadjipanayis, G. C. (1991). Size-dependent Curie temperature in nanoscale MnFe 2 O 4 particles. *Physical Review Letters*, *67*(25), 3602.

20. Kulkarni, G. U., Kannan, K. R., Arunarkavalli, T., & Rao, C. N. R. (1994). Particle-size effects on the value of T c of MnFe 2 O 4: Evidence for finite-size scaling. *Physical Review B*, *49*(1), 724.

21. Tang, Z. X., Sorensen, C. M., Klabunde, K. J., & Hadjipanayis, G. C. (1991). Size-dependent magnetic properties of manganese ferrite fine particles. *Journal of Applied Physics*, *69*(8), 5279-5281.

22. Çay, A., Vassiliadis, S., Rangoussi, M., & Tarakçıoğlu, I. (2007). On the use of image processing techniques for the estimation of the porosity of textile fabrics. *International Journal of Materials and Textile Engineering*, *1*(2), 421-424.

23. Çay, A., & Tarakçioğlu, I. (2008). Relation between fabric porosity and vacuum extraction efficiency: Energy issues. *Journal of the Textile Institute*, *99*(6), 499-504.

24. Çay, A., & Tarakçioğlu, I. (2008). Relation between fabric porosity and vacuum extraction efficiency: Energy issues. *Journal of the Textile Institute*, *99*(6), 499-504.

25. Duran, K., Çay, A., & Atav, R. (2007). Pamuklu kumaşların atkı-çözgü sıklığı ve gözenekliliği ile reaktif boyamalarda elde edilen renk efektleri arasındaki ilişki..

26. Fukui, T. (2018). 1.7. composite structure *Nanoparticle Technology Handbook*, 22.

27. Blackham, D. V., & Pollard, R. D. (1997). An improved technique for permittivity measurements using a coaxial probe. *IEEE Transactions on Instrumentation and Measurement*, *46*(5), 1093-1099.

Pimenta dioica leaf extract used in the synthesis of silver nanoparticles: Characterization and evaluation of antimicrobial applications.

Abhishek Prakash Tiwari[1*], Rajkamal Tiwari[2], and Bal Chandra Yadav[1]

[1]Nanomaterials and Sensor Research Laboratory, Department of Physics, School for Physical and Decision Science, Babasaheb Bhimrao Ambedkar University, Lucknow 226025, U.P., India.

[2]Central Institute of Petrochemicals Engineering & Technology (CIPET), Department of Chemicals and Petrochemicals, Ministry of Chemicals & Fertilizers, Govt. of India, Lucknow 226008, U.P., India.

Corresponding Author's Email: **aptiwari@bbau.ac.in**

ABSTRACT-

A novel, simple and eco-friendly green synthesis method for Silver Nanoparticles (Ag NPs) has been developed using *Pimenta dioica* floral extract as reducing agent. In this protocol, Silver Nitrate ($AgNO_3$) solution was reduced with the help of *Pimenta dioica* flower extract. The synthesised Silver NPs were then characterized using UV-vis Spectroscopy, Field Emission - Scanning Electron Microscopy (FE-SEM), X-Ray Diffraction (XRD) technique for their morphological and structural analysis. The average size of synthesized AgNPs was estimated using FESEM image and found to be ~12 nm. Synthesized nanoparticles may further be studied for their potential applications such as antimicrobial activity, bio-imaging, sensing and drug delivery owing to the known properties of the silver NPs and *Pimenta dioica*.

Keyword: Silver Nanoparticles, *Pimenta dioica*, Green Synthesis, Metal oxides, Nanoparticles, Antimicrobial activity

1. Introduction

In the recent years, green synthesis approach for synthesis of nanomaterials and their various applications is continuously pursued and attracted the attention of researchers (1-5). Thegreen synthesis of noble metal nanoparticles emerged as a great tool for the advent and development in the

field of Nanotechnology. The plant mediated synthesis (phyto synthesis) is known as green synthesis because it occurs without involving any harmful/toxic chemicals (6, 7). Metallic nanoparticles are prepared by several synthesis techniques including biological, physical, chemical and others to control morphology, size, and stability of synthesized Nano-sized structures but an approach for green synthesis of metallic nanoparticles is the most fascinating synthesis process. Green synthesis methods using plant extracts have received great significance because these are eco-friendly and cost-effective (8-10)due to the presence of plentiful as well as diversified biomolecules acting as reducing and capping agents (11,12).In green synthesis methods; morphology, shape, size, surface to volume ratio and composition of NPs can be varied easily which plays a vital role to obtain enhanced physical, chemical, and biological properties for desirable applications in several areas such as electronics, house-hold devices, agriculture, cosmetics, and pharmaceutical industries (13-17). Phyto synthesized silver nanoparticles (Ag NPs) exhibit many potential applications in several fields because of its safe and environment friendly nature. Researchers are in continuous search of less hazardous, easy to handle, efficient, large scale production and eco-friendly methods of synthesis fornano-technological developments and their impact on living organisms (18-21). Out of metals, Ag NPs have become an intense topic of researchers due to their distinctive physiochemical properties and promising biomedical applications (22-27). The scientific community is exploiting the use of silver nanoparticles (Ag NPs) in nano-medicine and its combinations with other biomaterials to reduce microbial contamination. These nanoparticles have also been explored for bio-imaging applications owing to their surface-plasmon-resonance property (28).

N. Jayaprakash et al. have synthesized Ag NPs using Tamarind fruit extract and studied for antimicrobial applications against 09 well known bacteria (29). Synthesized nanoparticles by tamarind fruit extracts were found to be well suitable for antimicrobial applications. S. Saravanan et al. have synthesised AgNPs by using Peltophorumpterocarpum plant extract and used them in different concentrations in fabricating dye-sensitized solar cells. They found that the plasmonic effect of the silver nanoparticles enhances substantially the energy conversion efficiency in DSSCs (30). In another study, S. Gurunathan et al. have synthesized silver nanoparticles using Escherichia coli and synthesized silver nanoparticles were purified using sucrose density gradient centrifugation. Study infers that the particle size can be controlled by varying the reaction temperature, pH andconcentration of $AgNO_3$ (31).

Present paper delineates a neat protocol which describes the synthesis of silver nanoparticles using *Pimenta dioica*flower extract as reducing as well as capping agent. To the best of our knowledge, this is the unique protocol that explores the green synthesis of silver nanoparticles by *Pimenta dioica*flower extract. Synthesized nanoparticles have been studied with various characterization techniques for their morphological and structural analysis. *Pimenta dioica*is an evergreen species of *Plumeria* native to Panama, Colombia and Venezuela. The plant *Pimenta dioica*(wild plumeria/frangipani) belongs to the family *Apocynaceae*. This Plant is a beautiful shrub which usually has one or two slender trunks.It is also called Bridal Bouquet or crown (32). Leaves are dark green and unique fiddle-shaped or spoon-shaped. Large clusters of bright white 3-inch flowers with small light-yellow centres, cover the most of the tree. The flowers are not fragrant.

To determine the antibacterial activity of silver nanoparticles, against bacterial strains such as *E.coli*, *Staphylococcus sps*, and *Pseudomonas sps*. The bacterial cultures were grown overnight in nutrient broth on a rotary shaker (200 rpm) at 37°C and then they were seeded into nutrient agar plates. Silver nanoparticles with concentration at 60µl were loaded into the wells. The plates were incubated at 37°C for 24hours, after incubation, zone of inhibition around the wells were measured.Antibiotic sensitivity describes the susceptibility of bacteria to various antibiotics. Clinical microbiologists have a major role to play in prescribing antibiotics for either treatment or prophylaxis of infection. The antibiotics for therapy are selected after performing Antibiotic Susceptibility Test (AST). It is often done by the Kirby-Bauer method in which antibiotic impregnated discs are used to test the susceptibility of any bacterial strain to a specific antibiotic.

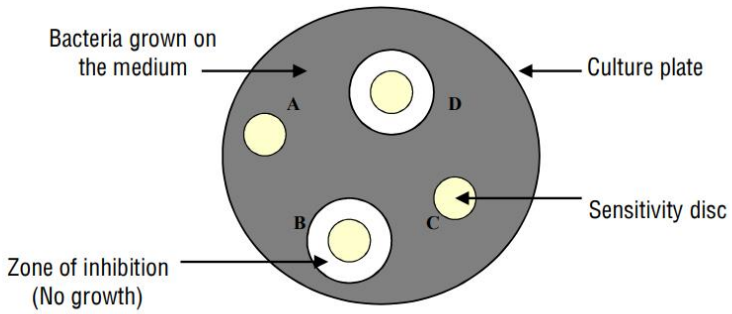

Fig1: Sensitivity of Bacteria to antibiotics B and D but not to A and C.

2. Materials and Methods

2.1 Materials

Silver Nitrate ($AgNO_3$) with 99.99% purity and other chemical required for washing & cleaning purpose were purchased from Merck. All chemicals were used as received without further purification. Fresh Pimenta dioica(Pimenta dioicaJacq.) flowers, commonly known as White Frangipani or Bridal Bouquet were collected from Indira Gandhi Planetarium, Lucknow, U.P., India premises in the month of July-August 2020. Double distilled water was used throughout the experiment.

2.2 Preparation of flower Extract

Fresh Pimenta dioica (Pimenta dioica Jacq.) flowers thoroughly rinsed and surface cleaned with running tap water to remove debris, dust particles and other contaminated organic contents, followed by washing three times in double distilled water. After then flower petals were air dried at room temperature. About 5 gm of flower petals were kept in a beaker containing 100 mL double distilled water and boiled for 15 minutes. The extract was cooled down and then filtered thrice with sartorius filter discs of grade 292. Final volume of the extract was found to be 80 ml and it was stored at 4℃ for further experiment.

2.3 Synthesis

For the synthesis of silver nanoparticles, 10mM aqueous solution of Silver Nitrate ($AgNO_3$) was prepared and used as a precursor solution. 100 ml of 10 mM aqueous $AgNO_3$ solution was stirred at room temperature and 5 ml of *Pimenta dioica* flower extract was added to the solution. Reaction was continued for 20 minutes but no change in colour was observed. Afterwards, mixture solution was stirred at 45℃ on a magnetic hot plate cum stirrer. It was found that the colour of the mixture solution was changed to brownish yellow within 20 minutes which indicates the formation of Ag NPs. In order to ensure the completion of the reaction, the mixture solution was stirred at the same temperature for additional 25 minutes but no further change in colour was observed. Synthesized Ag NPs were well dispersed and stable for several months. Schematic representation of the synthesis procedure is shown in figure 1.

2.4 Characterizations

The synthesised silver nanoparticles were studied with the help of UV-vis Spectroscopy, Field Emission-Scanning Electron Microscopy (FE-SEM) and X-Ray Diffraction (XRD) technique for their morphological and structural analysis.

The UV-Vis absorption spectra of *Pimenta dioica* flower extract and synthesized silver nanoparticles were recorded using UV-Vis Spectrophotometer (Evolution 201) at Babasaheb Bhimrao Ambedkar University, Lucknow.

The morphology and particle size of the synthesized nanoparticles were examined using Field-Emission Scanning Electron Microscope (JEOL, JSM-7100F, Tokyo, Japan) at Advanced Centre of Materials Science, IIT Kanpur with an accelerating voltage of 15 kV. The samples for FESEM imaging were prepared by adding few drops of diluted solution of synthesised silver NPs on a cleaned glass substrate by spin coating technique followed by drying at USIC, Babasaheb Bhimrao Ambedkar University, Lucknow.

Crystalline nature of the synthesized Ag NPs was studied using X-Ray Diffraction (XRD) technique and XRD Pattern was recorded with the help of PANalytical X'Pert X-Ray Diffractometer at Advanced Centre of Materials Science, IIT Kanpur. Instrument was operated using monochromatic Cu Kαradiation (λ=1.54 Å)at 45 kV and 40 mA with the minimum step size (2θ) of 0.0010.The sample for XRD analysis was prepared by adding several drops of synthesized silver nanoparticles by drop casting method followed by drying under IR lamp at BBAU, Lucknow.

2. Results and Discussions

Figure 2(a) shows UV-Vis Spectra of *Pimenta dioica*flower extract while the inset picture shows the flower and its extract. It is evident from the inset of figure 2(a) that the colour of the flower extract is faint yellow. The UV-Vis Spectra show a strong absorption peak at ~267 nm which may be attributed to the presence of function groups in the extract. Figure 2(b) shows UV-Vis Spectra of synthesized silver nanoparticles. An absorption peak at ~415 nm is observed in the spectra which is a characteristic peak of silver nanoparticles due to surface plasmon resonance. This is also evident by change in colour of the mixture solution from transparent to brownish yellow. This colour change is observed because of the excitation of surface plasmon resonance band of free electrons in silver nanoparticles. The appearance of plasmon's peak depends upon size and shape of the synthesized nanoparticles.

Figure3 shows the XRD spectra of synthesised silver nanoparticles. The XRD pattern exhibits sharp reflections which are characteristics of Face Centred Cubic (FCC) structure of silver. Four peaks are observed at 2θ values of 38.35, 43.01, 64.72, 77.65 correspondingly indexed as (111), (200), (220), and (311) planes of FCC structure of silver (JCPDS File No. 04-0783). Therefore, it is found that the synthesized silver nanoparticles using *Pimenta dioica* flower extract are crystalline in nature. The

lattice parameter ‘a’ was calculated from most intense peak (111) and found to be 4.06 Å which is in close agreement with standard value 4.0865 Å (JCPDS File No. 04-0783). The full-width at half-maximum of (111) diffraction was used to estimate the average crystallite size of synthesized Ag NPs by the Scherrer formula (33). The calculated crystallite size was found to be ~18 nm.

Figure 4 (a-d) show the FESEM images of synthesized silver nano particles synthesized by *Pimenta dioica* flower extract. FESEM images revealed that synthesized silver nano particles are nearly spherical in shape, having smooth surface and uniformly distributed. Figure 4(b) is used to estimate the average particle size by measuring more than 300 particles and it is found that particles size ranges from 7 to 27 nm with an average particle size of ~12 nm. Distribution of particle size is shown in figure 5 (a, b).

3. Conclusion

Silver nanoparticles have been synthesised by using *Pimenta dioica* flower extract as a reducing agent. The synthesis is very simple, cost effective and less hazardous. Synthesized silver nanoparticles are characterized using UV-vis Spectroscopy, Field Emission - Scanning Electron Microscopy (FE-SEM), X-Ray Diffraction (XRD) technique for their morphological and structural analysis. Synthesized silver nano particles are nearly spherical in shape, having smooth surface and uniformly distributed. The average size of synthesized AgNPs was estimated using FESEM image and found to be ~12 nm and may find potential applications in antibacterial, bioimaging and drug delivery applications.

Table: Susceptibility of each organism

Sr. No.	**Antibiotics/Sample**	**Organism**		
		Escherichia coli	***Staphylococcus aureus***	***Pseudomonas aeruginosa***
1.	AgNPs by Flower	S	S	S
2.	AgNPs by Leaf	S	S	S

Sensitive (S): An organism is called ‘sensitive’ to a drug when the infection caused by it is likely to respond to the treatment with that specific drug at the recommended dosage.

Intermediately sensitive (I): It is applicable to organisms that are moderately sensitive to an antibiotic that can be used for treatment at a higher dosage and as a result leads to uncertain therapeutic effect.

Resistant (R): An organism is called 'resistant' to a drug when the organism does not respond to a given drug irrespective of the dosage.

References

1. Elumalai, E.K.; Prasad, T.N.V.K.V.;Hemachandran,J. ;TherasaS.V.; Thirumalai T.; David E. Extracellular synthesis of silver nanoparticles using leaves of Euphorbia hirta and their antibacterial activities. *J. Pharm. Sci. & Res.* 2010, 2(9), 549-554.

2. Dhumale, V.A.; Gangwar, R.K.; Pande, N. Importance of gold nanoparticles for detection of toxic heavy metal ions and vital role in biomedical applications. *Materials Research Innovations.*,https://doi.org/10.1080/14328917.2020.1825770.

3. Mason, C.;Vivekanandhan, S.;Misra, M.; Mohanty, A.K.Switchgrass (Panicum virgatum) Extract Mediated Green Synthesis of Silver Nanoparticles. *World Journal of Nano Science and Engineering*. 2012, 02(02), 47–52.

4. Vinay, S.P.; Chandrasekhar, N.;Udayabhanu.;Nagarju, G.;Chandrappa, C.P. Ixora coccinea extract-mediated green synthesis of silver nanoparticles: photodegradative and antimicrobial studies. *International Journal of Biosensors & Bioelectronics.* 2019, 5(4), 100-105.

5. Mata, R.;Nakkala, J.R.;Sadras, S.R. Catalytic and biological activities of green silver nanoparticles synthesized from Plumeria alba (frangipani) flower extract. *Materials Science and Engineering C.* 2015, 51, 216–225.

6. Johnsona, P.;Krishnana, V.;Loganathana, C.;Govindhan, K.; Raji, V.; Sakayanathan, P.; Vijayan, S.; Sathishkumar, P.; Palvannan, T.Rapid biosynthesis of Bauhinia variegata flower extract-mediated silver nanoparticles: an effective antioxidant scavenger and α-amylase inhibitor.*Artificial Cells, Nanomedicine and Biotechnology*. 2018, 46(7), 1488–1494.

7. Raj, L.F.A.A.;Jayalakshmy E. Biosynthesis and characterization of zinc oxide nanoparticles using root extract of Zingiber officinale. *Oriental Journal of Chemistry.* 2015, 31(1), 51–56.

8. Srikar, S.K.;Giri, D.D.; Pal, D.B.; Mishra, P.K.; Upadhyay, S.N.; Light Induced Green Synthesis of Silver Nanoparticles Using Aqueous Extract of Prunus amygdalus. *Green and Sustainable Chemistry*. 2016, 06(01), 26–33.

9. Gangwar, R.K.;Dhumale, V.A.;Gosavi, S.W.; Sharma, R.B.;Datar, S.S. Catalytic activity of allamanda mediated phytosynthesized anisotropic gold nanoparticles. *Advances in Natural Sciences*: *Nanoscience and Nanotechnology*. 2013, 4, 045005.

10. Jyoti, K.; Singh, A.; Fekete, G.; Singh, T. Cytotoxic and radiosensitizing potential of silver nanoparticles against HepG-2 cells prepared by biosynthetic route using Picrasmaquassioides leaf extract. *Journal of Drug Delivery Science and Technology*. 2020, 55, 101479.

11. Venugobal, J.;Anandalakshmi, Prasad, G.S.;Janakiraman, K.;Muthukumar, V.;Senthilraj R. Green synthesis and characterisation of silver nanoparticles using Aristolochiabracteata leaf extract and their antibacterial activity. *International Journal of Chemical and Pharmaceutical Sciences*. 2015, 6(2), 60-64.

12. Prasannaraj, G.; Venkatachalam, P.; Enhanced Antibacterial, Anti-biofilm and Antioxidant (ROS) Activities of Biomolecules Engineered Silver Nanoparticles Against Clinically Isolated Gram Positive and Gram Negative Microbial Pathogens. *Journal of Cluster Science*. 2017, 28(1), 645–64.

13. Iravani, S.;Korbekandi, H.;Mirmohammadi, S.V.;Zolfaghari, B. Synthesis of silver nanoparticles: chemical, physical and biological methods. *Res. Pharm. Sci.*, 2014, 9(6), 385-406.

14. Mahadevan, S.; Vijayakumar, S.;Arulmozhi, P. Green synthesis of silver nano particles from Atalantiamonophylla (L) Correa leaf extract, their antimicrobial activity and sensing capability of H_2O_2. *Microbial Pathogenesis*., 2017, 113(1), 445–450.

15. Nava, O.J.;Luque, P.A.; Gómez-Gutiérrez, C.M.;Vilchis-Nestor, A.R.; Castro-Beltrán, A.;Mota-González, M.L.; Olivas, A. Influence of Camellia sinensis extract on Zinc Oxide nanoparticle green synthesis. *Journal of Molecular Structure*. 2017, 1134(15), 121–125.

16. Philip, D. Mangifera Indica leaf-assisted biosynthesis of well-dispersed silver nanoparticles. *Spectrochimica Acta - Part A: Molecular and Biomolecular Spectroscopy*. 2011, 78(1), 327–331.

17. Mukherjee, P.; Ahmad, A.; Mandal, D.; Senapati, S.;Sainkar, S.R.; Khan, M.I.; Parishcha, R.; Ajaykumar, P.V.; Alam, M.; Kumar, R., et al. Bioreduction of $AuCl_4$-Ions by the Fungus, Verticillium sp. and Surface Trapping of the Gold Nanoparticles Formed**. *Angew. Chem. Int. Ed.*, 2001, 40(19), 3585-3588

18. El-Sonbaty, S.M. Fungus-mediated synthesis of silver nanoparticles and evaluation of antitumor activity. *Cancer Nanotechnology*. 2013, 4, 73–79.

19. Maliszewska, I.;Szewczyk, K.;Waszak, K. Biological synthesis of silver nanoparticles. J. Phys.: Conf. Ser., 2009, 146, 012025

20. Li, G.; He, D.; Qian, Y.; Guan, B.; Gao, S.; Cui, Y.; Yokoyama, K.; Wang, L. Fungus-mediated green synthesis of silver nanoparticles using aspergillus terreus. *Int. J. Mol. Sci.*, 2012, 13, 466-476, DOI:10.3390/ijms13010466.

21. Mukherjee, P.; Ahmad, A.; Mandal, D.; Senapati, S.;Sainkar, S.R.; Khan, M.I.;Parishcha, R.; Ajaykumar, P.V.; Alam, M.; Kumar, R., et al. Fungus-Mediated Synthesis of Silver Nanoparticles and Their Immobilization in the Mycelial Matrix: A Novel Biological Approach to Nanoparticle Synthesis. *Nano Letters*. 2001, 1(10), 515–519.

22. Ahmad, N.; Bhatnagar, S.; Ali, S.S.; Dutta, R. Phytofabrication of bioinduced silver nanoparticles for biomedical applications. *International Journal of Nanomedicine*. 2015, 10, 7019–7030.

23. Shanmuganathan, R.;Karuppusamy, I.; Saravanan, M.;Muthukumar, H.;Ponnuchamy, K.; Ramkumar, V.S.; Pugazhendhi, A. Synthesis of Silver Nanoparticles and their Biomedical Applications - A Comprehensive Review. *Current Pharmaceutical Design*. 2019, 25(24), 2650–2660.

24. Karthik, L.; Kumar, G.;Kirthi, A.V.;Rahuman, A.A.;Bhaskara-Rao, K.V. Streptomyces sp. LK3 mediated synthesis of silver nanoparticles and its biomedical application. *Bioprocess and Biosystems Engineering*. 2014, 37(2), 261–267.

25. Saravanan, M.;Amelash, T.;Negash, L.;Gebreyesus, A.; Selvaraj, A.;Rayar, V.; Dheekonda, K. Extracellular Biosynthesis and Biomedical Application of Silver Nanoparticles Synthesized from Baker's Yeast. *International Journal of Research in Pharmaceutical and Biomedical Sciences*. 2013, 4(3), 822-828.

26. Abbasi, E.; Milani, M.; Aval, S.F.;Kouhi, M.;Akbarzadeh, A.;Nasrabadi, H.T.; Nikasa, P.;Joo, S.W.; Hanifehpour, Y.; Nejati-Koshki, K.;et al. Silver nanoparticles: Synthesis methods, bio-applications and properties. *Critical Reviews in Microbiology*. 2016, 42(2), 173–180.

27. Priyadarshini, S.; Gopinath, V.;Priyadharsshini N.M.; MubarakAli, D.;Velusamy, P. Synthesis of anisotropic silver nanoparticles using novel strain, Bacillus flexus and its biomedical application. *Colloids and Surfaces B: Biointerfaces*. 2013, 102, 232–237.

28. Alaqad, K.; Saleh, T.A. Gold and Silver Nanoparticles: Synthesis Methods, Characterization Routes and Applications towards Drugs. *Journal of Environmental & Analytical Toxicology*. 2016, 6(4), 1000384.

29. Jayaprakash, N.; Vijaya, J.J.;Kaviyarasu, K.;Kombaiah, K.; Kennedy, L.J.; Ramalingam, R.J.; Munusamy, M.A.; Al-Lohedan, H.A. Green synthesis of Ag nanoparticles using Tamarind fruit extract for the antibacterial studies. *Journal of Photochemistry and Photobiology B: Biology*. 2017, 169, 178–185.

30. Saravanan, S.; Kato, R.; Balamurugan, M.; Kaushik, S.; Soga, T. Efficiency improvement in dye sensitized solar cells by the plasmonic effect of green synthesized silver nanoparticles. *Journal of Science: Advanced Materials and Devices.* 2017, 2(4), 418–424.

31. Gurunathana, S.;Kalishwaralala, K.;Vaidyanathana, R.; Deepak, V.; Pandian, S.R.K.; Muniyandi, J.; Hariharan, N.; Eom, S.H. Biosynthesis, purification and characterization of silver nanoparticles using Escherichia coli. *Colloids and Surfaces B: Biointerfaces.* 2009, 74, 328–335.

32. Chamakuri, S.R.; Suttee, A.; Mondal, P. An eye-catching and comprehensive review on Pimenta dioica jacq. (bridal bouquet). *Plant Archives*. 2020, 20(2), 2076-2079.

33. Muniz, F.T.L.; Miranda, M.A.R.; Santos, C.M.D.; Sasaki, J.M. The Scherrer equation and the dynamical theory of X-ray diffraction. *Acta Crystallographica Section A: Foundations and Advances*. 2016, 72(3), 385–390.

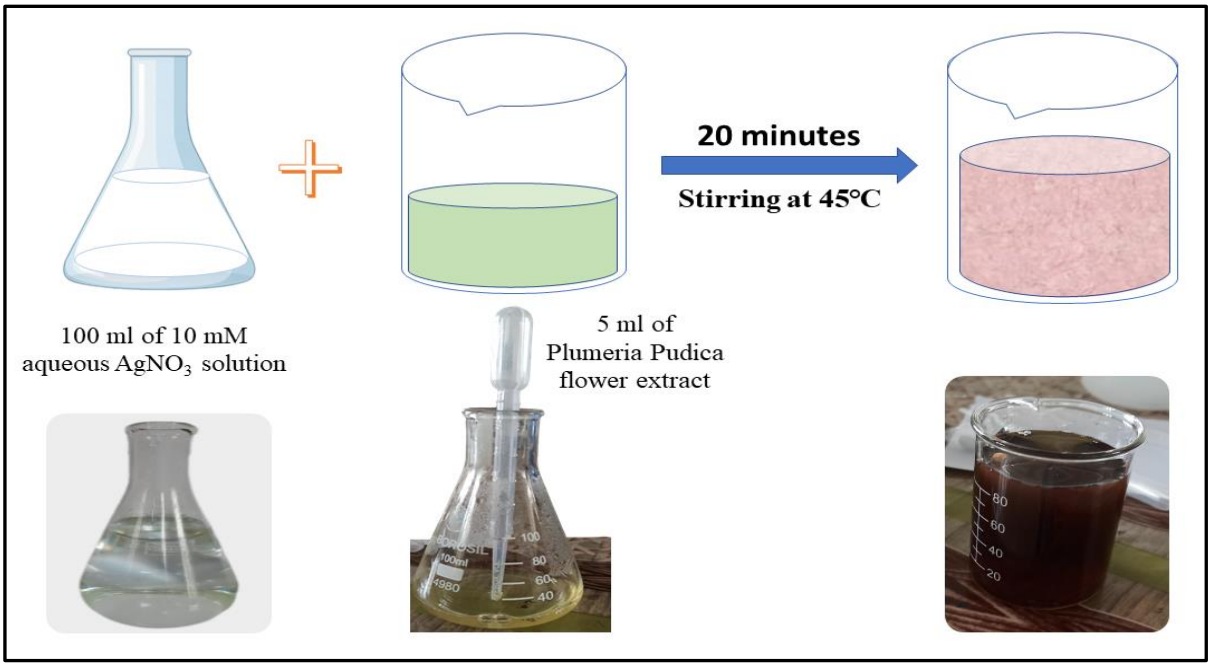

Figure 1: Schematic representation of synthesis procedure

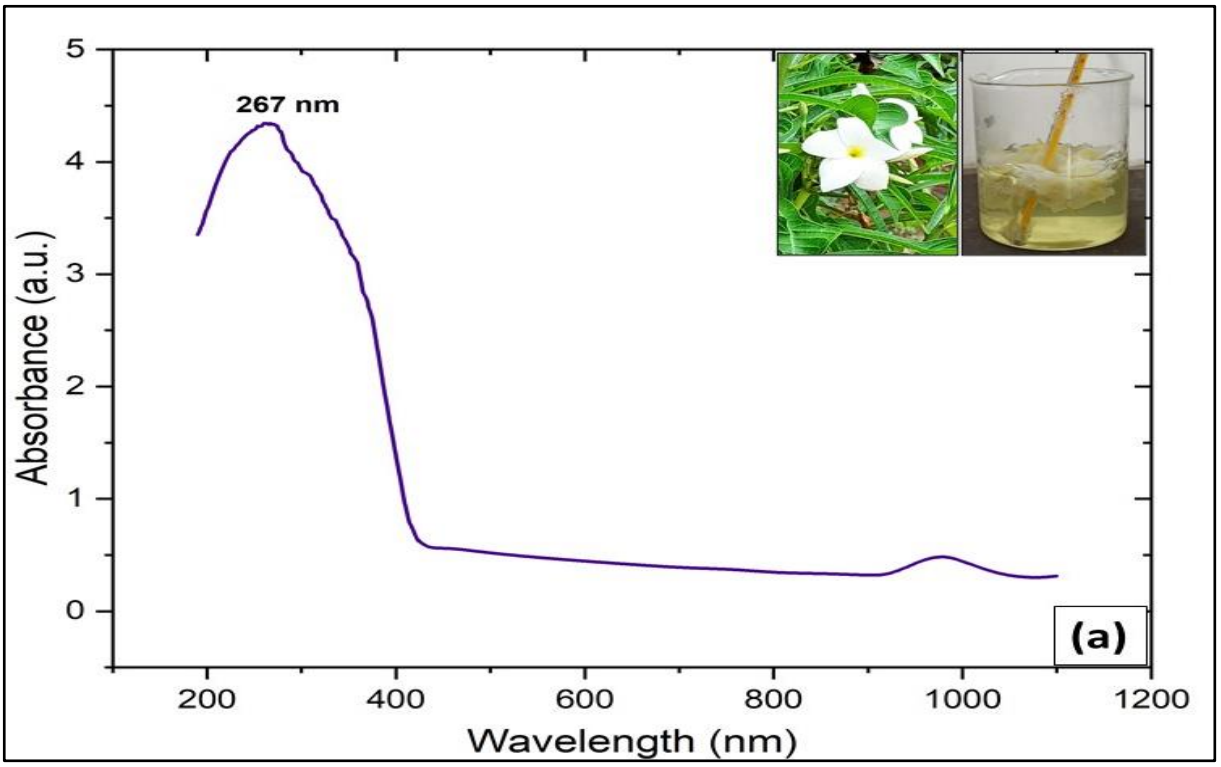

Figure 2(a): UV-Vis spectra of *Pimenta dioica*flower extract. Inset shows the flower and its extract

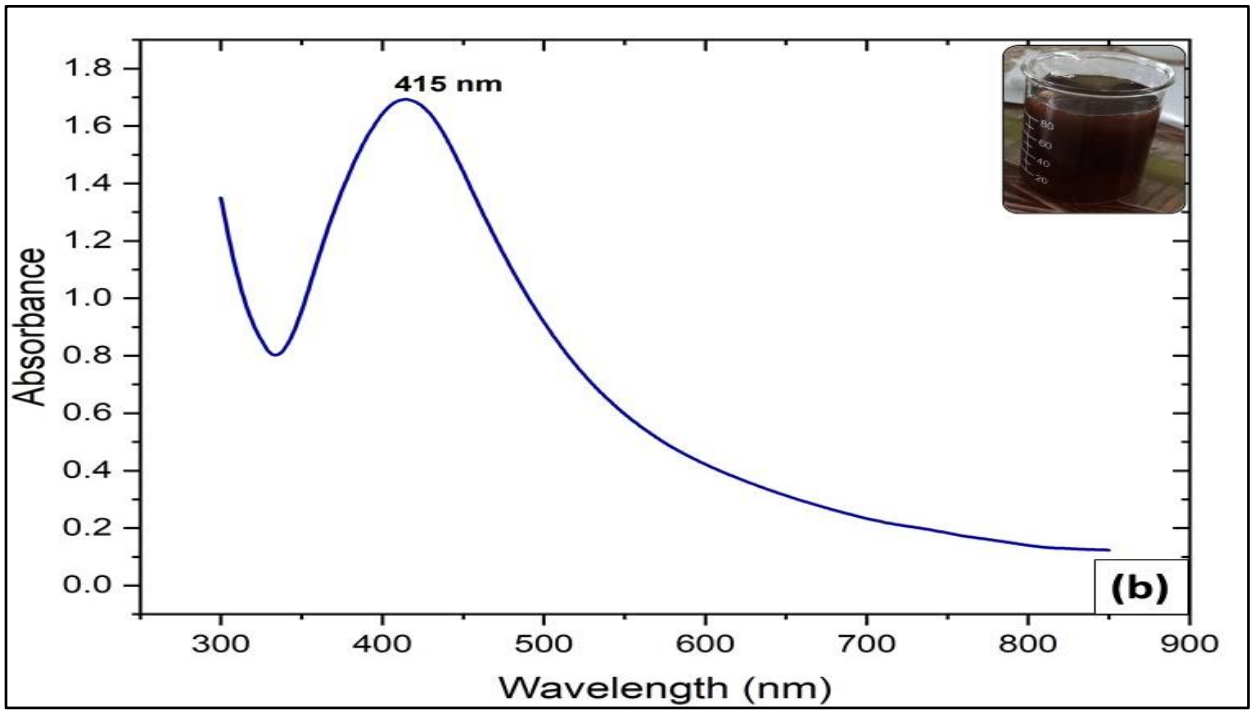

Figure 2(b): UV-Vis spectra of synthesized Ag Nanoparticles.

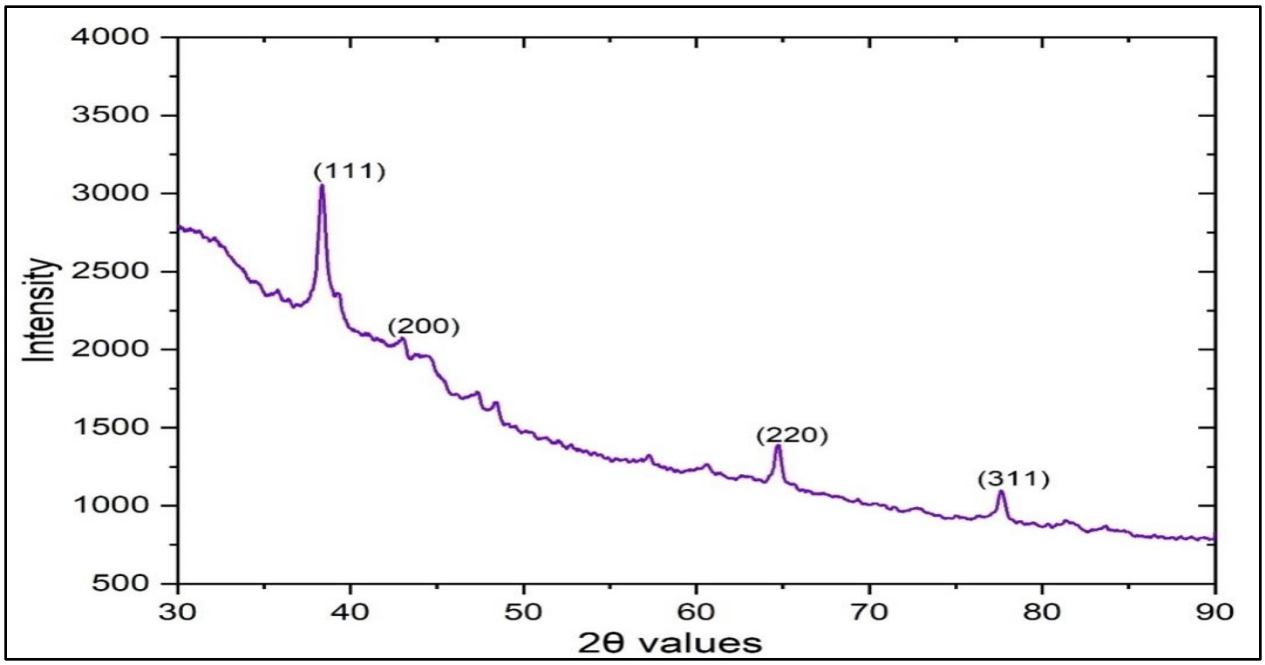

Figure 3: XRD spectra of synthesised Ag Nanoparticles

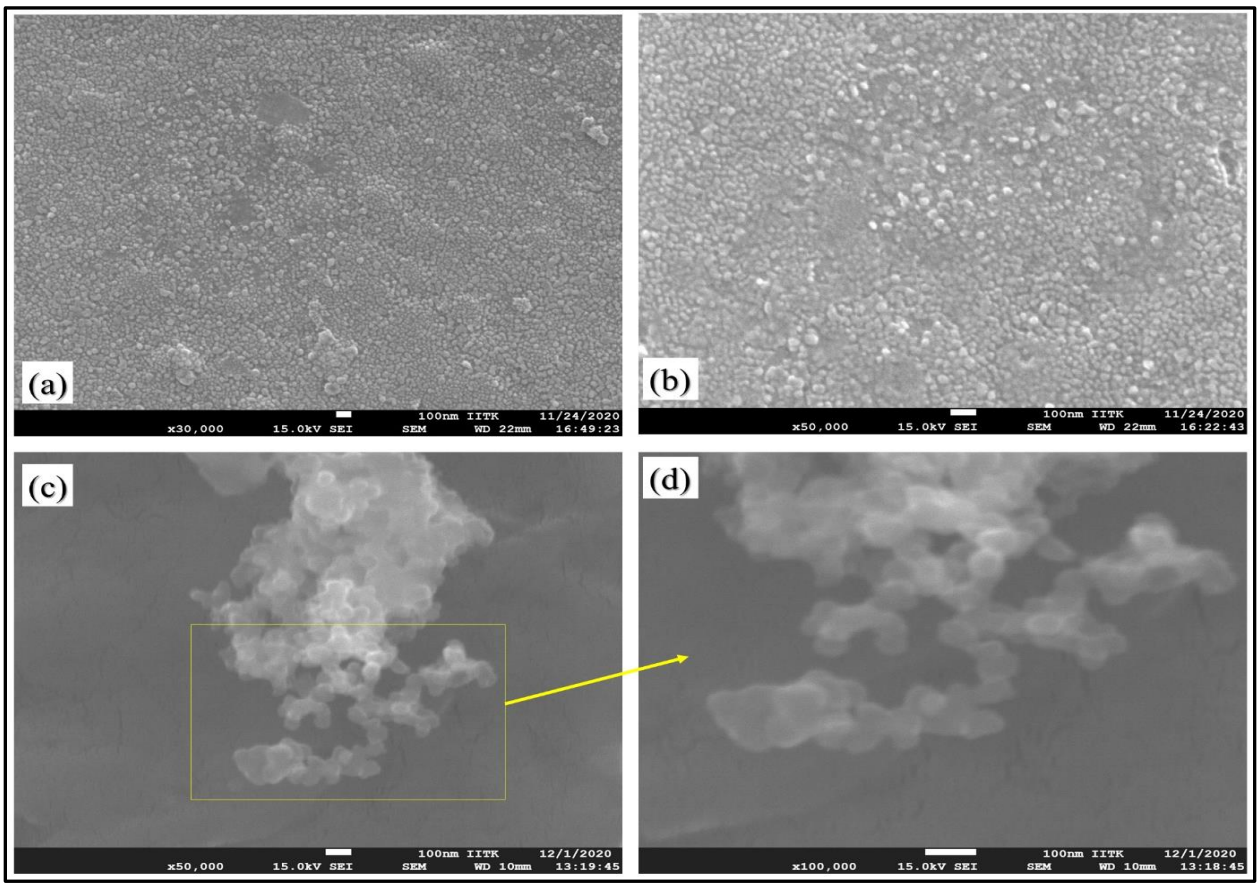

Figure. 4 (a,b,c,d): FESEM images of synthesised Ag Nanoparticles

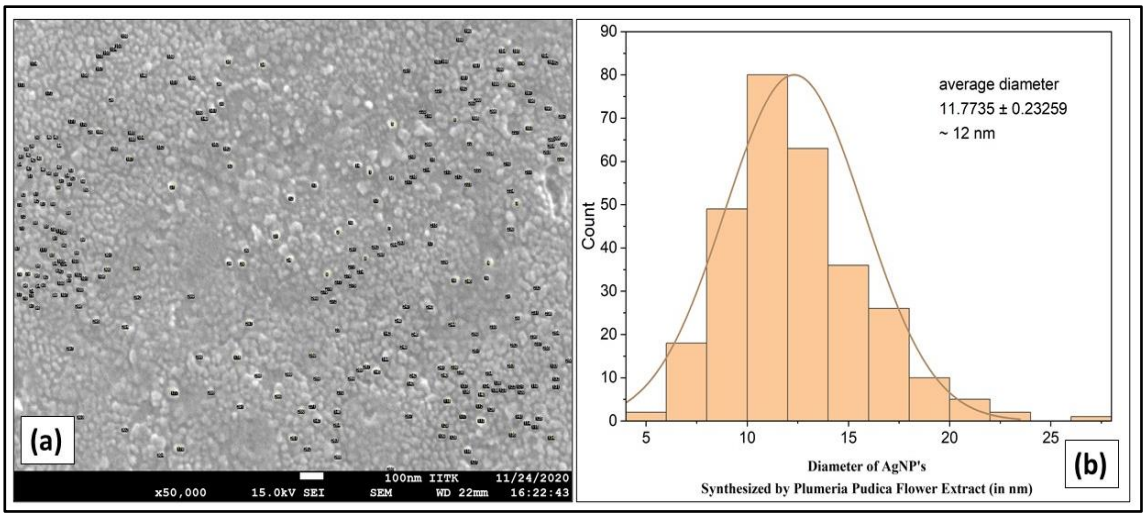

Figure. 5 (a,b): Particle size distribution of synthesized Ag Nanoparticles

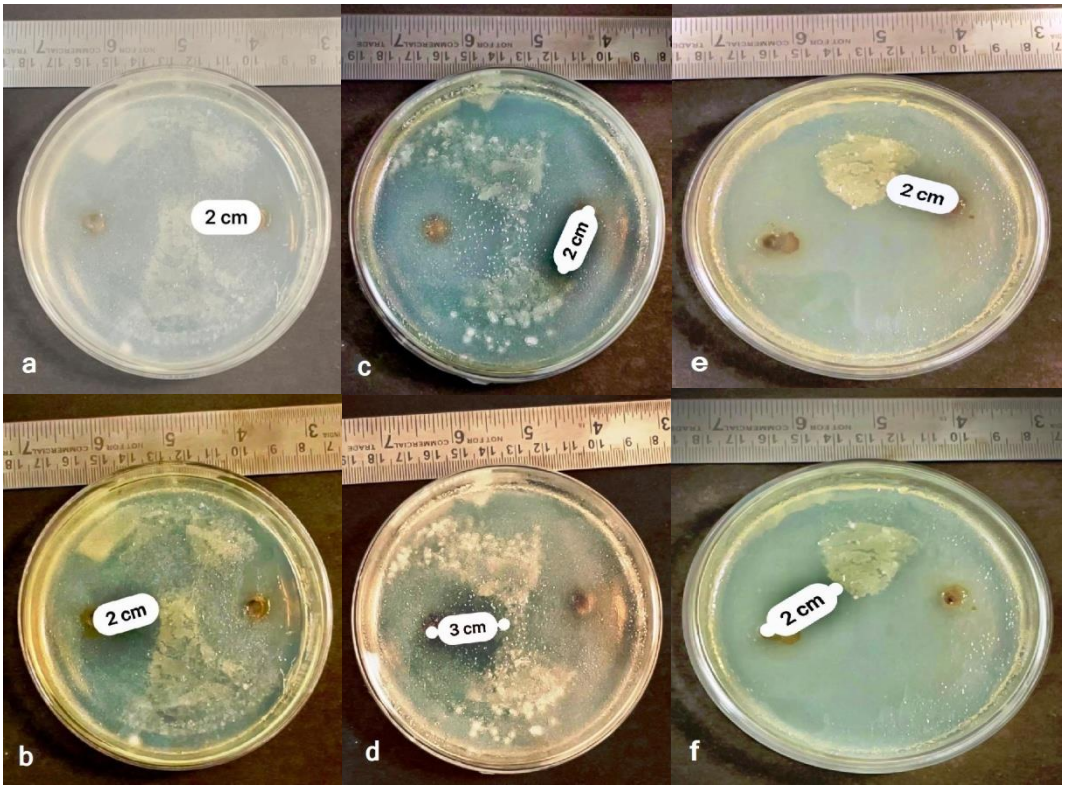

Figure 6 (a,b,c,d,e,f): Susceptibility of *Pseudomonas aeruginosa* (a,b), *Staphylococcus aureus* (c,d), *Escherichia coli* (e,f) with respect to AgNPs (by Fower) & AgNPs (by leaf).

Analysis of thermal properties and bulk modulus of liquid at different temperatures

P. Singh[1], C. P. Singh[1] and R. Singh[2]

[1]Department of Physics, R.B.S. College, Agra 282002, Uttar Pradesh, India

[2]Department of Physics, Gov. P.G. College, Khair, Aligarh 282138, Uttar Pradesh, India

Corresponding Author's Email: drpsolanki@gmail.com

Abstract

In the present paper, we have analyzed that the spinodal model produces very well. The isothermal compressibility of liquid methanol (CH_3OH) for a wide range of pressures and temperatures. We have used the pseudo spinodal model further to determine pressure derivatives, first-order as well as second-order of isothermal compressibility and bulk modulus for liquid methanol in the range of pressure (0 – 100 MPa) and temperatures (208.17K – 298.16K). The results have been found to present closed agreement with the available experiment data.

Keywords: Liquid methanol, Thermal expansivity, isothermal compressibility, Bulk modulus, Pseudo spinodal model.

1. Introduction

The study of thermodynamic properties of liquid methanol (CH_3OH) have been of great interest over the years [1-5]. The methanol is prototypical substance for the study of hydrogen-bonding phenomena [6-8]. There been continuous efforts describing the effect of temperature and pressure on the hydrogen bond strength of liquid methanol. A number of theoretical and experimental studies have been performed to understand the thermodynamic properties of liquid methanol at different temperatures [9-14]. To understand the high-pressure behavior of liquid methanol (CH_3OH) attempts have been made [11-13] to study the thermodynamic properties of the liquid at the room temperature and above. The limited number of reliable high-pressure measurements available [13, 14] at temperatures close to the melting line.

The equation of state and isothermal compressibility of liquid methanol (CH_3OH) along different isotherms and different isobars. In the present paper, we study the isothermal compressibility of liquid methanol at different temperatures and pressures using the equation of state approach [15-20]. We have used the data for liquid methanol reported by Taravillo et al. [21-23] which are more accurate and reliable than those reported previously Sun et al. [8, 9].

In the present study we have used the pseudo spinodal model [24-28] formulated along different isotherms for evaluating the isothermal compressibility and bulk modulus both with the change in pressure along selected isotherms. It is found that the spinodal pressure depends on the temperature and is a characteristic of the material. It has been demonstrated [26-28] in the present study that the some spinodal pressure is responsible for the variations of isothermal compressibility and bulk modulus with the change in pressure. Values of compressibility and its pressure derivatives up to second order are obtained for methanol at different pressure and temperatures. The compressibility and their pressure derivatives are then transformed to the corresponding pressure derivatives of bulk modulus using the formulations given in the following section.

2. Method of analysis

The pressure derivative of thermal expansivity α_p is directly related to the temperature derivative of isothermal compressibility K_T. It is found that α_p decreases with the increase in pressure whereas compressibility increases with the increase in temperature. However, both α_p and K_T decrease with the increase in pressure. These variations with the change in pressure can be explained with the help of the pseudo spinodal model [27, 28]. We write the following expressions:

$$\alpha_p = A\left(P - P_{sp}\right)^{-\beta} \qquad \text{.....(1)}$$

and

$$K_T = K^*\left(P - P_{sp}\right)^{-\gamma} \qquad \text{.....(2)}$$

where P is the pressure and P_{sp} is the spinodal pressure at which α_p and K_T diverge, that is, tend to infinity. In equation (1) A and P_{sp} are constants at a given temperature. Their values change with the change in temperature. K^* is also dependent on temperature for different liquids. The exponents β and γ are material-dependent constants. For many liquids, the exponent γ is found to be close to 0.50 whereas γ is higher than 0.50 [22, 23]. In this study, we take $\gamma = 0.85$ for methanol as revealed by experimental data [21-23]. Values of input parameters for compressibility of methanol are given in Table 1.

In the present study we focus on isothermal compressibility and bulk modulus which are inverse to each other. Thus, we write for isothermal bulk modulus

$$B_T = \frac{1}{K_T} \qquad \text{.....(3)}$$

On successive differentiation of equation (3), we get

$$B'_T = -\frac{K'_T}{K_T^2} \qquad \text{.....(4)}$$

and

$$B_T B''_T = -\frac{KT''}{K_T^3} + 2\frac{K_T'^2}{K_T^4} \qquad \text{.....(5)}$$

where

$K'_T = \left(dK_T / dP\right)_T$, $B'_T = \left(dB_T / dP\right)_T$,

$K''_T = \left(d^2K_T / dP^2\right)_T$ and $B''_T = \left(d^2B_T / dP^2\right)_T$.

The product $B_T B''_T$ has been written so as to make it dimensionless. In order to determine the higher order derivatives B'_T and $B_T B''_T$ with the help of equations (4) and (5), we need K'_T and K''_T. These are determined in the present study using the pseudo spinodal model.

Equation (2) on successive differentiation with respect to pressure gives

$$K'_T = -\gamma K^* \left(P - P_{sp}\right)^{-\gamma-1} \qquad \text{.....(6)}$$

and

$$K''_T = \gamma(\gamma+1) K^* \left(P - P_{sp}\right)^{-\gamma-2} \qquad \text{.....(7)}$$

The results obtained using equations (1) to (7) are given in Figures 1 to 3 for K_T, K'_T and K''_T. Values of B_T, B'_T and $B_T B''_T$ are given in Tables 2 to 4. The results thus obtained are utilized to study the equation of state (EOS) [29].

3. Results and Discussion

Values of isothermal compressibility at different pressures along selected isotherms have been compared with the experimental data in Figure 1. The first-order as well as second-order pressure derivatives of isothermal compressibility are given in Figures 2 and 3. The results for compressibility and its pressure derivatives have been determined with the help of the spinodal model [22, 23] using the parameters given in Table 1. The spinodal model has been found to yield good agreement with the experimental data for liquid methanol (CH_3OH).

We have used the values of isothermal compressibility and its pressure derivatives to determine bulk modulus and its pressure derivatives at different pressures and temperatures using Eqs. no. (3), (4) and (5). These are important physical quantities useful for the studies based on equation of state and higher order thermoelastic properties of materials [29-31].

Table 1 : Values of input parameters for compressibility of liquid methanol, γ = 0.85 [21-23].

T(K)	10^3K^* (MPa $^{0.15}$)	$-P_{sp}$(MPa)
208.17	41.60	125.13
223.17	42.68	115.50
248.19	44.78	101.91
263.17	45.08	91.47
273.17	44.19	81.53
298.16	45.88	69.57

Table 2 : Values of bulk modulus B_T (GPa) for liquid methanol at different pressures and temperatures.

P/MPa	208.17K	223.17K	248.19K	263.17K	273.17K	298.16K
0	1.4577	1.3273	1.1373	1.0306	0.9534	0.8025
10	1.5561	1.4242	1.2315	1.1257	1.0519	0.8995
20	1.6531	1.5202	1.3245	1.2192	1.1488	0.9957
30	1.7497	1.6152	1.4162	1.3116	1.2444	1.0883
40	1.8453	1.7091	1.5071	1.4029	1.3386	1.1806
50	1.9398	1.8021	1.5969	1.4929	1.4316	1.2716
60	2.0337	1.8942	1.6857	1.5822	1.5236	1.3614
70	2.1267	1.9853	1.7736	1.6705	1.6147	1.4503
80	2.2187	2.0759	1.8611	1.7580	1.7047	1.5382
90	2.3105	2.1659	1.9477	1.8450	1.7940	1.6252
100	2.4015	2.2552	2.0337	1.9312	1.8825	1.7111

Table 3: First pressure derivatives of bulk modulus (dB_T/dP) for liquid methanol.

P/MPa	208.17K	223.17K	248.19K	263.17K	273.17K	298.16K
0	9.90	9.77	9.48	9.58	9.94	9.80
10	9.79	9.64	9.35	9.43	9.77	9.61
20	9.68	9.54	9.23	9.30	9.62	9.46
30	9.59	9.44	9.13	9.18	9.48	9.29

40	9.50	9.34	9.03	9.07	9.36	9.16
50	9.41	9.26	8.94	8.97	9.25	9.04
60	9.34	9.17	8.85	8.88	9.15	8.93
70	9.26	9.10	8.77	8.79	9.06	8.83
80	9.19	9.02	8.70	8.71	8.97	8.74
90	9.13	8.96	8.62	8.64	8.89	8.66
100	9.07	8.90	8.56	8.57	8.81	8.58

Table 4: Second pressure derivatives of bulk modulus [$-B_T(d^2B_T/dP^2]$ for liquid methanol.

P/MPa	208.17K	223.17K	248.19K	263.17K	273.17K	298.16K
0	17.33	16.77	16.09	16.07	17.42	17.16
10	16.83	16.61	15.56	15.70	16.77	16.25
20	16.53	15.91	15.22	15.12	16.22	15.53
30	16.08	15.56	14.53	14.79	16.02	15.23
40	15.86	15.49	14.27	14.53	15.56	14.75
50	15.82	14.96	13.91	14.23	15.15	14.40
60	15.35	14.98	13.78	13.87	14.77	14.11
70	15.30	14.51	13.54	13.76	14.37	13.85
80	15.01	14.59	13.19	13.55	14.20	13.54
90	14.73	14.10	13.15	13.24	13.94	13.13
100	14.41	13.74	13.01	13.08	13.89	12.89

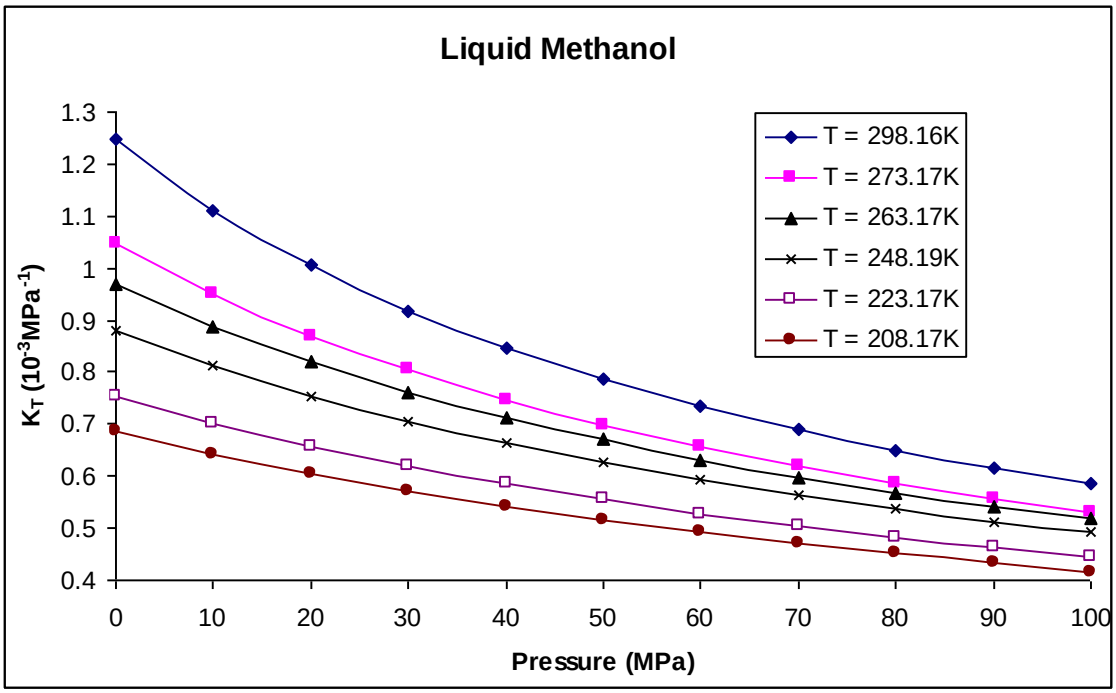

Figure 1: Calculated values of isothermal compressibility K_T for liquid methanol at different temperatures represented by continuous curves are compared with the experimental data [22, 23] represented by symbols ●□ x▲■

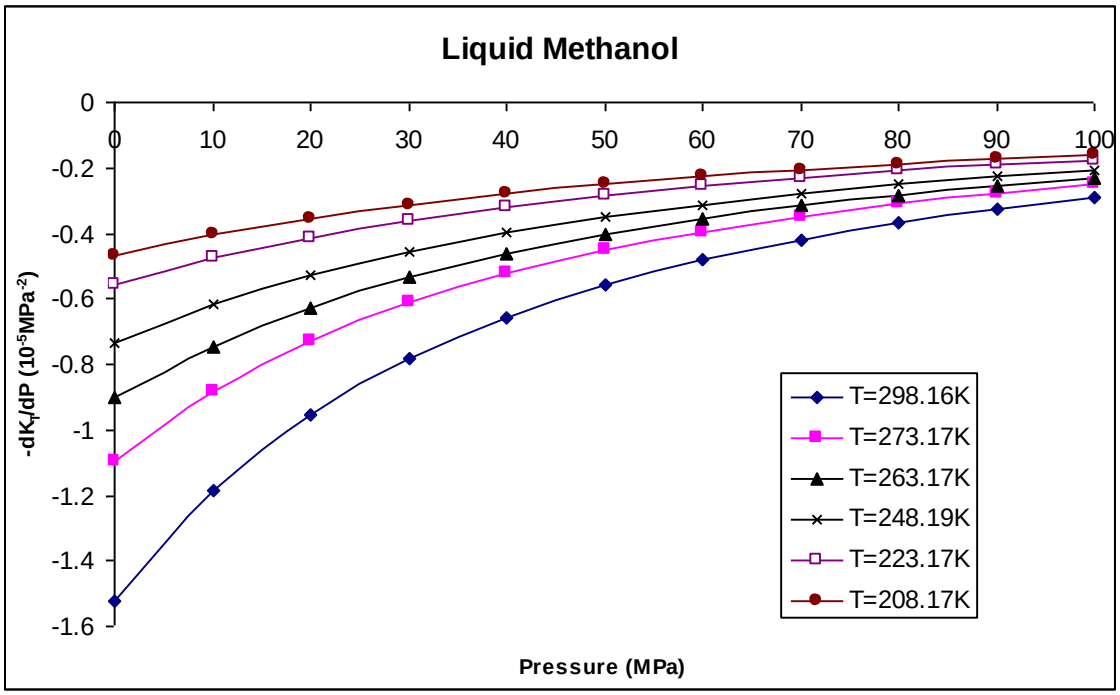

Figure 2: Calculated values of first-order pressure derivative of isothermal compressibility for liquid methanol represented by continuous curves are compared with the experimental data represented by symbols ●□ x▲■ ♦.

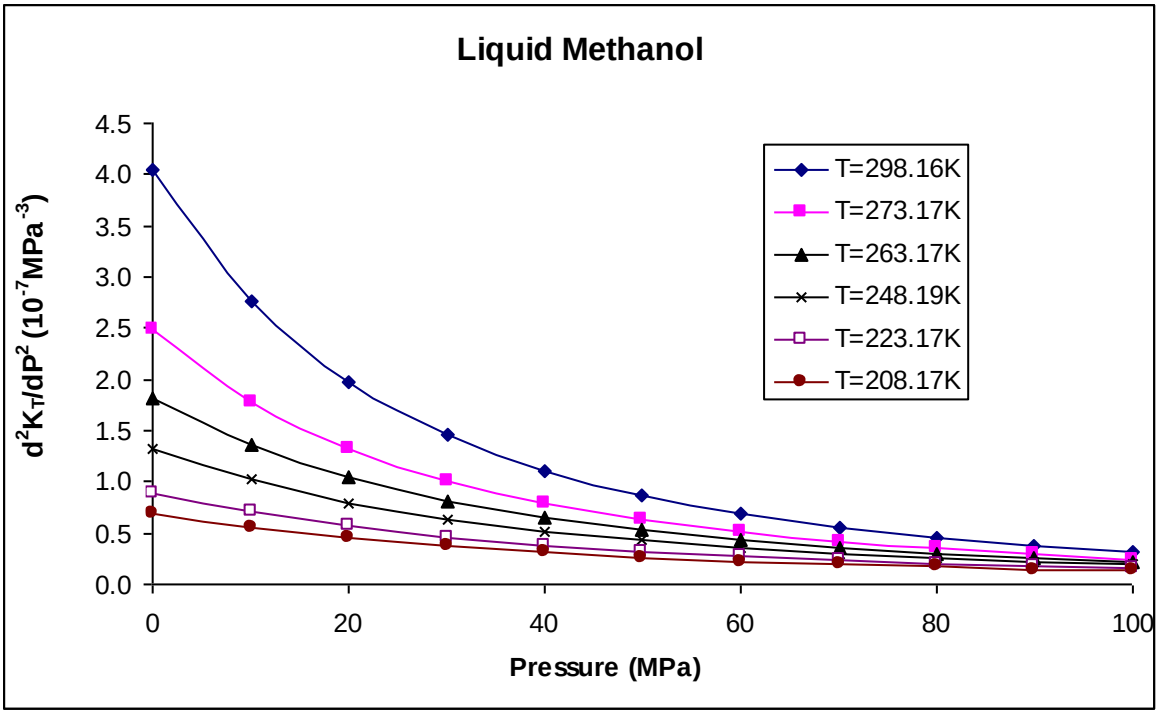

Figure 3 : Calculated values of second-order pressure derivatives of isothermal compressibility for liquid methanol represented by continuous curves are compared with the experimental data represented by symbols ●□ x▲■ ♦.

REFERENCES-

[1] E. H. Amagat Traisieme memoire, *Liq. Ann. Chim. Phys.* **29** 505 (1893).

[2] W. Seitz, H. Alterthum and G. Lechner, *Ann. Physik. (Leipzig)* **49** 85 (1916).

[3] T. Moriyoshi and H. Inubushi, *J. Chem. Thermodyn.* **9** 587 (1977).

[4] J. R. S. Macado and W. B. Streett, *J. Chem. Eng. Data* **28** 218 (1983).

[5] A. J. Easteal and L. A. Woolf, *J.Chem. Thermodyn.* **17** 49 (1985).

[6] R. D. Goodwin, *J. Phys. Chem. Ref. Data* **16** 799 (1987).

[7] H. Kubota, Y. Tanaka and T. Makita, *Int. J. Thermo Phys.* **8** 47 (1987).

[8] T. F. Sun, S. N. Biswas, N. J. Trappeniers and C. A. Ten Seldam, *J. Chem. Eng. Data* **33** 395 (1988).

[9] T. F. Sun, J. A. Schouten and S. N. Biswas, *Ber. Bunsenges. Phys. Chem.* **94** 528 (1990).

[10] M. Riembaucr, L. Schulte and A. Würflinger, *Z. Phys. Chem. Neue Folge* **166** 53 (1990).

[11] V. Vacek and A. M. Hany, *Fluid Phase Equilib.* **76** 187 (1992).

[12] K. M. Reuck and R. J. B. de : Craven, *Methanol International Thermodynamic Tables of the Fluid State* – 12; IUPAC Chemical Data Series No – 38; Black well Scientific Publications: (1993).

[13] J. Hruby, J. Klomfar and O. Sifner, *J. Chem. Thermodyn.* **25** 1229 (1993).

[14] D. Papaioannou and C. Panayiotou, *J. Chem. Eng. Data* **40** 202 (1995).

[15] E. U. Franck and R. Deul, *Faraday Discuss. Chem. Soc.* **66** 191 (1978).

[16] R. Ledwig and A. Würflinger, *Z. Phys. Chem. Neue Folge* **132** 21 (1982).

[17] K. Vedam and P. Limsuwan, *J. Chem. Phys.* **69** 4772 (1982).

[18] J. Shanker, S.S. Kushwah and P. Kumar, *Physica B* **239** 337 (1997).

[19] B. Grocholski and R. Jeanloz, *J. Chem. Phys***123** 204503 (2005).

[20] W. L. Jorgensen and M. Ibrahim, *J. Am. Chem. Soc.* **104** 373 (1982).

[21] M. Taravillo, V. G. Baonza, M. Caceres and J. Nunez, *J. Phys. Condens. Matter* **15** 2979 (2003).

[22] M. Taravillo, V. G. Baonza, M. Caceres and J. Nunez, *J. Phys. Condens. Matter* **18** 10213 (2006).

[23] M. Taravillo, F. J. Perez, J. Nunez, M. Caceres and V. G. Baonza, *J. Chem. Eng. Data* **52** 481 (2007).

[24] M. Hareng and J. Lebeland, *J. Chem. Phys.* **73** 622 (1980).

[25] Ph. Pruzan, *J. Phys. Lett* **45L** 273 (1984).

[26] I. C. Sanchez, J. Cho and W. J. Chen, *Macromolecules* **26** 3234 (1993).

[27] I. C. Sanchez, J. Cho and W. J. Chen, *J. Phys. Chem.* **97** 6120 (1993).

[28] R. S. Chauhan, P. Singh and C. P. Singh, *Indian J. Phys.* **85** 421 (2011).

[29] R. S. Chauhan, P. Singh and C. P. Singh, *Chinese Journal of Physics* **63** 45 (2020).

[30] R. S. Chauhan, P. Singh and C. P. Singh, *Indian Journal of Pure & Applied Physics* **49** 535 (2011).

[31] R. S. Chauhan, P. Singh and C. P. Singh, *Physics and Chemistry of Liquids* **51** 294 (2013).

The Grüneisen parameter and its higher order derivatives for the interior of the Earth

[1]Pushpendra S. Sikarwar
[1]Department of Physics, RBS College, Agra, 282002
Corresponding Author's Email- psikarwar1991@gmail.com

Abstract- On the basis of the free volume theory of Grüneisen parameter it is found that the second order Grüneisen parameter (q) and the second pressure derivative of bulk modulus (KK") changes in a similar manner in the limit of extreme compression. The ratio of second order Grüneisen parameter and second pressure derivative of bulk modulus becomes finite at infinite pressure. It has been found that the relationships under study satisfy the boundary conditions at infinite pressure for the higher order Grüneisen parameter. Using above result, the Grüneisen parameter and its higher order derivative for the interior of the earth can be calculated using the input data from Stacy and Davis (2004).

Keywords- Grüneisen parameter, free volume theory, higher order derivatives, Extreme compression behavior, Thermal expansivity.

Introduction- In the condensed matter physics the Grüneisen parameter is used to measure the thermoelastic properties of solids in the limit of extreme compression. The pressure derivative of (γ) play a central role in predicting the thermal behavior equation of state and melting at high pressure free volume theory of (γ) has been generalized to obtain (γ) as a function of pressure P bulk modulus K and pressure derivative of bulk modulus K' = dK/dP This generalized free volume formula can be written as

[K'/2-1/6-f/3(1-P/3K)]/[1-2fP/3K]

Where f is the free volume parameter. The behavior of solids at high pressures and high temperatures, required an adequate knowledge of equation of state and thermoelastic properties of materials [1-4]. Stacey [1-3] has developed a fundamental theory for the analysis of thermoelastic properties of materials at extreme compression (volume V → 0, pressure P → ∞). One of the most important findings in the result that thermal expansivity of materials decreases with the increase in pressure, and tend to zero in the limit of infinite pressure.

Analysis-

The analysis performed by Stacey [1-3] starts with the following identity.

$$\left[\frac{d\ln(\gamma\alpha T)}{d\ln V}\right]_S = (1+\gamma\alpha T)(\partial_S+q) \qquad \ldots\ldots\ldots\ldots\ldots(1)$$

Where γ is the Gruneisen parameter [4]

$$\gamma = \frac{\alpha K_T V}{C_V} = \frac{\alpha K_s V}{C_P} \qquad \text{.....(2)}$$

Where α is thermal expansivity, K_T and K_s are isothermal and adiabatic bulk moduli, C_V and C_P are specific heats at constant volume and constant pressure respectively. ∂_S is the adiabatic Anderson- Grüneisen parameter

$$\partial_S = -\frac{1}{\alpha K_s}\left(\frac{dK_s}{dT}\right)_P \qquad \text{.....(3)}$$

and q is the second order Gruneisen parameter

$$q=\left(\frac{d\ln\gamma}{d\ln V}\right)_T \qquad \text{.....(4)}$$

Equation (1) represents an identity which is valid at all values of pressure, temperature and volume. This has been derived using the Maxwell thermodynamic relations [3,4]. The product $\gamma\alpha T$ appearing in Eq. (1) is physically meaningful as it is directly related to the ratio, K_s/K_T or C_P/C_V . Eq. (2) has been derived [4] using the fundamental relationship between thermal pressure and thermal energy. It is found that γ remains nearly constant for different solids, although other thermoelastic properties appearing in Eq. (2) differ much from one solid to other. ∂_S is an important parameter (Eq. (3)) introduced and used by Anderson [4] to describe the temperature dependence of bulk modulus. ∂_S does not vary much from material to material, and also it remains approximately constant with the change in temperature. q is the second order Grüneisen parameter (Eq. (4)) which decreases with the increase in pressure, and becomes zero in the limit of infinite pressure.

Stacey's consequence of vanishing thermal expansivity at infinite pressure was derived on the basis of mathematical identities used by Shanker et al. [5,6]. The vanishing thermal expansivity then leads to the fact that the first and second pressure derivatives of bulk moduli become temperature independent constants at infinite pressure. These thermodynamic consequences under extreme compression constitute important boundary conditions for thermodynamic properties of substances under extreme compression.

If y is a function of x such that y remains positive finite at $x \rightarrow 0$, then

$$\left(\frac{d\ lny}{d\ ln\ x}\right)_{x\rightarrow 0} = 0 \qquad \text{.....(5)}$$

If y tends to zero at $x \rightarrow 0$, then

$$\left(\frac{d\ lny}{d\ ln\ x}\right)_{x\rightarrow 0} = \text{positive finite} \qquad \text{.....(6)}$$

With the help of Eq. (5) and (6), one can understand conveniently from Eq. (1) that $\partial_{S\infty}$ is positive finite when $(\gamma\alpha T)_\infty$ is zero, and $\partial_{S\infty}$ must be zero when $(\gamma\alpha T)_\infty$ is positive finite. In Eq. (1), q becomes $(q)_\infty$ equal to zero since γ_∞ remains positive finite, Eq. (4).

The parameter $\partial_{S\infty}$ is related to γ_∞ and K'_∞ the pressure derivative of bulk modulus at infinite pressure. One has the thermodynamic identity which reduces at infinite pressure as follows

$$\partial_{S\infty} = K'_\infty - 1 - \gamma_\infty \qquad \text{.....(7)}$$

$$K'_\infty = 1 + \gamma_\infty \qquad \text{.....(8)}$$

When $\partial_{S\infty}$ is positive finite, Eq. (7) yields

$$K'_\infty > 1 + \gamma_\infty \qquad \text{.....(9)}$$

Although Eq. (8) is satisfied by γ_∞ =2/3 and K'_∞=5/3, values according to the Thomas-Fermi model [7], but Eq. (9) is a fundamental constraint found by Stacey [2,3]. Eq. (9) must be satisfied by all physically acceptable equations of state. Of particular interest are the following thermodynamic identities at infinite pressure derived from the expressions given by Stacey [3]

$$\left[\frac{d\ ln(\alpha K_T V)}{d\ ln\ V}\right]_{S\infty} = \delta_{T\infty} - C'_{T\infty} - K'_\infty + 1 \qquad \text{.....(10)}$$

and

$$\delta_{T\infty} = K'_\infty - 1 + C'_{T\infty} \qquad \text{.....(11)}$$

where

$$\delta_T = \frac{-1}{\alpha K_T}\left(\frac{d\ K_T)}{dT}\right)_P \qquad \text{.....(12)}$$

$$C_T' = \frac{d\ln C_v}{d\ln V} \qquad \text{……..(13)}$$

Equations (10) and (11) gives

$$\left[\frac{d\ln(\alpha K_T V)}{d\ln V}\right]_{S\infty} = 0 \qquad \text{……..(14)}$$

$$(\alpha K_T V)_\infty = \text{positive finite} \qquad \text{……..(15)}$$

In the limit of infinite pressure, K_T varies as $V^{-K_\infty'}$ [8], one can rewrite Eq. (15) as follows:

$$\alpha_\infty = \text{constant } V^{-K_\infty'-1} \qquad \text{……(16)}$$

At extreme compression ($V \to 0$), Eq. (16) reveals that α_∞ tends to zero since $K_\infty' > 1$. One has the following expressions for the adiabatic and isothermal Anderson-Gruneisen parameters [4]

$$\partial_S = \left[\frac{d\ln(\alpha T/C_p}{d\ln V}\right]_S \qquad \text{…….(17)}$$

and

$$\partial_T = \left[\frac{d\ln\alpha}{d\ln V}\right]_T \qquad \text{…….(18)}$$

Equations (17) and (18) reveals that $\partial_{S\infty}$ and $\partial_{T\infty}$ both remain positive finite because α_∞ tends to zero. This is derived from Eq. (6) it should be mentioned that the RHS of Eq. (3) is equal to that of Eq. (17). Also the RHS of Eq. (12) is equal to that of Eq. (18). Stacey [3] has obtained the following identities,

$$\left(\frac{dK_T'}{dT}\right)_P = \alpha\delta_T\left[\delta_T - K_T' + \left(\frac{d\ln\delta_T}{d\ln V}\right)_T\right] \qquad \text{....……..…(19)}$$

$$\left(\frac{dK_S'}{dT}\right)_S = \alpha\delta_S\left[\delta_S - K_S' + \left(\frac{d\ln\delta_S}{d\ln V}\right)_S\right] \qquad \text{…..……(20)}$$

Since $\partial_{S\infty}$ and $\delta_{T\infty}$ both are positive finite, one have

$$\left[\left(\frac{d\ln\delta_T}{d\ln V}\right)_T\right]_\infty = 0 \qquad \text{……..(21)}$$

$$\left[\left(\frac{\mathrm{d}\ln\delta_S}{\mathrm{d}\ln V}\right)_S\right]_\infty = 0 \qquad \ldots\ldots\ldots\ldots(22)$$

Equations (21) and (22) are derived from Eq. (5). Equations (19) and (20) at infinite pressure reveal that K_T' and K_S' both become independent of temperature Since α_∞ tends to zero. At infinite pressure, Equations (19) and (20) are reduced as follows:

$$\left[\frac{1}{\alpha}\left(\frac{\mathrm{d}\,K_T'}{\mathrm{d}T}\right)_P\right]_\infty = \partial_{T\infty}(\partial_{T\infty} - K_\infty') \qquad \ldots\ldots\ldots\ldots (23)$$

$$\left[\frac{1}{\alpha}\left(\frac{\mathrm{d}\,K_S'}{\mathrm{d}T}\right)_P\right]_\infty = \partial_{S\infty}(\partial_{S\infty} - K_\infty') \qquad \ldots\ldots\ldots\ldots\ldots(24)$$

Thus Equations (23) and (24) the ratio reveal that the ratios of $(\mathrm{d}K_T'/\mathrm{d}T)$ and at infinite pressure are finite. One can write using Eq. (5)

$$\left[\frac{\mathrm{d}\ln\left(\frac{1}{\alpha}\frac{\mathrm{d}\,K_T'}{\mathrm{d}T}\right)}{\mathrm{d}\ln V}\right]_\infty = 0 \qquad \ldots\ldots\ldots\ldots\ldots(25)$$

At infinite pressure $K_{S\infty}' = K_{T\infty}'$ [3], so both of them are represented by K_∞' . On rewriting Eq. (25), one gets:

$$\left[\frac{\mathrm{d}}{\mathrm{d}P}\frac{\mathrm{d}\,K\prime}{\mathrm{d}T}\right]_\infty = -\frac{\partial_{T\infty}}{K_\infty}\left[\frac{\mathrm{d}\,K\prime}{\mathrm{d}T}\right]_\infty \qquad \ldots\ldots\ldots\ldots..(26)$$

In deriving Eq. (26), one has used

$$\partial_T = \left(-\frac{K}{\alpha}\frac{\mathrm{d}\alpha}{\mathrm{d}P}\right)_T \qquad \ldots\ldots\ldots\ldots\ldots\ldots (27)$$

which is equivalent to Eq. (18)

The RHS of Eq. (26) tends to zero since $\partial_{T\infty}$ is finite, $[\mathrm{d}K'/\mathrm{d}t]_\infty$ is zero and K_∞ tends to infinity. Equation (27) them gives

$$\left[\frac{\mathrm{d}}{\mathrm{d}P}\left(\frac{\mathrm{d}\,K\prime}{\mathrm{d}T}\right)\right]_\infty = \left(\frac{\mathrm{d}\,K''}{\mathrm{d}T}\right)_\infty = 0 \qquad \ldots\ldots\ldots\ldots\ldots\ldots(28)$$

The basic principles of calculus have been used along with some thermodynamic identities [3] to demonstrate that α_∞ tends to zero, $\partial_{S\infty}$ and $\partial_{T\infty}$ remain positive finite, and logarithmic

volume derivatives $(d\ln\delta_S/d\ln V)_\infty$ and $(d\ln\delta_T/d\ln V)_\infty$ become zero. Higher order thermoelastic parameters $\frac{1}{\alpha}\left(\frac{d\,K'_T}{dT}\right)_P$ and $\frac{1}{\alpha}\left(\frac{d\,K'_S}{dT}\right)_P$ at infinite pressure are found to remain finite, although α, $\left(\frac{d\,K'_T}{dT}\right)_P$ and $\left(\frac{d\,K'_S}{dT}\right)_P$ all become zero in the limit P tends to infinity. The temperature derivatives of K'_T and K'_S become independent of pressure, and second pressure derivatives K'' become independent of temperature at extreme compression.

These Consequences owe much to Stacey's thermodynamic identities. it is desirable to illustrate to claim by referring to the specific experimental results. It is not trivial to measure the second derivative of bulk moduli. Stacey and Davis [2] have reported the values of K' and K K'' become quite small.

Conclusions-

The Consequences based on Stacey's thermodynamic identities are important boundary conditions for the thermodynamic properties of substances under extreme compression. Recent studies [9-12] on the thermoelastic properties of materials at high pressures are consistent with the results obtained in the limit of extreme compression [13-16] and others [14] to discuss the nature of variation of αK_T with volume.

References:

[1] F.D. Stacey. Geophys J. Int., **143**,621 (2000).

[2] F.D. Stacey, P. M. Davis, Phys. Earth Planet Inter., **142,**137 (2004).

[3] F.D. Stacey, Rep. Prog. Phys., **68**, 341 (2005).

[4] O.L. Anderson, Equations of State for geophysics and ceramic sciences, Oxford University Press, New York. (1995).

[5] J. Shanker, P. Dulari, P. K. Singh, Physica B **404**, 4083 (2009).

[6] J. Shanker, K. Sunil, B.S. Sharma, Physica B **407**, 2082 (2012).

[7] J. Shanker, B.P. Singh, H. K. Baghel, Physica B **387**,409 (2007)

[8] L. Knopoff, J. Geophys. Res., **68**, 2929 (1963)

[9] J. Shanker, B.P. Singh, K. Jitendra, Condens. Matter Phys., **11**, 681 (2008).

[10] J. Shanker, B.P. Singh, K. Jitendra, Condens. Matter Phys., **12**, 205 (2009).

[11] S. S. Kushwah, A.K. Upadhyay, M.P. Sharma, High temperatures- High Pressures, **44**, 59 (2014).

[12] S.K. Srivastava, Solid State Commun., **151**, 1472 (2011).

[13] K.S. Singh, Physica B **407**, 668 (2012).

[14] R. S. Chauhan, C. P. Singh, Physica B, **387** (2007) 352

[15] K. Anand, Pushpendra S. Sikarwar, Vijay S. Sharma Condens. Matter Phys., **29**,602(2021).

[16] S. Kumar, S.K. Sharma, O.P. Pandey, High temperatures- High pressures, **44,** 339 (2015).

Optimized Hardware Implementation of Diabetic Sensorimotor Polyneuropathy Severity Classifier using FPGA

Sandeep Kumar Pandey, Geetika Srivastava

Department of Physics and Electronics, Dr. Rammanohar Lohia Avadh University, Ayodhya, 224001

Email: Sandeep.avadh@gmail.com, geetika_gkp@rediffmail.com

Abstract- Diabetic Sensorimotor Polyneuropathy (DSPN) disease increases rapidly in diabetic patients. It cause permanent disability and also in some cases death of patients occurred. Early detection and prevention like changes in lifestyle helps the patients to recover from DSPN. As we seen that use of machine learning is increases rapidly in disease diagnosis of human being. Therefore taking the problem of early detection of DSPN in patients we designed a neural network taking Electromyography (EMG) signal from different lower limb muscles during gait and hardware implemented over a Xilinx Zed Board which provided 70.9% accuracy in detection with optimum resource utilization. Although the accuracy is low but improved version of this device will become helpful in DSPN diagnosis in patients in near future.

Keywords—DSPN, EMG, SVM, NN, GL, VL, TA

Introduction: Diabetes disease has become most dangerous and chronic, due to which permanent disability and in many cases death of patients also occurred. Due to diabetes Diabetic Sensorimotor Polyneuropathy is a growing disease in humans all over the world [1]. DSPN is an early sign of non-healing wound and diabetic foot ulcer [2]-[3]. Approximately 50% diabetic patients are suffering from DSPN and among them 50% patients not reported the symptoms of DSPN [4]-[5]. 34% of diabetic patients are reported to experience pain sensations, and type 2 diabetic patients have a far higher incidence of painful neuropathic symptoms than type l diabetes. Reduced physical and psychological functioning, anxiety, and depression may also be linked to these pain symptoms. Quantitative sensory technique such as vibration perception threshold (VPT), nerve conduction studies (NCS), Neuropathy Disability Score (NDS), Michigan Neuropathy Screening Instrument, Achilles tendon reflexes, pinprick and temperature sensation etc. are the famous method to diagnose DSPN [6]. They are costly, needs expert person and also some are painful. Although there have been significant improvements in treating symptomatic pain, such as with the use of drugs, there are few therapy options that focus on the underlying pathophysiology of DSPN. Early diagnosis and prevention is help in the treatment of DSPN [7]. To overcome these difficulties, we proposed to design a DSPN severity classifier using Machine Learning (ML) as we seen that applicability of ML increases

in bio signal processing day by day [8]. DSPN affects lower limb muscles [9], therefore by recording the Electromyography signal of patients from different lower limb muscles during gait and processed them using machine learning algorithm we designed a DSPN severity classifier and hardware implemented over Xilinx Zed Board. Implemented hardware provided good result in testing. In literature many works are reported which gives approximately 99% accuracy in software but as per my study no work reported on hardware implementation of DSPN severity classifier. Presented work provided an approach to develop a patient friendly portable device which classifies the normal and abnormal patients without more criticality and expertise. Rest of the paper is arranged as EMG signal Pre-processing, EMG Signal Processing using machine learning algorithm, proposed method, dataset preparation, neural network design, results and discussion, conclusion and future work.

EMG Signal Pre-Processing: EMG is short form of Electromyography. It is the study of muscle electrical signals or in other words it is the process of measuring the electrical activity produced by muscles throughout the body using electrodes [10]. When recording EMG signal, there are two main things that affects the quality of signal. First is the signal to noise ratio and second is the distortion [10]-[12]. Therefore after the collection of raw signals, a proper method of de-noising must be applied to the signals to remove the unwanted noises introduced by any inner or outer source of electrical activity or any other types of artefacts. Figure 1 shows the pre-processing steps of EMG signal.

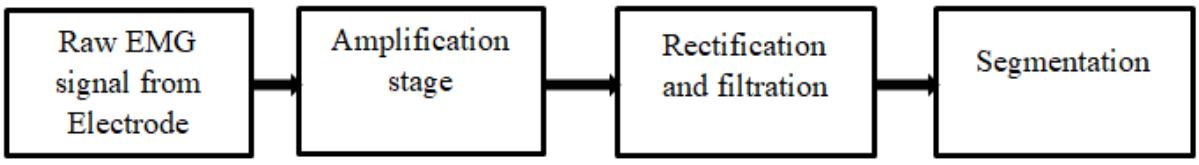

Figure 1. Pre-processing stage of EMG signal

The raw signal is collected using electrode and amplified. Usually, a differential amplifier is used at the first stage. The signal further processed to eliminate low or high-frequency noise, or other artefacts. Mostly, the users are interested in the amplitude of the EMG signal. Therefore, the signal is rectified and averaged in some format to show the EMG amplitude.

EMG Signal Processing Using Machine Learning Algorithm [13]-[15]:

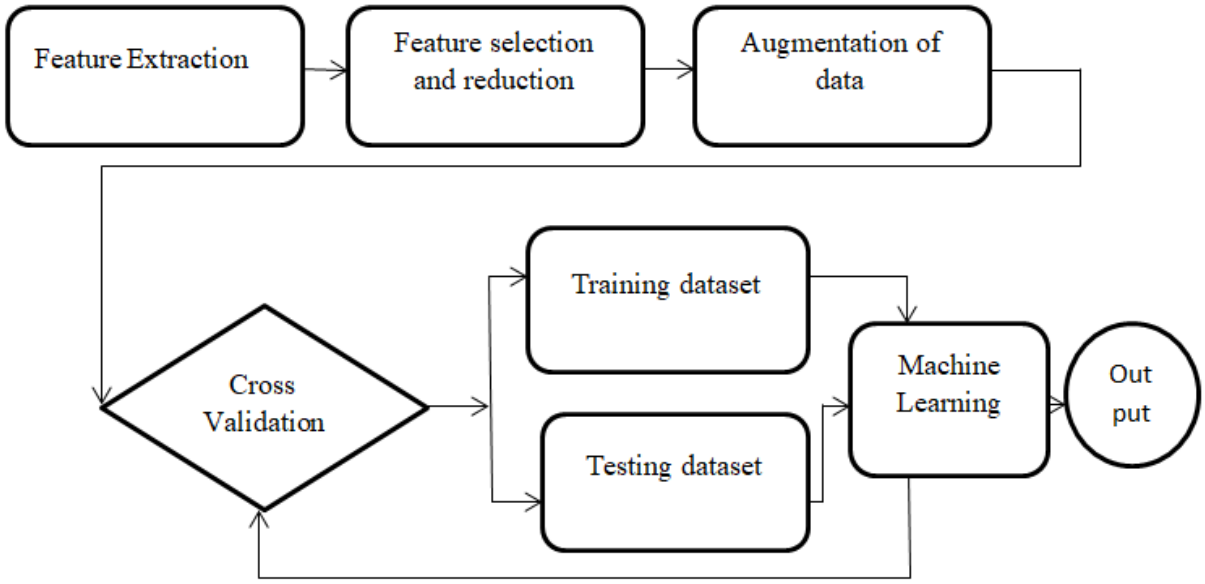

Figure 2. EMG signal processing using Machine learning

Figure 2. shows the steps of EMG signal processing using Machine learning. First we extract the features from EMG data and then select the most important features. For imbalanced training dataset using data augmentation techniques we create a balanced dataset and also create a testing dataset. Using cross validation, we apply machine learning algorithm which provided desired output.

Proposed Method: Taking the idea from Muthuramalingam et al [16] where authors design NN based SVM which provided good results in resource utilization we proposed a linear support vector machine based bi-layered neural network. First, we trained SVM in MATLAB and calculated the weighted output. The weighted output of SVM is used as input of neural network which utilised optimum resource and provided reasonable accuracy in diagnosis.

Dataset Preparation: Lower limb muscles Vastus Lateralis [VL], Gastrocnemius Lateralis [GL], Tibialis Anterior [TA] are most affected during gait [17]. We took EMG data from the study of Watari et al [18]. We took 142 sample of non DSPN condition from 29 patients and 72 sample of severe DSPN condition from 14 patients and not considered the mild and moderate condition in our study. Output for normal patients was allotted as ‘0’ and for abnormal patients as ‘1’. Using SMOTE data augmentation technique [19]-[20] we equate the number of data for normal and abnormal patients. For the given three set of EMG data from GL, VL, and TA using Relief feature selection algorithm [21] we found 19 most significant features from each dataset as shown in figure 3, 4 and 5.

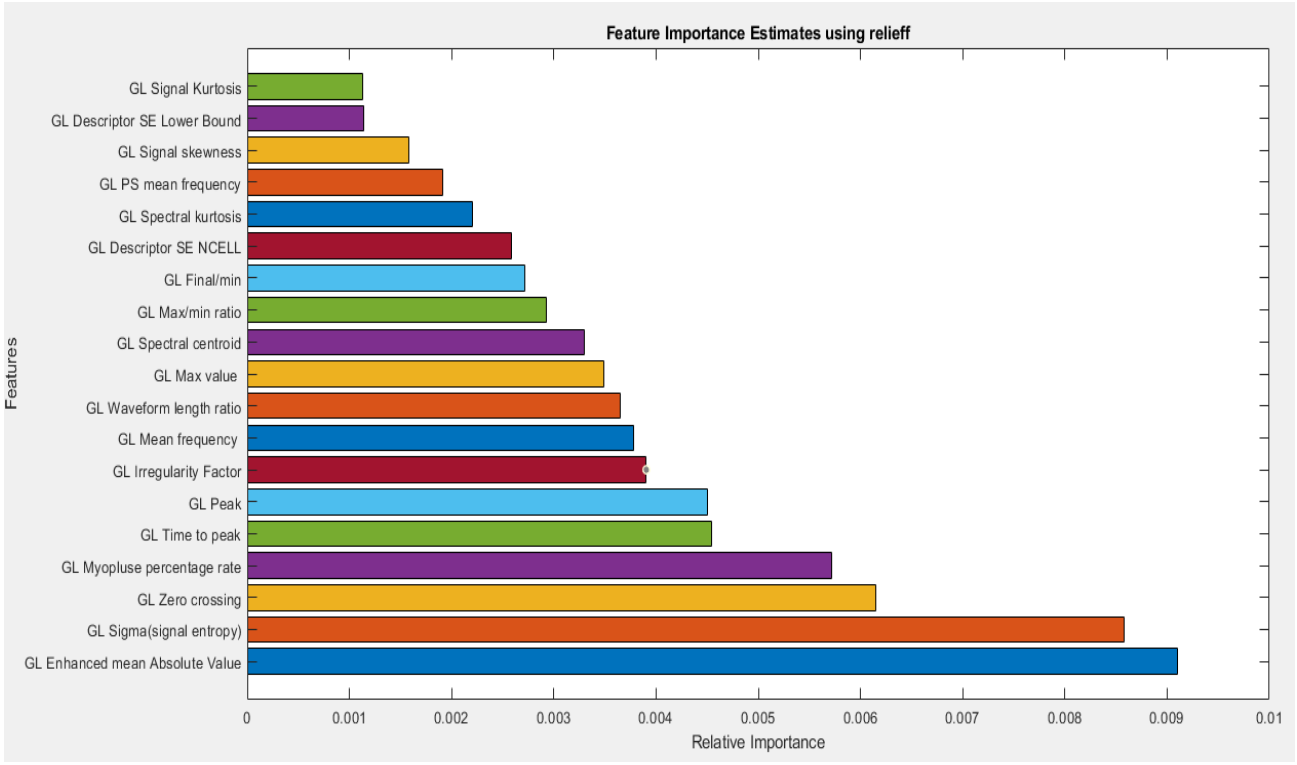

Figure 3. GL Extracted feature using Relief method

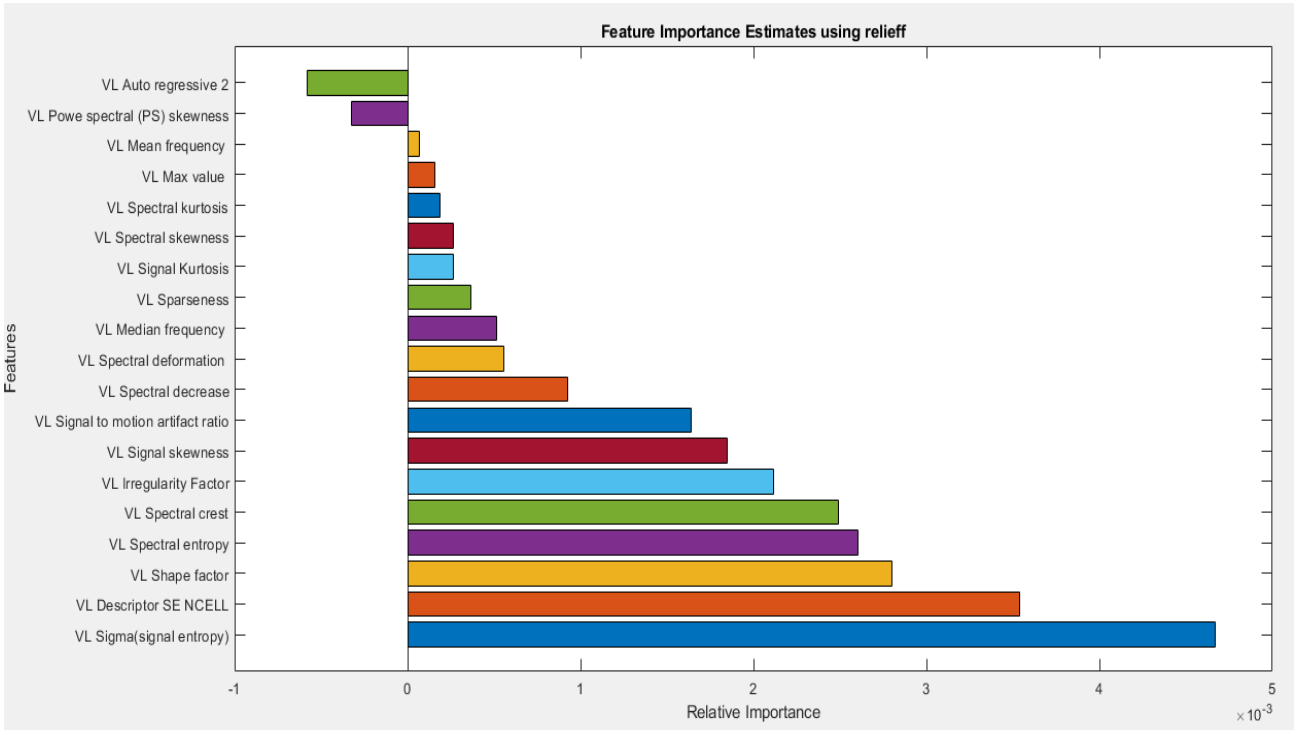

Figure 4. VL Extracted feature using Relief method

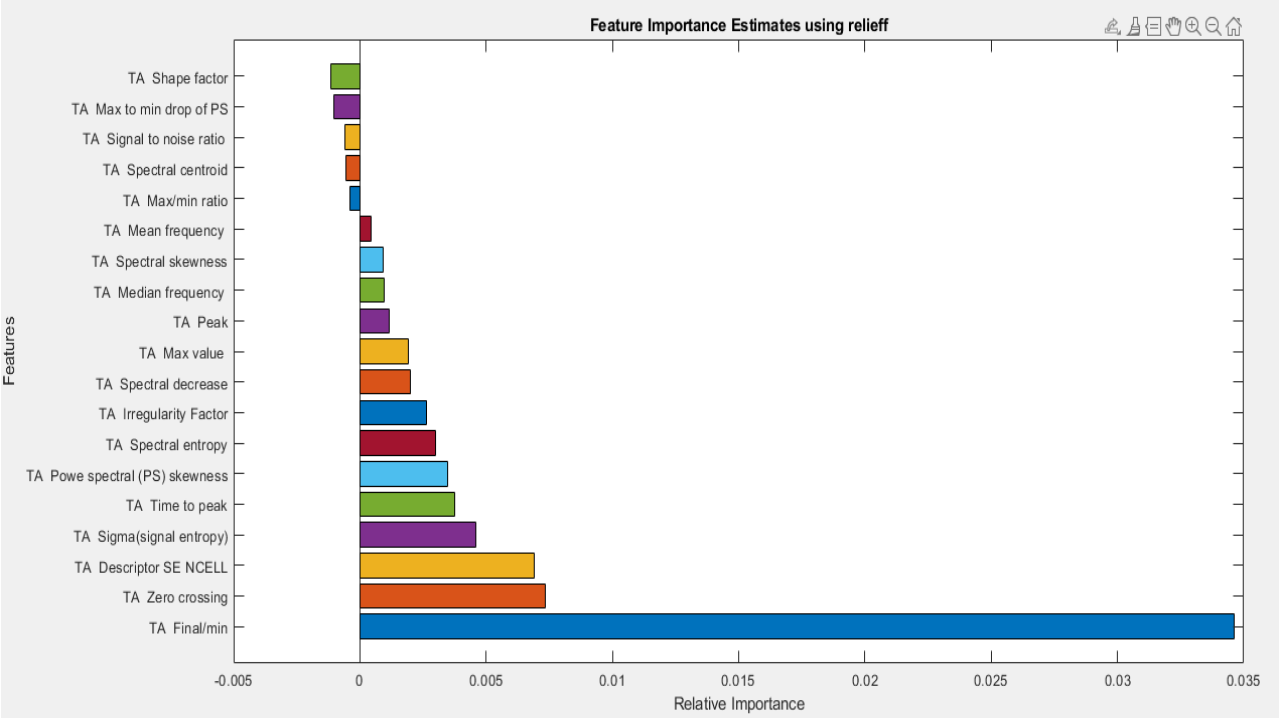

Figure 5. TA extracted feature using Relief method

First we trained support vector machine classifier at MATLAB taking total six features. Two most significant feature of GL data named as GL enhanced mean absolute value and GL sigma (signal entropy), two most significant features of VL data named as VL sigma (signal entropy) and VL Descriptor SE NCELL and two most significant feature of TA data named as TA Final/min and TA zero crossing are included in six feature data of SVM. Using six feature dataset we trained linear SVM at MATLAB which provided 74.8% accuracy. After that for trained SVM model we calculated weighted output for given dataset. Calculated weighted output is used as input of designed neural network.

Neural Network Design: Using the weighted output of SVM as input of neural network we designed a bi-layered neural network in MATLAB which provided 72.5 % accuracy. For the designed model in MATLAB using VHDL and Vivado design suite 2022.2 we created a neural network, synthesized and hardware implemented at Xilinx Zed Board which shown in figure 6 and designed device package is shown in figure 7.

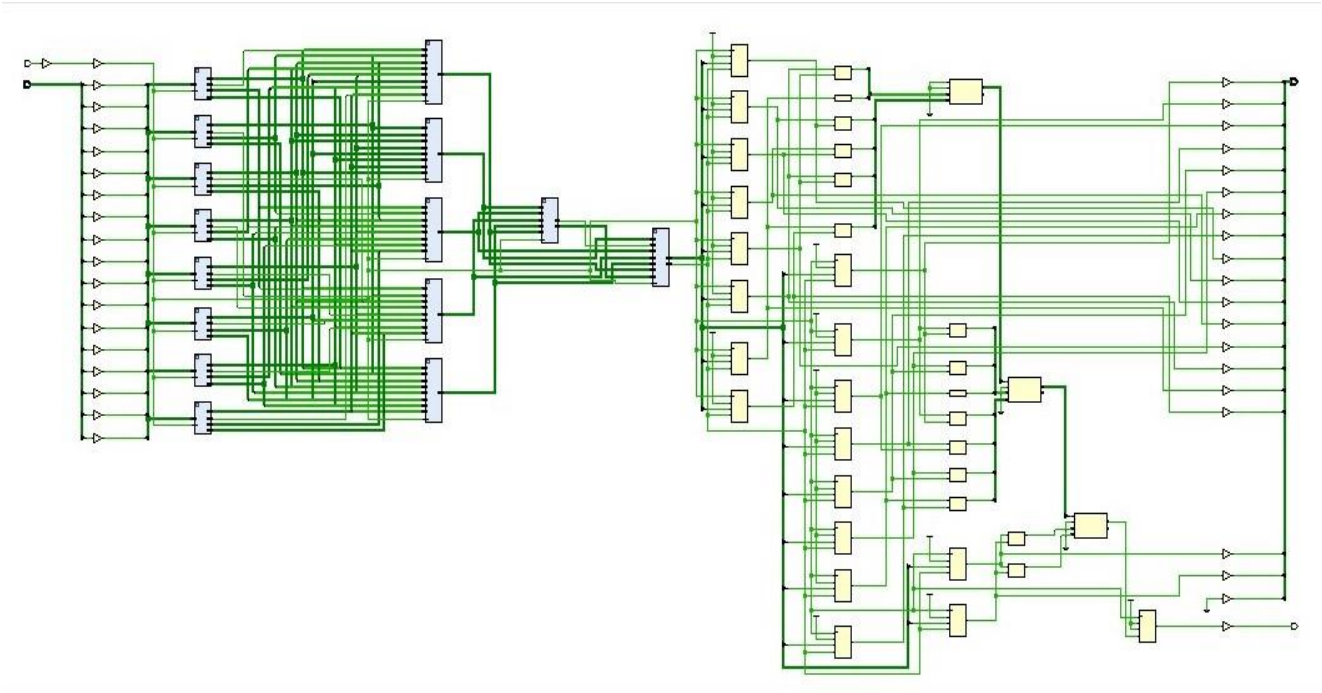

Figure 6 Neural Network Schematic design in Vivado

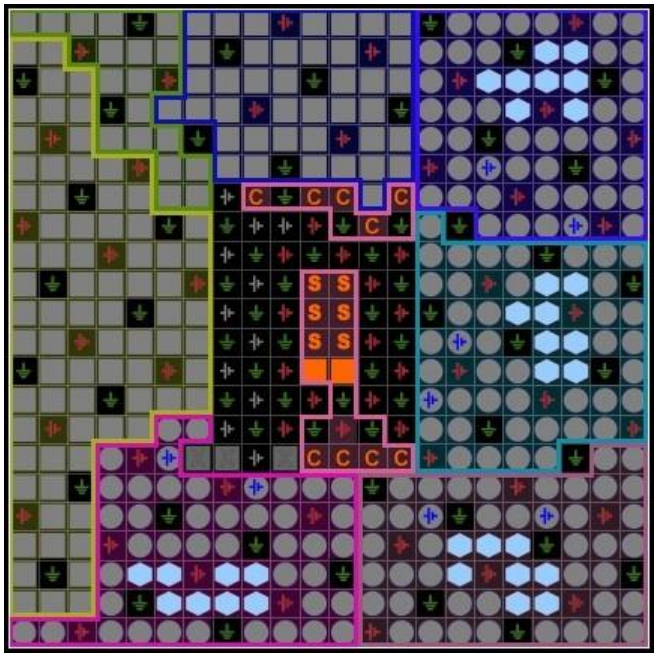

Figure 7. Device Package

Result and Discussion: Hardware implemented on Zed board provided 70.9 % accuracy with optimum resource utilization. All other performance parameters are also satisfactory. We only classified DSPN and non DSPN patients but there are a lot of class in DSPN severity such as mild, moderate, according to severity score. Although the accuracy is low but this work will

help to design a hardware with improved accuracy and minimum resource and power utilization. Also after upgradation in future it will help in the diagnosis of severity level and we continuously work on the performance improvement and reduction of resource utilization and in near future it will be possible that a compact and efficient model is developed which will thoroughly help to diagnose DSPN severity without any expert person. A resource utilization report is shown in table 1 and percentage utilization of resources are shown in figure 8.

Table 1. Resource Utilization Summary

Name	Total	Utilization
Slice LUTS	**53200**	**1206**
Slice Register	**106400**	**99**
F7 Muxes	**26600**	**144**
BRAM Tiles	**140**	**128**
DSPs	**220**	**58**
Bonded IOB	**200**	**38**

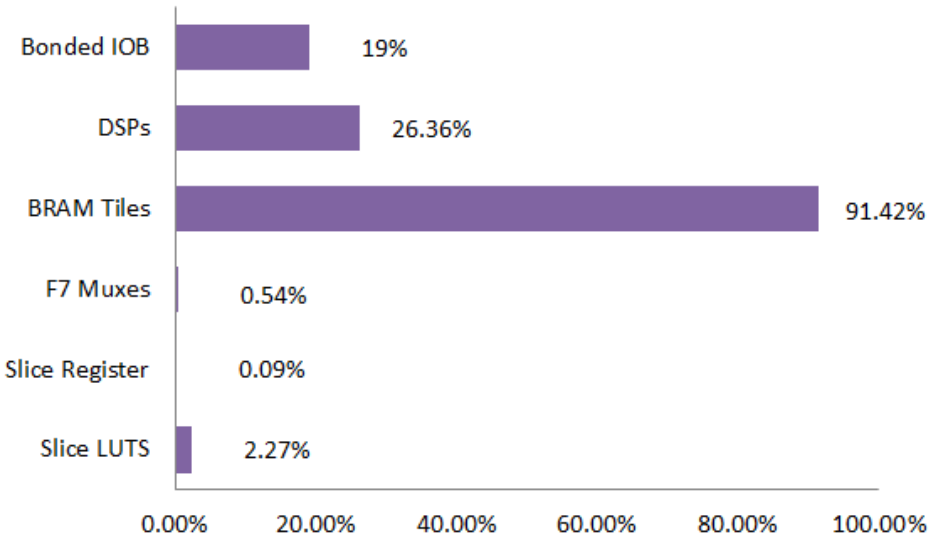

Figure 8. Resource Utilization Report

Conclusion and Future Work: Early diagnosis can help to prevent DSPN severity. For this purpose a machine learning based model is hardware implemented at Xilinx Zed Board which provided 70.9% accuracy in binary class classification. Resource utilization summary shows that utilization of BRAM tiles is more than 90%, except this all-other utilization is optimum. Also the accuracy is moderate, it should be more for accurate diagnosis. In our future work we aimed to improve performance of software model and hence implemented hardware so that it utilize the minimum resource and provide maximum accuracy so that it can help to diagnose DSPN patients from normal patients and also diagnose the severity level of the patients in near future.

References-

[1] Pop-Busui, Rodica, Andrew JM Boulton, Eva L. Feldman, Vera Bril, Roy Freeman, Rayaz A. Malik, Jay M. Sosenko, and Dan Ziegler. "Diabetic neuropathy: a position statement by the American Diabetes Association." Diabetes care 40, no. 1 (2017): 136.

[2] Haque, Fahmida, Mamun BI Reaz, Muhammad EH Chowdhury, Fazida H. Hashim, Norhana Arsad, and Sawal HM Ali. "Diabetic sensorimotor polyneuropathy severity classification using adaptive neuro fuzzy inference system." IEEE Access 9 (2021): 7618-7631.

[3] Haque, Fahmida, Mamun Bin Ibne Reaz, Muhammad Enamul Hoque Chowdhury, Geetika Srivastava, Sawal Hamid Md Ali, Ahmad Ashrif A. Bakar, and Mohammad Arif Sobhan Bhuiyan. "Performance analysis of conventional machine learning algorithms for diabetic sensorimotor polyneuropathy severity classification." Diagnostics 11, no. 5 (2021): 801.

[4] Dyck, Peter J., James W. Albers, Henning Andersen, Joseph C. Arezzo, Geert-Jan Biessels, Vera Bril, Eva L. Feldman et al. "Diabetic polyneuropathies: update on research definition, diagnostic criteria and estimation of severity." Diabetes/metabolism research and reviews 27, no. 7 (2011): 620-628.

[5] Haque, Fahmida, Mamun Bin Ibne Reaz, Muhammad Enamul Hoque Chowdhury, Serkan Kiranyaz, Mohamed Abdelmoniem, Emadeddin Hussein, Mohammed Shaat et al. "Evaluating Performance of Machine Learning Models for Diabetic Sensorimotor Polyneuropathy Severity Classification using Biomechanical Signals during Gait." arXiv preprint arXiv:2205.10581 (2022).

[6] Boulton, Andrew JM, Peter Kempler, Alexander Ametov, and Dan Ziegler. "Whither pathogenetic treatments for diabetic polyneuropathy?." Diabetes/Metabolism Research and Reviews 29, no. 5 (2013): 327-333.

[7] Vas, Prashanth RJ, and Michael E. Edmonds. "Early recognition of diabetic peripheral neuropathy and the need for one-stop microvascular assessment." The lancet Diabetes & endocrinology 4, no. 9 (2016): 723-725.

[8] Karlik, Bekir. "Machine learning algorithms for characterization of EMG signals." International Journal of Information and Electronics Engineering 4, no. 3 (2014): 189.

[9] Almurdhi, Monirah M., Neil D. Reeves, Frank L. Bowling, Andrew JM Boulton, Maria Jeziorska, and Rayaz A. Malik. "Reduced lower-limb muscle strength and volume in patients with type 2 diabetes in relation to neuropathy, intramuscular fat, and vitamin D levels." Diabetes care 39, no. 3 (2016): 441-447.

[10] Reaz, Mamun Bin Ibne, M. Sazzad Hussain, and Faisal Mohd-Yasin. "Techniques of EMG signal analysis: detection, processing, classification and applications." Biological procedures online 8 (2006): 11-35.

[11] Phinyomark, Angkoon, Evan Campbell, and Erik Scheme. "Surface electromyography (EMG) signal processing, classification, and practical considerations." Biomedical Signal Processing: Advances in Theory, Algorithms and Applications (2020): 3-29.

[12] Merletti, Roberto, and Loredana R. Lo Conte. "Surface EMG signal processing during isometric contractions." Journal of Electromyography and Kinesiology 7, no. 4 (1997): 241-250.

[13] Zgallai, Walid A., ed. Biomedical signal processing and artificial intelligence in healthcare. Academic Press, 2020.

[14] Subasi, Abdulhamit. Practical guide for biomedical signals analysis using machine learning techniques: A MATLAB based approach. Academic Press, 2019.

[15] Di Nardo, Francesco, Christian Morbidoni, Alessandro Cucchiarelli, and Sandro Fioretti. "Influence of EMG-signal processing and experimental set-up on prediction of gait events by neural network." Biomedical Signal Processing and Control 63 (2021): 102232.

[16] Muthuramalingam, A., S. Himavathi, and E. Srinivasan. "Neural network implementation using FPGA: issues and application." International Journal of Electrical and Computer Engineering 2, no. 12 (2008): 2802-2808.

[17] Sacco, Isabel CN, Paula MH Akashi, and Ewald M. Hennig. "A comparison of lower limb EMG and ground reaction forces between barefoot and shod gait in participants with

diabetic neuropathic and healthy controls." BMC musculoskeletal disorders 11, no. 1 (2010): 1-9.

[18] Watari, Ricky, Cristina D. Sartor, Andreja P. Picon, Marco K. Butugan, Cesar F. Amorim, Neli RS Ortega, and Isabel CN Sacco. "Effect of diabetic neuropathy severity classified by a fuzzy model in muscle dynamics during gait." Journal of neuroengineering and rehabilitation 11, no. 1 (2014): 1-9.

[19] Chawla, Nitesh V., Kevin W. Bowyer, Lawrence O. Hall, and W. Philip Kegelmeyer. "SMOTE: synthetic minority over-sampling technique." Journal of artificial intelligence research 16 (2002): 321-357.

[20] Elreedy, Dina, and Amir F. Atiya. "A comprehensive analysis of synthetic minority oversampling technique (SMOTE) for handling class imbalance." Information Sciences 505 (2019): 32-64.

[21] Urbanowicz, Ryan J., Melissa Meeker, William La Cava, Randal S. Olson, and Jason H. Moore. "Relief-based feature selection: Introduction and review." Journal of biomedical informatics 85 (2018): 189-203.

Design of single stage CMOS Op-amp and two stage CMOS Op- amp with .9 volt of supply voltage and 10 micro amperes of current in 90 nm technology

Vaibhav, Raj Kumar Tiwari
Department of Physics and Electronics
Dr Ram Manohar Lohia Awadh University, Ayodhya

ABSTRACT

This article outlines a clear process for creating single-stage and 2 stage CMOS operational amplifiers. The single stage op-amp which has been designed exhibits a gain of 27.453 dB with GBW of 3.84 M Hz and two stage op-amp which has been designed, exhibits a gain of 45.3970 dB with GBW of 482.579 k Hz. Design and simulation results have been carried out in 90nm Cadence virtuoso tool with supply voltage of .9 V and 10 micro amperes of current.

KEYWORDS: Analog Circuit, Low Power Supply, Lower size, High Frequency, 1stage CMOS Operational amplifier, 2 stage CMOS Operational amplifier, GBW.

INTRODUCTION

The technology sector has seen tremendous growth over the past few years. In analog processing devices, operational amplifiers are essential components. A lot of analog and mixed signal devices depend on operational amplifiers. The construction of analog circuits, such as operational amplifiers (op-amps) in CMOS technology, becomes more crucial as the demand for mixed mode integrated circuits rises.

Operational amplifiers (op-amps) with a reasonable open loop gain band width product (GBW), high output swings, and moderate DC gains are typically applied with two-stage structures . The design methodology presented in this article aims to simplify yet accurately simulate the design of high-gain CMOS op-amps. CMOS technology is currently advancing with smaller feature areas. CMOS technology has an advantage over NMOS technology due to its flexibility in design and comparatively simple circuit configurations. Operational amplifiers, also known as OPAMPs, are crucial components of analogue processing devices. An analogue circuit's primary barrier can be attributed to the OPAMP. In an ideal world, they serve as an unlimited voltage gain voltage controlled current source. Numerous analogue and mixed-signal devices must have operational amplifiers. OPAMPs with vastly different levels of complexity are used to comprehend functions ranging from dc bias generation to high-speed amplification or filtering. The design of OPAMPs

continues to pose a challenge as the supply voltage and transistor channel lengths scale down with each generation of CMOS technologies [1].

DESIGN OF SINGLE STAGE OP-AMP

CMOS operational amplifier formed by transistor N_1 and N_2, and loaded by current mirror circuit formed by transistor P_1 and P_2. The drain current of transistor N_1 i.e. I/2 is fed to the input of the mirror transistor P1 thus replica of this current ids provided by the output transistor of mirror P4. At the output node the two current balance out each other leaving a zero current to flow out of the next stage. If transistor P2 is perfectly matched to the transistor P1, its drain voltage is track the voltage at the drain of P1 [2]

Design parameter and Result of single stage CMOS Op-amp

NMOS N1 and N2

L=300nm, W= 6u

PMOS P1 and P2

L=300nm, W=390nm

Vdd = 900 mv

Id= 10 uA

Gain in dB= 27.453

GBW of 3.84 M Hz

Input voltage= 1mv

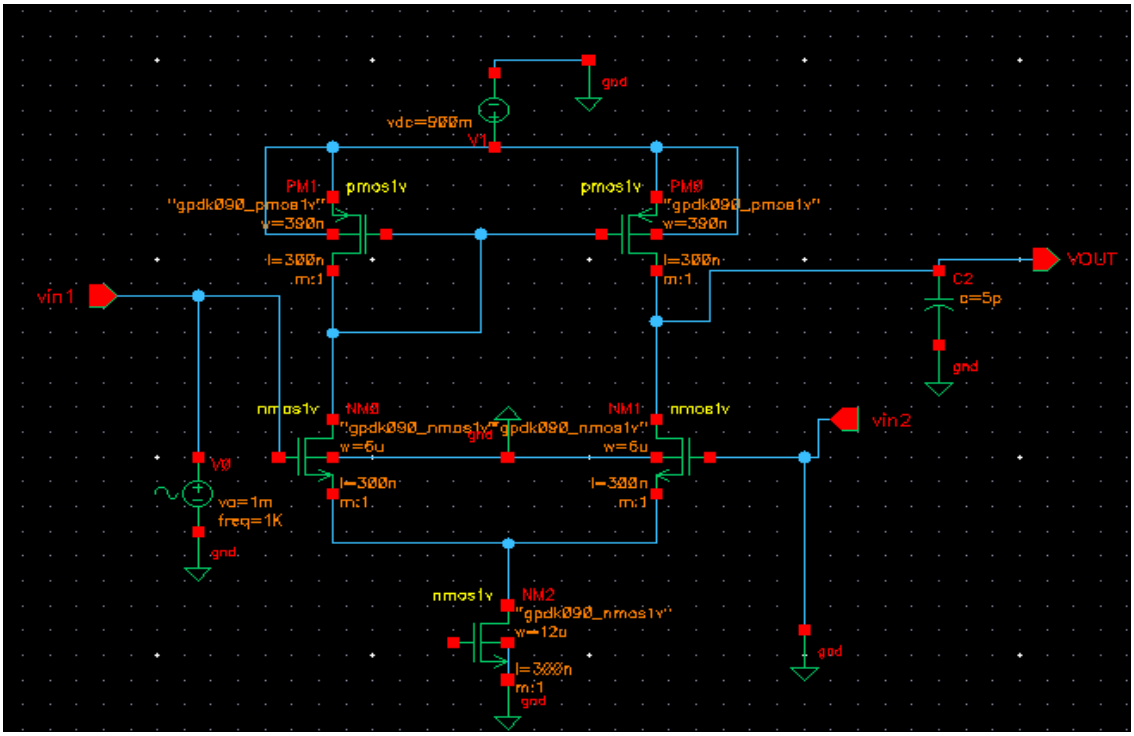

Single stage Op-amp

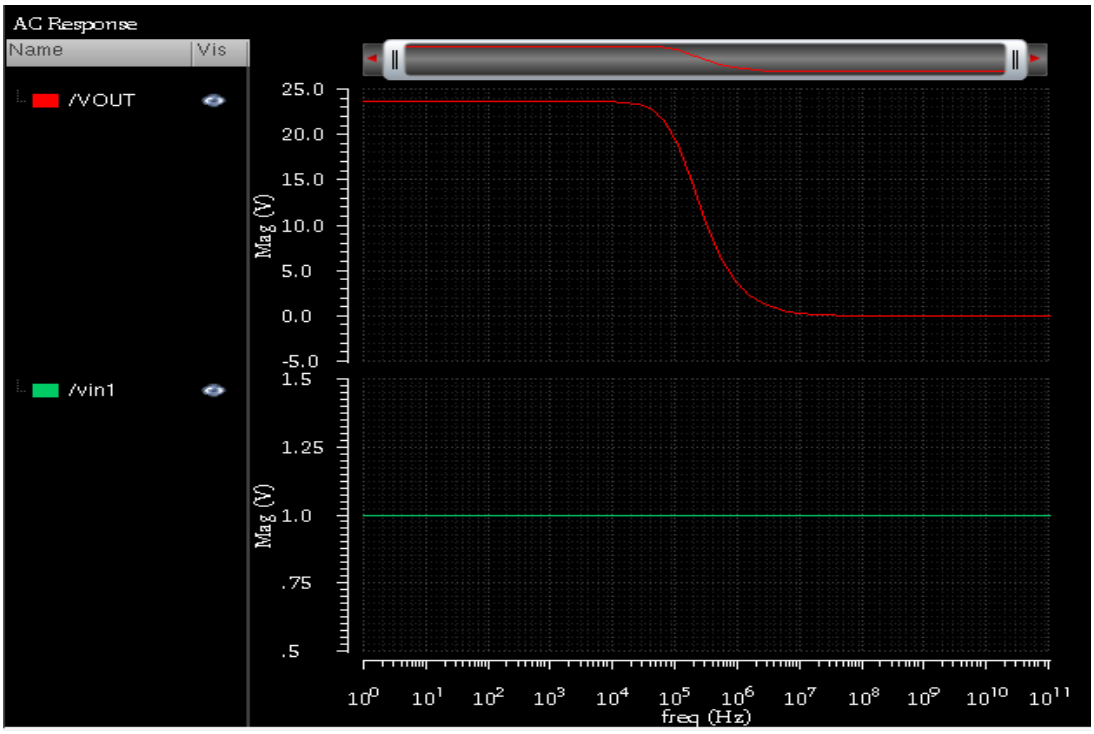

(a) Gain in Magnitude

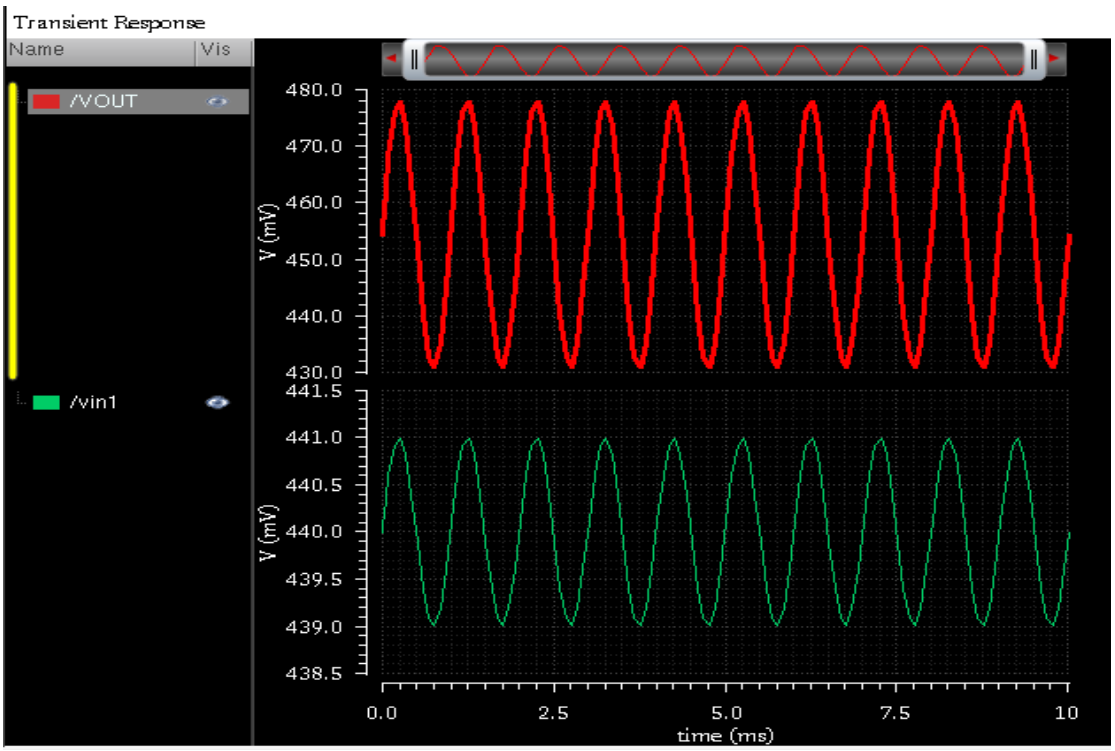

(b) Transient Analysis

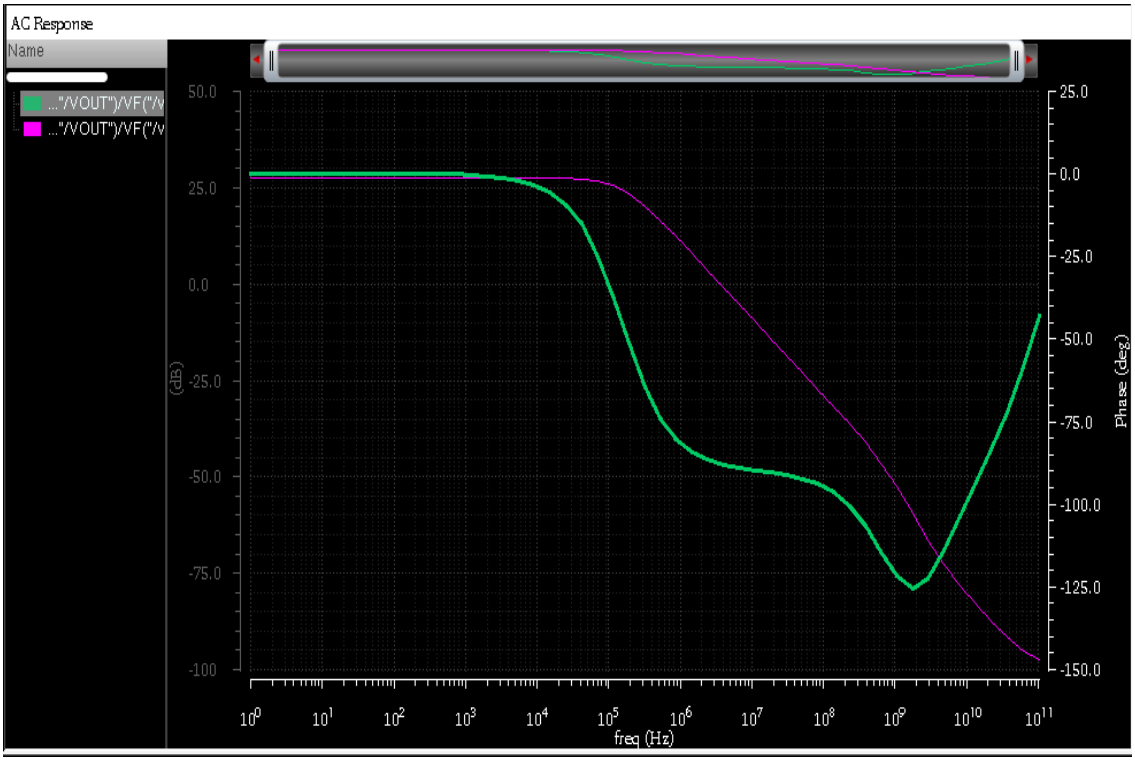

(c) Gain and Phase margin in dB

DESIGN OF TWO STAGE OP-AMP

The ubiquitous MOS Op-Amp is an essential component of many analogue and mixed-signal circuitry and systems. Operational amplifiers are amplifiers with a high enough forward gain to effectively insulate the closed loop transfer function from the op-amp's gain when negative feedback is applied. Numerous practical analogue circuits and systems have been created using this concept. An op-amp must have an open loop gain big enough to implement the negative feedback concept as its main requirement. The circuit comprises of a common-source second stage followed by an input differential transconductance stage that forms the op-amp's input. For a given voltage input, the output signal swing is maximized by the common source second stage while the DC gain is increased by an order of magnitude. This is crucial for lowering power usage [3].

If the Op-Amp is required to drive a low resistance load, the second stage must be followed by a buffer stage whose objective is to reduce the output resistance and maintain a high signal amplitude [4]. To determine each transistor's operating point during its quiescent state, a bias circuit is available. To obtain stable closed loop performance, compensation is necessary.

However, a right-half-plane (RHP) zero is also produced and the phase margin is weakened as a result of an unintentional feed forward route through the Miller capacitor. [5].

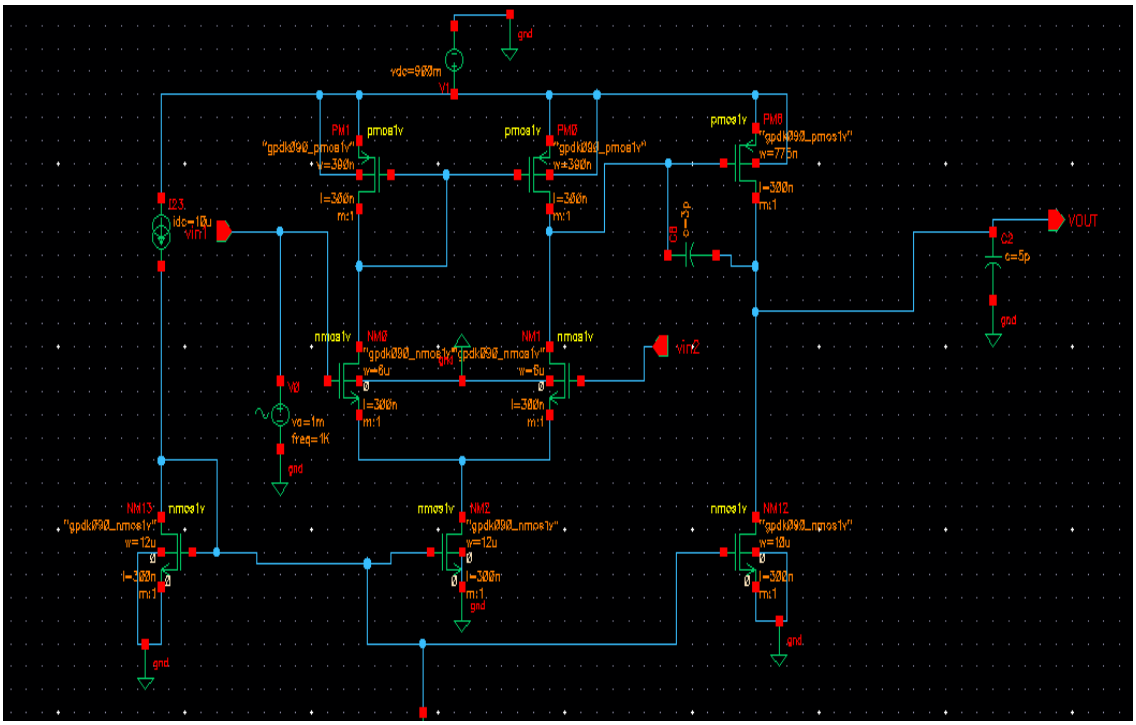

Two stage Op-amp

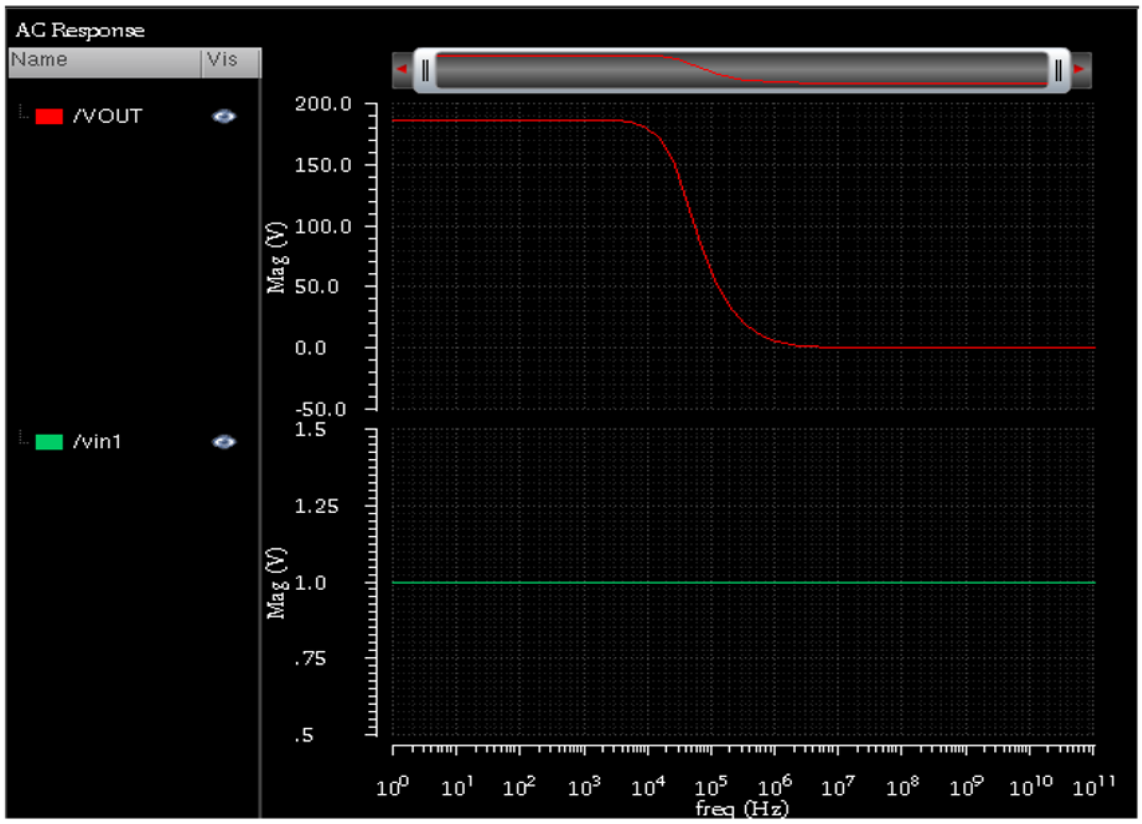

(a) Gain in Magnitude

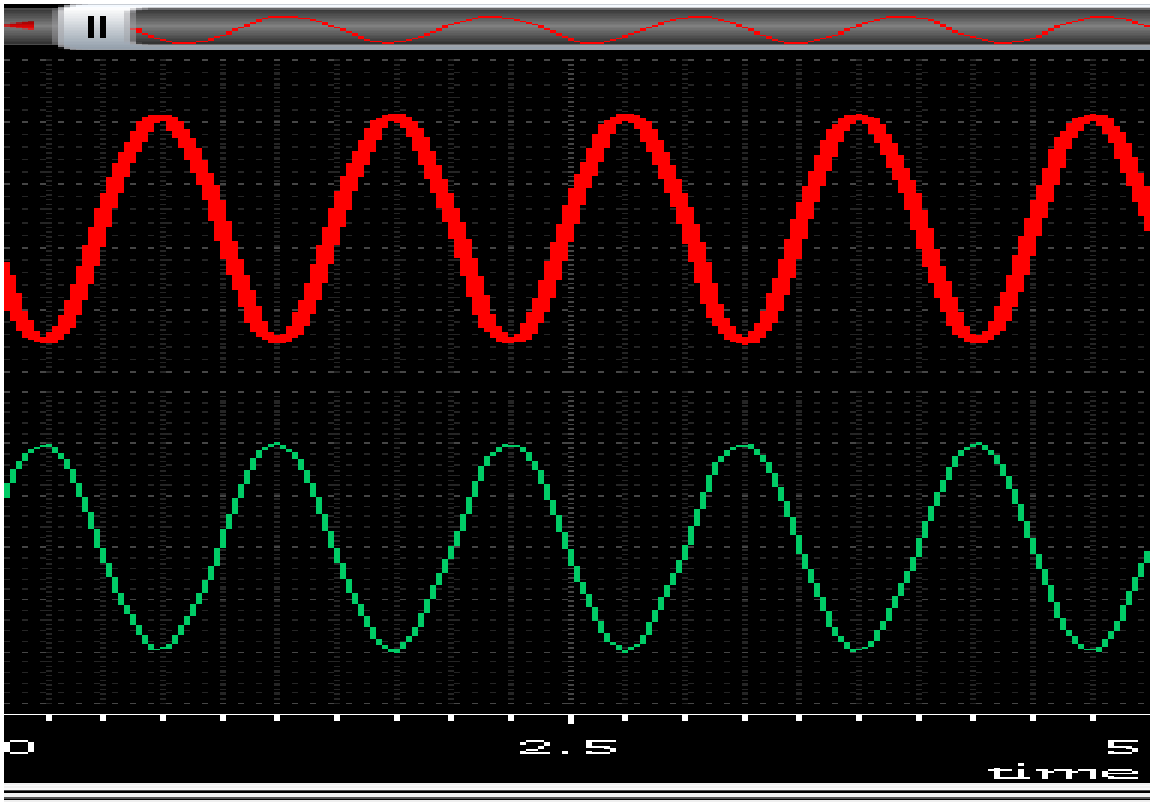

(b) Transient Analysis

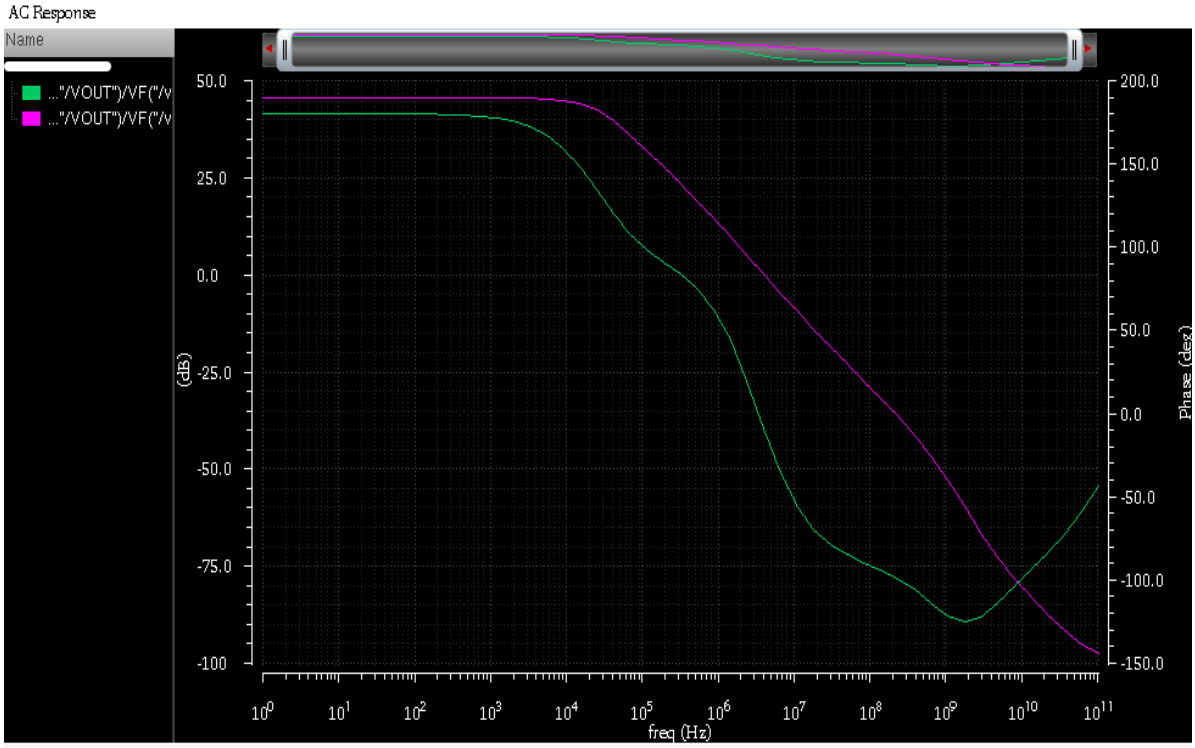

(c) Gain and Phase margin in dB

Design parameter and Result of Two stage CMOS Op-amp

NMOS N_1 and N_2, L=300nm, W= 6u, NMOS N_3, L=300nm, W= 10u

PMOS P_1 and P_2, L=300nm, W=390nm, PMOS P_3

L=300Nm, W=775nm, Vdd = 900 mv

Id= 10 uA, Gain in dB= 45.3970dB

GBW = 482.579 k Hz , Input voltage= 1mv

CONCLUSION

Here single stage and 2 stage CMOS op-amp and analyzed its behavior. The proposed design process can be used to create op-amps that satisfy all necessary requirements, according to simulation findings. Design techniques for this op-amp were also given. Simulations confirm that the there is remarkable increase in gain as move form first stage Op-amp27.453 dB to two stages Op-amp i.e. 45.3970dB.

REFRENCES-

1. B. Razavi, Design of Analog CMOS Integrated Circuits. McGraw-Hill, 2002
2. Microelectronic circuits sedra-smith
3. Fiez Terri S., Yang Howard C., Yang John J., Yu Choung, Allstot David J., " A Family of High-Swing CMOS Operational Amplifiers", IEEE J. Solid-State Circuits, Vol. 26, NO. 6, Dec. 1989.
4. R. Castello, "CMOS buffer amplifier," in Analog Circuit Design, J.Huijsing, R. van der Plassche, and W. Sansen, Eds. Boston, MA: Kluwer Academic, 1993, pp. 113–138.
5. Jhon and Ken Martin "Analog Integrated Circuit Design", Wiley India Pvt. Ltd, 1997
6. Priyanka Kakoty, "Design of a high frequency low voltage CMOS Operational amplifier", International Journal of VLSI design & communication System (VLSICS), Vol.2, No.1, pp. 73-85, March 2011
7. P. Allen and D. Holmberg "CMOS Analog Circuit Design", 2nd Edition. Saunders college publishing/HRW, Philadelphia, PA, 1998.

Simulation and designing of Voltage Controlled Oscillator: A Review

Nikhat Akhtar[1], Raj Kumar Tiwari[2], Gaya Prasad[3]

[1]Prof. Department of Physics and Electronics Dr. Rammanohar Lohia Avadh University, Ayodhya, U.P. 224001, India.

Abstract- "CMOS" refers to digital circuit design, and the processes used to implement that design on integrated circuits. CMOS circuits in VLSI consume less power when static. This paper presents a brief study of various types voltage-controlled oscillator and their function like a complementary metal–oxide–semiconductor (CMOS) ring oscillators and LC-VCO.

The high performance VCO on 45 nm technology to achieve the desired objectives such as both non-linear and linear operations. The circuits used is a modified design of VCO.

The study of an improved design of four-stage CMOS differential ring voltage-controlled oscillator (VCO) with high-output frequency, low phase noise, and low power consumption is proposed in this paper. A new differential delay cell has been used for differential ring VCO which utilizing dual-delay-path topology to attain both high-output frequency and low phase noise.

Keywords: Voltage control oscillator, ring oscillator, low power consumption, cmos-technology, phase noise, oscillation frequency etc.

Introduction: Electronic oscillators belong to the very first electric circuits at the beginning of the twentieth century a complete systematic design concept for this class of electronic circuits is not available until now. One of the reasons is that the behavior of these dynamical circuits depends in an intrinsic manner on the nonlinearities of within the circuit and therefore we are confronted with nonlinear differential equations. The oscillatory circuit behavior is related from a mathematical point of view to the so-called limit cycles. However electronic oscillators are fascinating circuits in many senses because the progress in manufacturing technologies of electronic devices and circuits led to new challenges in oscillator modeling and new mathematical concepts for solving the descriptive equations of oscillators. In certain cases, the behavior of an electronic oscillator should be influenced by the behavior of other electronic systems in a desired manner such that entrainment and synchronization effects arise. Therefore, driven nonlinear oscillators and their descriptive equations have to be considered where even chaotic behavior can appear. From a physical point of view electronic oscillators can be interpreted as such systems where dissipative structures occur. Ilya Prigogine coined this phrase as a name for the patterns which self-organize in far-from-equilibrium dissipative systems and limit cycles are a special case of them; see Nicolis,

Prigogine [1]. Such dissipative systems are nonlinear and have to be connected with a DC power supply for delivering energy into the system. Furthermore, these systems interact with a heat bath where energy is dissipated.

Accordingly, the fluctuations of the heat bath influence electronic oscillators belong to the very first electric circuits at the beginning of the twentieth century a complete systematic design concept for this class of electronic circuits is not available until now. One of the reasons is that the behavior of these dynamical circuits depends in an intrinsic manner on the nonlinearities of within the circuit and therefore we are confronted with nonlinear differential equations. The oscillatory circuit behavior is related from a mathematical point of view to the so-called limit cycles. However electronic oscillators are fascinating circuits in many senses because the progress in manufacturing technologies of electronic devices and circuits led to new challenges in oscillator modeling and new mathematical concepts for solving the descriptive the oscillator as electronic noise. As a result, electronic oscillators have to be modeled by driven nonlinear stochastic differential equations with limit cycle type solutions. In most cases analytical solutions for this type of equations are not available and approximation concepts have to be developed. From this point of view electronic oscillator circuits are until now a source of inspiration for new mathematical and physical concept; see e.g. Guckenheimer [2]. Fig. (1). Dissipative structure.

However, for the oscillator circuit design not only approximative solutions of certain descriptive equations are needed since at the first stages of a design process only very few circuit parameters are known. Note that a circuit design concept consists of two steps where it is starting from the specifications of a circuit under design. These specifications are closely related to the solutions of the descriptive equations of the designed circuit. In a first design step the circuit architecture - circuit shape (O'Dell [3]) - has to be chosen whereas in the second step the free parameters of this circuit shape have to be determined. Therefore, if not all circuit parameters are available, it is even not possible to know whether the descriptive equations possess oscillatory or limit cycle solutions.

For this reason, Mandelstam and Papalexi [4] developed in 1931 the concept of parametrized descriptive equations for oscillator circuits based on ideas of the French mathematician Henry Poincare. This concept was also the basis for the bifurcation theory of electronic oscillators; today it is called Andronov-Hopf theorem in the theory of dynamical systems. In contrast to the quantitative analysis of nonlinear differential equations this theorem studies these equations from a qualitative point of view. By means of the qualitative analysis we are able

to consider the qualitative change of different types of solutions of nonlinear differential equations in dependence on certain circuit parameters. In the case of the Andronov-Hopf theorem the change from an equilibrium point to a limit cycle is explained. Although this theorem is known in electronic oscillator analysis since 1935 [5] (see Maggio et al. [6] for a more recent publication) it was never used for a systematic design process of electronic oscillators until recently; see Mathis & Russer [7], Prochaska et al. [8]. As mentioned above the circuit description with parametrized equations is well suited for the second step of the design process and therefore the Andronov-Hopf theorem should be used in design processes for electronic oscillator circuits; a first concept idea was presented by Mathis [9].

Literature Review

A- Early Oscillator Circuits-

Since in 1895 Marconi showed for the first time that the laboratory arrangement of Hertz can be used for the wireless transmission of information along larger distances more powerful electrical arrangements were desired. Around 1900 several researchers (e.g. Thompson, Tesla, Slaby, Braun, von Arco and others) suggested improved versions of Marconi's arrangement. Probably it was a milestone as Duddel published his paper “On rapid variations in the current through the direct-current arc” [10] where he used results of the German physicist Simon [11]. A few years later Poulsen improved Duddel's oscillatory generator substantially from a technical point of view and as a result he presented in 1906 a new powerful arrangement with an arc as electronic device for wireless transmission of telephony signals. For further studies we refer to Blake [12] and Nesper [13]. Although the physical processes in arcs are rather difficult to understand at this time because of their electronic nature reasonable nonlinear models were developed by Kaufman, Duddel, Simon, Wagner and others. In the dissertation thesis of Wagner many aspects of such circuits were discussed [14]. Using these results Zenneck [15], a former co-worker of the above-mentioned Braun, published in 1914 an interesting paper where he studied the start-up behavior of such RLC circuit including a nonlinear arc device. In contrast to his predecessors, he described the behavior of the circuit by means of a nonlinear differential equation that described the energy (or power) balance. After solving this equation, he got the approximative solution that is similar to the approximative of the van der Pol equation which was discovered several years later by van der Pol in the analysis of triode oscillators. From a mathematical point of view Zenneck's balance equation corresponds to an approximative first integral of the van der Pol equation. Zenneck's paper was also the first that studied the start-up behavior of oscillatory circuits in

more details. Further details are considered in another publication [16]. Circuits including sparks or arcs were the first successful generators for oscillatory currents. These electronic circuits had several disadvantages. Although engineers and physicists in the leading industrial companies (e.g. Marconi Comp., Telefunken, AT&T, Western Electric Comp.) tried to improve these circuits by using interesting ingenious ideas the robustness of these arrangements as well as their transmitting power were rather restricted. Therefore, a new generation of generators applied and now nonelectronic principle to get high-power oscillatory currents. For this purpose, the static frequency doubling effect which was studied by Epstein, Joly and Vallauri was used for the development of rotating alternators (see Kühn [17], Meißner [18]). These generators had much better properties than the spark or arc circuits. Only the frequency of oscillatory waves generated by these electrical machines was restricted. However, at this time transmitting stations worked with long waves. Around 1925 the situation was changed as the Heaviside layer was observed by nonprofessional users using transmitting stations with short waves. Within this range of frequencies rotating alternators cannot be applied. Moreover, short waves did not need high-power transmitting stations such that the power can be reduced for these frequencies. As a conclusion electronic vacuum tubes were used to build generators with oscillatory behavior for powerful transmitting stations.

B-Tubes and Oscillators

First ideas for a new electronic device were published by Fleming in 1904. For the invention of his thermionic diode (or Fleming detector) he used research results in the area of emission and transport of electrons (Edison effect, Richardson, Wehnelt; see Johannsen [19]) in vacuum although the physical details were not well-known at this time. A modulation of the current in Fleming's thermionic diode was achieved by adding a grid. This was done by de Forest in 1906. This electronic device was called by de Forest as Audion [20]. In the same year v. Lieben presented a patent of triode type of amplifier valve [21] that was improved by him in a patent from 1910 together with Reisz and Strauß [22]. The audion as well as the “Lieben-valve were three-pole devices with cathode, grid and anode. In contrast to de Forest's audion the “Lieben-valve was filled with mercury. Therefore, Lieben's valve was called “gas relay” and de Forest's “electron relay” (audion). This difference remained unclear in the following years and led to many discussions; see e.g. Armstrong [23] (p. 220) and Meißner [24] (p. 65).

Further references can be found in a paper of Tucker [25]; see also Johannsen [19]. After the discovery of these triode valves, it lasted further six years until first practical circuits were available. The first two classes of circuits were amplifiers and oscillators. Several groups in

Germany, USA, United Kingdom, and Austria were participated in these activities and there were many relationships between these groups. Therefore, it is difficult to solve the problem of priority with respect to the different electronic circuits; see e.g. Tucker [25], Johannsen [19], Barkhausen [26] (part II, pp.112), Meißner [24], and Skowronnek [27]. In 1913 Meißner presented a first high frequency transmitter including an electronic oscillator with a von Lieben tube (Fig. 2). It should be remarked that the principles of thermionic conduction were studied based on physical foundations by Langumir.

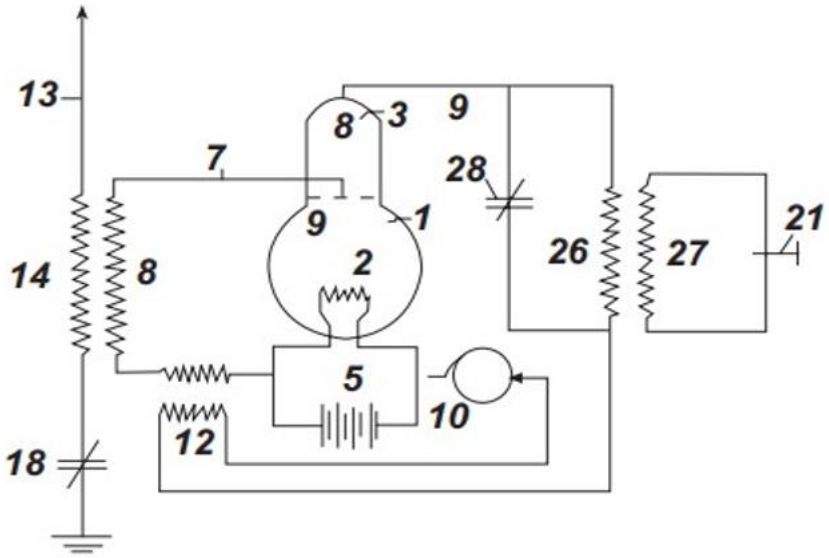

Fig. 1 Meißner Oscillator with a V. Lieben Tube.

A first example of an electronic oscillators with a valve which is the main subject of our paper was invented between 1912 and 1913 where the difference between De Forest's audion and the Lieben-Reisz valve is not considered (but see remarks of Meißner [24] (p. 65) and Hazeltine [30] (p. 98)). In agreement with Hazeltine [30] it seems that Meißner and Armstrong had similar ideas at the same time with respect to an oscillating circuit including a valve. The corresponding comments of Tucker [25] are a little bit obscure. Since the problem of the design of electronic circuits and especially oscillators with valves in order to transmit electromagnetic waves and receive them was a main subject in all military laboratories in all industrial states which are involved in the first world war many information became a secret. At the end of this war several electrical engineers and physicists published their results with a delay of one or more years (see corresponding remarks in the papers of Hazeltine [30], Barkhausen [26], Meißner [24] and others did not have an opportunity to publish it, just like Colpitts or Hartley). Hazeltine [30] (p. 98) gave some more references to interesting

collections of oscillating circuits. Obviously at the end of the first world war many different oscillator circuits were known and several authors began to publish their theoretical results about this interesting class of electronic circuits**.**

C. Descriptive Equations for Electronic Oscillators

Probably the first theoretical paper about electrical oscillators with a valve was published by Vallauri [31] which was published in German some montha sinusoidal oscillatory behavior already exists. By means of this approach Vallauri got "the exact determination of the conditions for oscillations in an audion circuit". After the publication of this paper many othe authors presented results that are more or less equivalent. These results were different in modifications of the valve model or the decomposition and its interpretation of the linearized oscillator circuit. We would like to mention only the comprehensive papers of Hazeltine [30], Heising [33] and Barkhausen [26]. The different approaches were compared by Albersheim [34].

Unfortunately, it was known already before 1920 that a linear theory cannot be complete for describing all aspects of electronic oscillators. Whereas the conditions of oscillatory behavior can be derived by a linear model a nonlinear model is essential to determine the amplitude of these oscillators. This statement was given by Möller [29] in a very similar manner (p. 331). Based on the idea of the feedback principle for the functionality of electronic oscillators this author developed a theory for these circuits that used again the idea of a power balance equation (just like Zenneck in 1914 for the case of oscillator circuits with an arc). For this purpose, Möller developed a concept that takes into consideration only the first harmonics of the oscillatory behavior and a nonlinear differential equation for the circuit was not derived. As a result, he got the method of the "oscillatory characteristic" (in German "Schwingkennlinie") that can be interpreted now as a variant of the harmonic balance or averaging method. Some remarks to the history of this methods can be found in the monograph of Sanders and Verhulst [35] (pp. 181).

Again, other authors presented similar approaches that correspond to the fundamental mathematical problem of nonlinear oscillatory systems or nonlinear differential equations. In contrast to Möller's approach van der Pol [36] derived in his doctorate thesis for the first time a nonlinear differential equation for an oscillatory electrical circuit and especially for an electronic oscillator circuit including a triode valve. Furthermore, he was able to apply a special perturbation method that resulted in a solvable nonlinear differential equation. It was a variant of an averaging method (Lagrange's secular perturbation method) that was known to van der

Pol from his studies in physics. In his famous paper from 1920 he states that the equation under consideration is closely related to some problems which arise in the analytical treatment of the perturbation of planets by other planets." The differential equation of van der Pol became an eminent impact to a new mathematical discipline "nonlinear oscillations" and at the end the mathematical theory of dynamical systems. On the other hand, we have to emphasize that although interesting from a theoretical point of view van der Pol's equation was not useful in practical situations at this time for two reasons: 1) Graphical differentiations of higher order arise. 2) Only in the simplest cases the perturbation method leads to a solvable differential equation. In other cases, only the steady amplitudes can be calculated.

Although Möller's method leads also to tedious calculations an semi-analytical approach was presented by Joos [37]. This author started with a good analytical approximation of the characteristic curves in form of an arctan-function and as a result he got another kind of oscillatory characteristics that did not include circuit parameters or valve constants. But also, this method did not become popular. Between 1920 and 1929 only very few scientific groups tried to develop new impacts to the theory of electrical oscillators. One of the few exceptions were van der Pol and Appleton. They published very interesting papers about the entrainment problem, forced oscillations and on relaxation problems as well as other aspects of nonlinear oscillators.

The main results of these authors are contained in van der Pol's review paper from 1934 [38]. A new era of oscillator theory began as the Russian school of Mandelstam and Papalexi entered this area. Although Papalexi had published a book about "The Theory of Oscillators with Electronic Valves" in 1922 and Mandelstam was already a well-known scientist who was involved also in aspects of wireless transmission of electromagnetic waves they considered electronic oscillators from a new point of view. In 1929 Andronov who had Mandelstam as his academic teacher published a brief paper [39] where he applied Poincare's theory of limit cycles to the van der Pol equation. Another paper together with Witt [40] followed in 1930. In a further paper [41] these two authors showed that Poincare's theory is useful for studying rather difficult aspects of the entrainment effect in nonlinear oscillations. By means of these results it could be shown that the theory of limit cycles of Poincare was a suitable framework to study problems in nonlinear oscillations. Another important step towards an unified theory of nonlinear oscillations was the introduction of parametrized nonlinear differential equations and again Poincare's ideas were used. Mandelstam and Papalexi showed [4] that first aspects of a theorem that is now called Andronov-Hopf theorem and describes a bifurcation of a limit cycle from a static equilibrium point. These ideas became a big impact in

Russia for the theory of nonlinear oscillations and several very active groups studied many aspects of this problem. The references of the famous book of Andronov, Witt and Chaikin [42] first published in 1937 illustrates this exciting area. In a review paper from 1935 Mandelstam, Papalexi, Andronov, Chaikin, and Witt [5] presented a complete concept of nonlinear oscillations that contains already almost all modern aspects of this theory; see also Mathis [43] and in particular the papers of Bissell [44], Aubin, Dalmedico [45] and Pechenkin [46]. It should be mentioned that at the same time Krylov and Bogoliubov [47] developed the mathematical foundations of a perturbation theory for oscillatory differential equations that is known now as averaging method or harmonic balance. It lasted more than 40 years until this subject was considered by Mees and Chua [48] in 1979. Afterwards Andronov-Hopf bifurcation became an essential subject in the theory of electrical circuits (e.g. Mathis [16]). It should be remarked that in higher dimensional systems (d > 2) additional methods are needed.

Example: Design of a 2.4 GHz LC-Tank VCO In this section we show the application of our proposed design concept to a practical oscillator design. The desired specifications are shown in Table 5 (a 0.25µm RF CMOS technology from IHP (SGB25V) is used). An inductor with a series inductance of Li,s = 11.1nH is chosen for the requested frequency range. Using our proposed model for the voltage dependent varactor capacitance [64] we are able to approximate the varactor dimensions. Fig. (1) shows an approximation of the frequency characteristic of the VCO in dependency of the varactor width Wv. Our calculations show, that as a first estimation a varactor width of Wn = 150µm is an appropriate choice for the requested frequency range (Table 1).

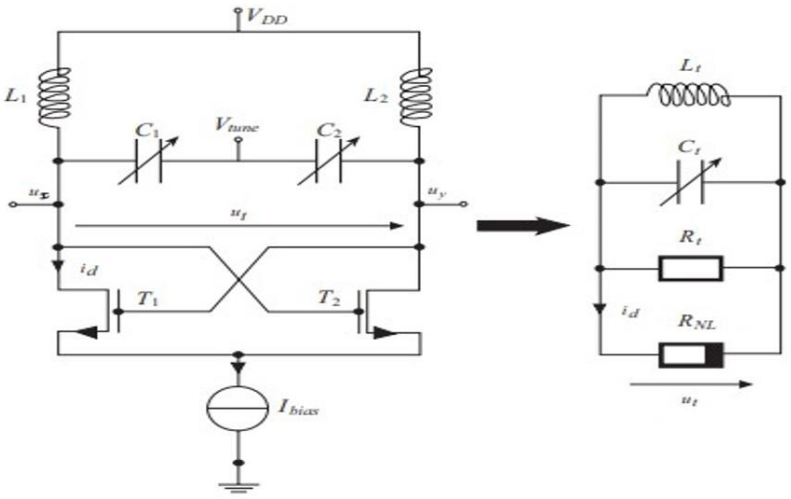

Fig. 2 SC tank voltage-controlled oscillator

Setting Lv to two times the minimum channel length is a good compromise between series resistance and Cv,max/Cv,min ratio [65]. In order to minimize the parasitic resistance, the length of the transistor pair Ln is set to the minimum channel length. We set the value of Ibias to the maximum value allowed by the specifications in order to maximize the output amplitude and optimize the phase noise characteristics of our VCO [66]. All design variables have been determined except the width Wn of the transistor pair. It is guaranteed that a variation of the width of the transistor pair Wn leads to a stable limit cycle as was shown in the previous section. Using expression (7) it is possible to calculate the needed width Wn. We find the bifurcation point and therefore the starting point of a stable oscillation at a parameter value of Wn = 2.03μm. Increasing Wn leads to an expansion of the limit cycle and accordingly to a rising of the oscillation amplitude (8) (Fig. 3).

Higher Dimensional State Space Representation-

A higher dimensional state space representation allows the inclusion of other parasitic effects and structural enhancements in comparison to the 2-dimensional state space modeling. Examples of possible parasitic effects could be the nonlinear effects of the cross-coupled transistor pair or substrate effects for instance. An example for a structural enhancement that could be included in the modeling using higher dimensional state space equations is a filtering capacitance parallel to the current source. In order to carry out the bifurcation analysis of a sinusoidal oscillator.

Param.	Spec.	Achieved
f_0	2.4 GHz	2.4 GHz
V_{DD}	2.5 V	2.5 V
I_{bias}	≤ 1 mA	1 mA
TR	≥ 20 %	34 %
v_t	≥ 1 V	≥ 1.37 V
C_{load}	≥ 100 fF	100 fF

Inductor		
Param.	Maple	Cadence
$L_{i,p}$	11.16 nH	-
$C_{i,p}$	16.6 fF	-
$R_{i,p}$	1824 Ω	-

Transistor Pair		
Param.	Maple	Cadence
W_n	> 2.03 μm	> 3.05 μm
L_n	250 nm	250 nm
R_0	10 kΩ	9.84 kΩ
C_{NMOS}	3.97 fF	3.77 fF

Varactor		
Param.	Maple	Cadence
W_v	150 μm	140 μm
L_v	500 nm	500 nm
$R_{v,p}$	3222 Ω	-
C_{v0}	378 fF	-

Table 1. Specifications and design parameters for $V_{tune} = 0$

The center manifold approach for simplifying dynamical systems has a nice geometric interpretation. Further investigations of the reduced system with analytical methods are well-known in system theory [2]. The following methods are predestinated for the use in common with center manifolds because they are formulated only in the 2- dimensional case or easier to handle in that dimension.

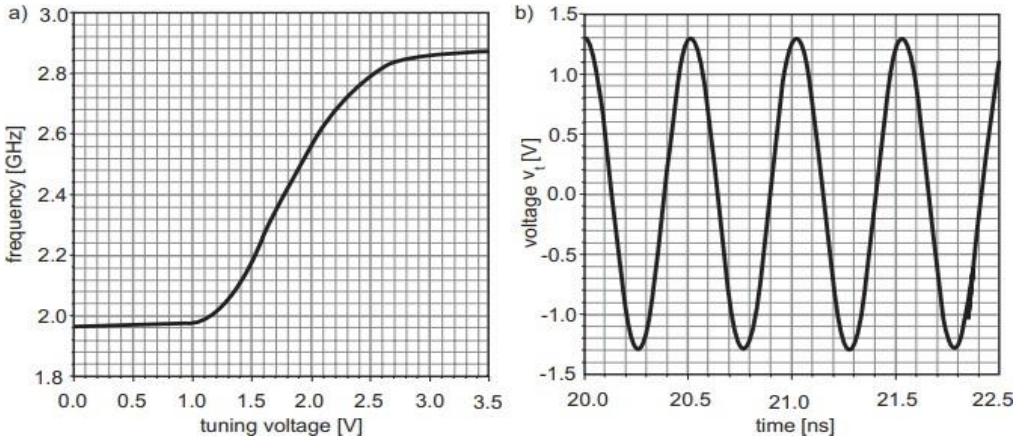

Fig. 3 (a) Graph between frequency and tunning voltage (b) Voltage and time.

CONCLUSION-

The essential steps of a systematic concept for the design of electronic oscillator circuits. It can be shown that by means of advanced mathematical methods the intrinsic nonlinear problem of oscillator design is manageable. Using a high-efficient computer algebra system (e. g. MAPLE or MATHEMATICA) semi-analytical expressions for the oscillator design can be derived. Based on previous work further research will be done in order to develop a computer aided design for electronic oscillators in the GHz area. It is our goal to enable expert analog designers to design oscillators by means of a variety of well-adapted tools instead of a general-purpose circuit simulator.

Reference-

1. H. Nicolis and I. Prigogine, Self-Organization in Nonequilibrium Systems: From Dissipative Structures to Order through Fluctuations, New York: John Wiley & Sons, 1977.
2. J. Guckenheimer and P. Holmes, Nonlinear Oscillations, Dynamical Systems and Bifurcations of Vector Fields, New York - Berlin - Heidelberg – Tokyo: Springer Verlag, 1983.
3. T. H. O'Dell, Electronic Circuit Design: Art and Practice, New York: Cambridge University Press, 1988.
4. L. Mandelstam and N. Papalexi, "About resonance phenomena of the frequency division" (in German), Zeitschrift für Physik., vol. 72, pp. 223-248, 1931.
5. L. Mandelstam, N. Papalexi, A.A. Andronov, S. Chaikin and A. Witt, "Recent results about nonlinear oscilltions" (in French), Zeitschr. f. Techn. Physik., vol. 4, pp. 81-134, 1935.
6. G. M. Maggio, O. De Feo and M. P. Kennedy, "A general method to predict the amplitude of oscillation in nearly sinusoidal oscillators", IEEE Trans. Circ. Syst. I, vol. 51, no. 8, 2004, pp. 1586-1595.

7. W. Mathis and P. Russer, "Oscillator Design", In: K. Chang, Ed., Encyclopedia of RF and Microwave Engineering, vol. 4, pp. 3563- 3589, New York: John Wiley, 2005.

8. M. Prochaska, A. Belski and W. Mathis, "Bifurcation Analysis of On-Chip Oscillators", Proc. IEEE Int. Sympos. Circ. Syst. (ISCAS), 2005.

9. W. Mathis, "Nonlinear Electronic Circuits - An overview", Proc. Conf. Mixed Des. Integr. Circ. Syst. (MIXDES), Poland 2000, pp.

10. W. Duddel, "On rapid variations in the current through the directcurrent arc", Electrician, vol. 46, pp. 269-273 and 330-313, 1900.

11. H. Th. Simon, "Acoustic phenomena of the electrical arc" (in German), Wiedemanns Annalen der Physik u. Chemie, vol. 64, pp. 233, 1898.

12. G. G. Blake, History of Radio Telegraphy and Telephotrotechn. Z., vol. 10, pp. 418-421 and 450-453, 1909.

13. K.W. Wagner, "The Arc as AC Generator" (in German), Ph.D. Thesis, University of Göttingen, 1910. [15] J. Zenneck, "About the onset of oscillations using electrical arcs" (in German), Ann. Phys., vol. 43, pp. 481-524, 1914.

14. W. Mathis, "An Efficient Method for the Transient Analysis of Weakly Damped Crystal Oscillators", Proc. MTNS-98 Symposium, Italy, IL POLIGRAFO, Padova, July 1998, pp. 313-316.

15. L. Kühn, "On wireless telephony" (in German), Z. Techn. Phys., vol. 3, pp. 109-118, 1922.

16. A. Meißner, "The time of high frequency alternator" (in German), Telefunken-Zeitschrift, vol. 26, pp. 159-164, 1953.

17. H. R. Johannsen, "The chronology of discoveries and inventions from amber to the microprocessors" (in German), BerlinOffenbach: VDE Verlag, 1986.

18. L. de Forest, "The Audion", Trans. Am. Inst. Electr. Eng., vol. 25, pp. 735, 1906.

19. R. V. Lieben, "Cathode ray relay" (in German), DRP 179807 (German Patent), March 4, 1906.

20. R. V. Lieben, E. Reisz and S. Strauß, "Grid between cathode and anode of a Lieben tube, a constant tunable voltage" (in German), DRP 249142 (German Patent), December 20, 1910.

21. E. H. Armstrong, "Some Recent Developments in the Audion Receiver", Proc. IRE 3, September 1915, pp. 215-247

22. A. Meißner, "On tube transmitters" (in German), Elektrotechn. Z, vol. 40, pp. 65-68 and 78-79, 1919.

23. D.G. Tucker, "The history of positive feedback: the oscillating audion, the regenerative receiver and other applications up to around 1923", Radio Electron. Eng., vol. 42, pp. 69-

80, 1972.

24. G. H. Barkhausen, "The vacuum tube and its technical applications I, II, III" (in German), Jahrbuch der Ddrahtlosen Telegraphie und Telephonie, vol. 14, pp. 27-47, 1919; vol. 16, pp. 82-114, 1920; vol. 18, pp. 402-419, 1921.

25. K. Skowrennek, "On the development of electron tube amplifiers" (in German), Arch. f. Geschichte Math., d. Naturwiss. u.d. Techn., vol. 13, pp. 225-276, 1931.

26. F. Paschke, "Walter schottkys first reseach areas" (in German), Siemens Forsch.-u. Entwickl.-Ber., vol. 15, pp. 287-290, 1986.

27. H. G. Möller, "Quantative treatment of oscillations in tube generators by means of the characteristic of oscillations (Schwingkennlinie)" (in German), Jahrbuch der Drahtlose Telegraphie und Telephonie, vol. 14, pp. 326-360, 1919.

28. L. A. Hazeltine, "Oscillating audion Circuits", Proc. Inst. Radio Eng., vol. 6, 1918, pp. 63-98.

29. G. Vallauri, "On the functionality of vacuum tubes with three electrodes (audion) and its application in radiotelegraphy Sul" (in Italian), L'Elettrotecnica, vol. 4, pp. 43-58, 1917.

30. G. Vallauri, "On the mode of operation of the vacuum tubes with three electrodes (Audion) used in the wireless telegraphy" (in German), Jahrbuch der Drahtlosen Telegraphie und Telephonie 12, pp. 349-364, 1917.

31. R. A. Heising, "The audion oscillator", Phys. Rev., vol. 16, pp. 216-237, 1920.

32. W. Albersheim, "Critical aspects of the problem of pulling and its literature" (in German), Archiv. Elektrotechnik, vol. 14, pp. 23-42, 1924.

33. J. A. Sanders and F. Verhulst, "Averaging Methods in Nonlinear Dynamical Systems", New York - Berlin - Heidelberg – Tokyo: Springer-Verlag, 1985.

34. B. van der Pol, "A theory of the amplitude of free and forced triode vibrations", Radio Rev., vol. 1, pp. 701-710, 1920.

35. G. Joos, "Theory of electron tube oscillators" (in German), Ann. d. Phys., vol. 69, pp. 505-547, 1922.

36. B. van der Pol, "The nonlinear theory of electric oscillators", Proc. Inst. Radio Eng., vol. 22, 1934, pp. 1051-1089. M. A. Andronov, "Limit cycles of poincare and the theory of oscillations" (in French), Comptes Rendus (Paris), vol. 189, pp. 559-561, 1929.

37. A. A. Andronov and A. Witt, "About the mathematical theory of auto-oscillations" (in French), Comptes Rendus (Paris), vol. 190, pp. 256-258, 1930.

38. A. A. Andronov and A. Witt, "About the theory of entrainment of van der pol" (in German), Archiv f. Elektrotechnik, vol. 24, pp. 99-110, 1930.

39. A. A. Andronov, A. Witt and S. Chaikin, Theory of Oscillators (Reprint), New York:

Dover Publication Inc., 1966 (first publication 1937).

40. W. Mathis, Theorie nichtlinearer Netzwerke, Berlin – Heidelberg - New York: Springer Verlag, 1987.

41. C. Bissell, "A.A. Andronov and the Development of Soviet Control Engineering", IEEE Control Syst. Mag., vol. 18, pp. 56-62.

42. D. Aubin and A.D. Dalmedico, "Writing the History of Dynamical Systems and Chaos: Longue Duree and Revolution, Disciplines and Cultures", Hist. Math., vol. 29, pp. 273-339, 2002.

43. A. Pechenkin, "The concept of self-oscillations and the rise of synergetics ideas in the theory of nonlinear oscillations", Stud. Hist. Philos. Modern Phys., vol. 33, pp. 269-295, 2002

Numerical Investigation of Burgers Equation By Differential Transformation Technique

Raju Prasad [1] and Vinay Saxena[2]

[1]Research Scholar, Department of Mathematics, Kisan PG College, Bahraich, UP, India-271801

[2] Professor, Department of Mathematics, Kisan PG College, Bahraich, UP, India-271801

Corresponding Author's E-mail: rajuprsd953@gmail.com

Abstract- This study presents a comprehensive numerical investigation employing the Differential Transformation Technique (DTT) to solve Burgers' Equation. The DTT, a powerful mathematical tool, is utilized to transform the differential equation into a set of algebraic equations, facilitating numerical solution. Through this method, the behavior of Burgers' Equation is examined, analyzing the influence of various parameters on the solution's characteristics. The numerical results illustrate the effectiveness and accuracy of the Differential Transformation Technique in approximating solutions for Burgers' Equation, providing insights into the dynamics and properties of this nonlinear partial differential equation in diverse scenarios.

Keywords: Non-linear PDE, One-dimensional Burgers equation, Two-dimensional Burgers equation, Differential Transformation Technique.

Introduction-

The Burgers' equation stands as a pivotal partial differential equation (PDE) with widespread applications across numerous branches of applied mathematics, including mathematical modeling, nonlinear acoustics, fluid mechanics, and gas dynamics. Originally introduced by Harry Bateman in 1915, it was further studied and elucidated by Johannes Martinus Burgers in 1948, thus bearing his name. This quasi-linear differential equation is foundational in its occurrence and is solvable through both analytical and numerical means.

The equation's versatile nature finds relevance in various real-world scenarios, serving as a mathematical model for an array of phenomena, thereby attracting substantial interest in scientific and engineering communities. Both analytical and numerical solutions for Burgers' equation have been explored extensively by numerous researchers utilizing a range of methodologies and techniques [1], [2].

The one-dimensional generalized form of Burgers' equation takes the shape:

$$U_t + U^p U_x - \nu U_{xx} = 0, \qquad a \le x \le b, \quad t \ge 0,$$

Here, $U(x,t)$ denotes the velocity at spatial coordinate x and time t, ν stands as a positive constant signifying the fluid's kinematic viscosity, and p represents a positive parameter. When $p=1$, it reverts to the classical Burgers' equation, while $p=2$ yields the modified Burgers equation.

The equation's broad applicability renders it invaluable in understanding and simulating various phenomena characterized by nonlinear behaviors. Its solutions offer insights into complex dynamics observed in fluid flow, shock wave propagation, and other nonlinear systems, playing a vital role in both theoretical analysis and practical applications.

This study aims to contribute to the exploration of Burgers' equation by focusing on its numerical solution. By employing numerical methods, particularly those like the Differential Transformation Technique or other applicable algorithms, this investigation seeks to compute approximate solutions for the equation under diverse conditions. The insights gained from this numerical exploration will provide a deeper understanding of the equation's behavior and its implications across different parameter values, spatial domains, and time evolution.

The significance of this study lies in its contribution to the existing body of knowledge surrounding Burgers' equation. By offering a numerical perspective, it aims to complement and enhance the understanding derived from analytical solutions, thereby aiding in the development of more accurate models and predictive tools for a wide array of physical phenomena encountered in various scientific and engineering disciplines [3].

2. Burgers Equation

The Burgers' equation is a fundamental partial differential equation (PDE) that describes nonlinear phenomena in various fields of applied mathematics, physics, and engineering. There are two primary forms of the Burgers' equation: the one-dimensional (1D) and the two-dimensional (2D) formulations, each with distinct characteristics and applications.

2.1 One-Dimensional Burger's Equation

The one-dimensional Burgers' equation is a nonlinear PDE that typically arises in one spatial dimension. It is commonly expressed as:

$$Ut + U\,Ux - \nu\,Uxx = 0$$

Where:

- $U(x,t)$ represents the velocity field as a function of spatial coordinate x and time t.
- Ut denotes the partial derivative of U with respect to time.

- Ux represents the partial derivative of U with respect to x, describing the spatial variation of the velocity.
- Uxx signifies the second partial derivative of U with respect to x, accounting for diffusion.
- v is the kinematic viscosity coefficient, a positive constant.

The 1D Burgers' equation models various phenomena involving one-dimensional flow and wave propagation, such as shock waves in compressible fluids, traffic flow, and nonlinear acoustics. It exhibits characteristics like shock formation, wave steepening, and the formation of rarefaction waves.

2.2 Two-Dimensional Burgers' Equation

The two-dimensional Burgers' equation extends the concept to two spatial dimensions and can be expressed as:

$$Ut + U\,Ux + V\,Uy - \nu\,(Uxx+Uyy) = 0$$

Where:

- $U(x,y,t)$ and $V(x,y,t)$ denote velocity components in the x and y directions, respectively.
- Ut, Ux, Uy, Vx, and Vy represent partial derivatives with respect to time t, and spatial coordinates x and y.
- Uxx, Uyy are second partial derivatives of U with respect to x and y, accounting for diffusion.
- v represents the kinematic viscosity coefficient.

The two-dimensional Burgers' equation describes more complex phenomena involving two-dimensional flow, such as vorticity dynamics, fluid turbulence, and certain heat transfer scenarios. It presents challenges in terms of numerical simulations due to increased complexity arising from the additional spatial dimension.

Both the 1D and 2D Burgers' equations play crucial roles in understanding nonlinear dynamics, serving as essential models in studying fluid mechanics, shock wave theory, and diverse nonlinear systems encountered in various scientific and engineering domains. Numerical methods are often employed to solve these equations, providing insights into the behavior of nonlinear systems and aiding in the development of accurate predictive models for practical applications [4]-[8].

2.3 Mathematical Model

Consider, one- dimensional Burgers equation in the form of

$$\frac{\partial u}{\partial t} + u\frac{\partial u}{\partial x} - \frac{1}{Re}\left(\frac{\partial^2 u}{\partial x^2}\right) = 0,$$

where initial condition u(x, 0) = ø(x, 0) ; boundary conditions are u(a, t) = ψ(a, t), u(b, t) = ψ(b, t) and computational domain for x is a ≤x ≤b and for t is $0 \le t \le t_{max.}$

And, two - dimensional Burger's equation in the form of

$$\frac{\partial u}{\partial t} + u\frac{\partial u}{\partial x} + v\frac{\partial u}{\partial y} - \frac{1}{Re}\left(\frac{\partial^2 u}{\partial x^2} + \frac{\partial^2 u}{\partial y2}\right) = 0$$

$$\frac{\partial u}{\partial t} + u\frac{\partial u}{\partial x} + v\frac{\partial u}{\partial y} - \frac{1}{Re}\left(\frac{\partial^2 u}{\partial x^2} + \frac{\partial^2 u}{\partial y2}\right) = 0,$$

where initial conditions are u(x, y, 0) = ø(x, y, 0) and v(x, y, 0) = ø(x, y,0) ; boundary conditions are u(a, t) = ψ(a, t), u(b, t) = ψ(b, t) v(a, t)= ψ(a, t), v(b, t)= ψ(b, t) and computational domain is a ≤x ≤b, c ≤y ≤d and $0 \le t \le t_{max}$ [9]-[11].

3. Numerical Solution of Problems

Here two test problems are taken and the results computed are tabulated and compared to analytical solutions for typical mesh-points with different grid-sizes.
Maximum error and runtime for the solution set computed is also recorded for further analysis.

3.1 Problem1:

Let computational domain: $0 \le x \le 1$, and $0 \le t \le t_{max}$, initial condition: $u(x,0)=\frac{2}{Re}\left(\frac{\pi \sin(\pi x)}{2+\cos(\pi x)}\right)$ and

Boundary Conditions: u(0, t)=0 , u(1, t)=0

Exact Solution: Exact solution to compare numerical results

$$U(x, t) = \frac{2\pi\, exp(-\pi^2 t/Re)\sin \pi x}{2+exp(-\pi^2 t/Re)\cos \pi x}$$

Step size $\Delta t = 0.00001$

Table 1: Numerical solutions for respective grid size at t=1.0 and Re=10

T.M.P x	Re=10		
	Numerical Solution		Exact Solution
	Δx=1/20	Δx=1/40	
0.1	0.03073532056	0.03073535698	0.03073535939
0.2	0.5980678869	0.05980685681	0.05980686132
0.3	0.08537566915	0.08537575991	0.08537576593
0.4	0.1052951509	0.1052952518	0.1052952585
0.5	0.1170895171	0.1170896144	0.1170896208
0.6	0.1181633843	0.1181634656	0.1181634709
0.7	0.1063798733	0.1063799310	0.1063799348
0.8	0.08104164267	0.08104167622	0.08104167843
0.9	0.04397681845	0.04397683275	0.04397683368
Max. Error	1.076747840e-007	6.715570683e-009	
Run Time	0.643	1.291	

Result and observation: The table 1 shows numerical results of fourth order compact scheme against exact solutions. The numerical results obtained are in good agreement with the analytical solution.

3.2 Problem 2:

Let computational domain $0 \leq x \leq 1$, and $0 \leq t \leq t_{max}$; Initial condition:

$U(x, 0) = \exp\left(\frac{1-\cos(\pi x)}{2\pi/Re}\right)$; Boundary conditions: u(0, t)=0, u(1, t)=0

Exact Solution: Exact solution to compare numerical results

$u(x, t)= \frac{2\pi}{Re}\frac{\sum_{n=1}^{\infty} c_n exp(-n^2\pi^2 t/Re) n \sin(n\pi x)}{c_0 \sum_{n=1}^{\infty} c_n exp(-n^2\pi^2 t/Re) n \cos(n\pi x)}$ where $c_0=\int_0^1 exp\left(-\frac{1-cos(\pi x)}{2\pi/Re}\right) dx$

$c_n=2\int_0^1 exp\left(-\frac{1-cos(\pi x)}{2\pi/Re}\right)\cos(n\pi x)\, dx,$ n=1, 2, 3 ……

Step size: varies

Table 2: Numerical solutions for different grid sizes at t=0 and Re=100

T.M.P.x	Numerical Solution			Exact Solution
	Δx=1/20 Δt=1/16	Δx=1/80 Δt=1/64	Δx=1/320 Δt=1/256	
0.1	0.0754110180	0.0753820256	0.0753819094	0.0753819089
0.2	0.1506561788	0.1506452219	0.1506451798	0.1506451797
0.3	0.2256096930	0.2256656625	0.2256658878	0.2256658887
0.4	0.3002197938	0.3003085026	0.3003088459	0.3003088472
0.5	0.3745355471	0.3744205239	0.3744200396	0.3744200376
0.6	0.4487326429	0.4478196540	0.4478161072	0.4478160933
0.7	0.5231517985	0.5202790162	0.5202684289	0.5202683874
0.8	0.5983745175	0.5914999452	0.5914762895	0.5914761967
0.9	0.6748436840	0.6600662860	0.6600195796	0.6600193912

Result and Observation: The table 2 shows results for short time steps as well as for large time-step that shows the robustness of the scheme against other schemes such as explicit schemes that require very small time step for stability issues, As the mesh is refined the values get closure the analytical solution [11]-[13].

4. Differential Transform

***Definition* 4.1** If u(t) is analytic in the domain T, then it can be differentiated continuously with respect time t,

$$\frac{d^k u(t)}{dt^k} = \emptyset(t,k) \quad \forall\, t \in T \qquad \text{.....(4.1)}$$

For t=t_i where $\emptyset(t_i,k)$ belongs to the set of non-negative integers, denoted as the K domain. Equation 4.1 can be written as

$$U_i(\mathrm{k}) = \emptyset(t_i,k) = \left[\frac{d^k u(t)}{dt^k}\right]_{t=t_i} \quad \forall\, k \in K \qquad \text{.....(4.2)}$$

where U_i(k) is called the spectrum of u(t) at t=t_i , in the K domain.

Definition 4.2 If u(t) can be expressed as a Taylor series, then u(t) can be represented as u(t)= $\sum_{k=0}^{\infty} \frac{(t-t_i)^k}{k!}$ U(k). .....(4.3)

Equation (4.3) is known as the inverse transformation of U(k). If U(k) is defined as

$$U(k)= M(k)\left[\frac{d^k q(t)u(t)}{dt^k}\right]_{t=t_i} \quad \text{where } k = 0,1,2\ldots\ldots\ldots..,\infty \quad \ldots\ldots\ldots\ldots\ldots\ldots(4.4)$$

Then the function u(t) can be described as

$$u(t) = \frac{1}{q(t)}\sum_{k=0}^{\infty}\frac{(t-t_i)^k}{k!}\frac{U(k)}{M(k)} \quad \ldots\ldots\ldots\ldots..\ldots(4.5)$$

where $M(k) \neq 0$, $q(t) \neq 0$. The function is M(k) called the weighting factor and q(t) is regarded as a kernel corresponding to u(t).M(k)= 1 and q(t)=1, then equation (4.3) and (4.5) are equivalent. In this way equation (4.3) can be treated as a special case of equation (4.5). In this paper, the transformation with $M(k)=\frac{1}{k!}$ and q(t)=1 applied. Then equation (4.4) becomes

$$U(k) = \frac{1}{k!}\left[\frac{d^k u(t)}{dt^k}\right]_{t=t_i} \text{, where } k= 0,1,2,\ldots\ldots\ldots..\infty \quad \ldots\ldots\ldots\ldots\ldots...(4.6)$$

Using the differential transform, a differential equation in the domain of interest can be transformed to be an algebraic equation in the K domain and u(t) can be obtained as a finite term Taylor series plus a remainder

$$u(t)=\frac{1}{q(t)}\sum_{k=1}^{n}\frac{(t-t_0)^k}{k!}\frac{U(k)}{M(k)}+R_{n+1}(t)=\sum_{k=0}^{n}(t-t_0)^k U(k)+ R_{n+1}(t) \quad \ldots\ldots\ldots\ldots\ldots\ldots(4.7)$$

In order to speed up the convergence rate and improve the accuracy of calculation, the entire domain of t need to be split into sub-domains [12]-[18].

5. Results And Discussions

The implementation of the numerical schemes designed for solving the Burgers' equations has exhibited commendable efficiency and accuracy throughout this study. A series of diverse numerical examples were employed to rigorously test these schemes, showcasing their robustness in handling different scenarios. These demonstrations underscored the schemes' efficacy, efficiency, and accuracy in approximating solutions for the Burgers' equations across various parameter settings, spatial domains, and time evolutions.

The robust nature of the schemes was particularly evident in their ability to accurately capture and simulate complex phenomena inherent in the Burgers' equations. From shock wave formation to wave steepening and rarefaction waves, the numerical solutions aligned

remarkably well with the expected behaviors, validating the schemes' reliability in modeling nonlinear dynamics.

Furthermore, the schemes were subjected to detailed analysis concerning their time-complexity and accuracy. This analysis, crucial for understanding the computational performance, supported the experimental observations obtained from solving problems governed by the Burgers' equations. The assessments confirmed that the schemes not only delivered accurate results but also did so within reasonable computational timeframes, emphasizing their efficiency in handling complex nonlinear problems.

The comparison between the numerical solutions and known analytical results, where available, further corroborated the schemes' accuracy and reliability. This alignment between the computed solutions and established theoretical findings reaffirmed the trustworthiness of the numerical methods employed.

6. CONCLUSION

The implemented numerical schemes have demonstrated exceptional performance, combining high efficiency with robust accuracy. Their ability to tackle the complexities of the Burgers' equations and replicate expected behaviors provides confidence in their applicability across a spectrum of scientific and engineering domains. The schemes' robustness, efficiency, and accuracy have been thoroughly analyzed, yielding results that consistently align with the expected accuracy and efficiency for the problems at hand. These findings contribute significantly to the understanding and utilization of numerical methods for solving nonlinear partial differential equations like the Burgers' equations in practical applications.

References-

[1] **J.M. Burger, (1948),** A mathematical model illustrating the theory of turbulence, *Adv, Appl. Mech.* I, 171-199.

[2] **Cole JD, (1951),** On a quasilinear parabolic equation occurring in aerodynamics, *Quart appl Math*; 9:225-36

[3] **E. R. Benton, G.W. Platzman**, **(1972),** A table of solutions of the one-dimensional Burgers' equation, *Quart. App. Math.* 30, 195-212.

[4] **P.C. Jain, D.N. Holla, (1978),** Numerical solution of coupled Burgers equations, *Int. J. Number. Meth. Eng.* 12, 213-222.

[5] **C.A.J. Fletcher, (1983),** Generating exact solutions of the two-dimensional Burgers equation, *Int. J. Numer. Meth. Fluids* 3,213-216.

[6] **J. K. Zhou, (1986),** Differential Transformation and its application for electrical circuits, *Huazhong University Press, Wuhan, china*.

[7] **R. Eymard, T. Gallouët, R. Herbin, (2000)** "Finite Volume Methods", Handbook of Numerical Analysis, Vol. 7.

[8] **A Refik Bahadir, (2003)**, A fully implicit finite-difference scheme for two dimensional Burgers equations, *Applied Mathematics and Computation* 137, 131-137.

[9] **Fatma Ayaz, (2004),** Solutions of the system of differential equations by differential transform method, *Appl. Math. Comput.* 147, 547-567.

[10] **F. Ayaz, (2004),** Application of differential transform method to differential-algebraic equations, *Appl. Math. Comput*.152, 649-657.

[11] **A. Arikoglu, I. Ozkol, (2006),** Solution of differential equations by using differential transform method, *Appl. Math. Comput.* 174, 1216-1228.

[12] **M. Mossa Al-Swalha, M.S.M. Noorani, (2009),** Application of Differential Transformation Method for solution of the hyperchaotic Rossler system, *Commun. Non-linear Sci. numer. Simul.* 14, 509-1514.

[13] **Borhanifar, Reza Abazari,** Exact Solutions for non-linear Schrodinger equations by differential transform method, *J. Appl. Math. Comput*. Dio:10.1007/s12190-009-0338-2.

[14] **Reza Abazari, (2009),** Solution of Reccati types matrix differential equations using matrix differential transform method, *J. App. Math. Inform*. 27, 1133-1143.

[15] **S. T. Mohyud-Din, Z. U. A. Warsi, M. Saleem, (2009),** "The Differential Transform Method for Solution of Burgers' Equation and Comparison with Adomian's Decomposition Method", International Journal for Numerical Methods in Fluids, Vol. 60, Issue 11.

[16] **S. Mukhopadhyay, S. Sinha, A. K. Banik, (2012**), "Solution of Burgers' Equation by Differential Transformation Method", International Journal of Applied Mathematical Research, Vol. 1, No. 3.

[17] **G. W. Bluman, S. Kumei, (2013),** "Symmetries and Differential Equations", Springer, 2013.

[18] **E. A. Al-Said, E. M. Hilal, A. H. Bhrawy, (2014),** "A New Modified Differential Transformation Method for the Solution of Time-Fractional Burgers' Equation", Mathematical Methods in the Applied Sciences, Vol. 37, Issue 10.

A Review article on Application of Fiber Optical Sensors in Aviation Industry

[1]Kishun Bir, [1]Bal Govind, [2]Vishalakshi Singh

[1]Kisan Post Graduate College, Bahraich, U.P. 271801, India.

[2]D.D.U. Government P. G. College, Saidabad, Prayagraj, U.P. 221508, India.

Abstract-

Fiber-optic technology emerged originally for applications in data transmission and telecommunications. However, sensors based on fiber-optics have been developed rapidly because of their excellent sensing performances and capability to function in remote and harsh environments.

A significant step forward in aviation technology has been the use of sensors. They are used to measure, monitor, and analyse data from numerous sources, as well as reporting back any potential dangers to pilots and on-ground support facilities instantly. Sensors can monitor the structural health of the plane, and enhance operations through reducing fuel usage and calculating the shortest flight paths.

Keyword: Aviation Industry, Fiber Optical Sensors, Aerospace and Aircraft

Introduction- In the year 1960, laser light was invented and after the invention of lasers, researchers had shown interest to study the applications of optical fiber communication systems for sensing, data communications, and many other applications. Subsequently the fiber optic communication system has become the ultimate choice for gigabits and beyond gigabits transmission of data.

Fiber-optic communication is a method of transmitting information from one place to another by sending pulses of light through an optical fiber. The light forms an electromagnetic carrier wave that is modulated to carry information. Fiber is preferred over electrical cabling when high bandwidth, long distance, or immunity to electromagnetic interference are required. This type of communication can transmit voice, video, and telemetry through local area networks, computer networks, or across long distances.

The fiber optic sensors also called as optical fiber sensors use optical fiber or sensing element. These sensors are used to sense some quantities like temperature, pressure, vibrations, displacements, rotations or concentration of chemical species. Fibers have so many uses in the field of remote sensing because they require no electrical power at the remote location and they have tiny size.

Fig. 1 Fiber Optic Sensors

The fiber optic communications industry has literally revolutionized the telecommunications and aviation industry by providing higher-performance, more reliable telecommunication links with ever-decreasing bandwidth cost, safety and easy to replace with traditional big old instruments. This revolution is bringing about the benefits of high-volume production to component users and a true information superhighway built of glass.

The process of communicating using fiber-optics involves the following basic steps:

1. Creating the optical signal involving the use of a transmitter, usually from an electrical signal
2. Relaying the signal along the fiber, ensuring that the signal does not become too distorted or weak

3. Receiving the optical signal

4. Converting it into an electrical signal

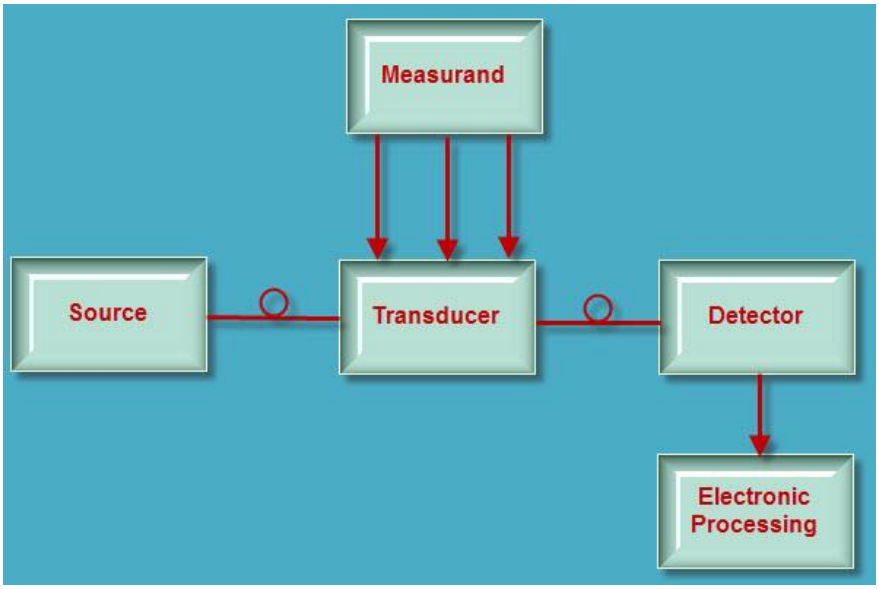

Fig. 2 Standard Block Diagram of Fiber Optic Sensors

Historical Background behind Fiber Optical Sensors-

First developed in the 1970s, fiber-optics have revolutionized the telecommunications industry and have played a major role in the advent of the Information Age. Because of its advantages over electrical transmission, optical fibers have largely replaced copper wire communications in core networks in the developed world.

Optical fiber was successfully developed in 1970 by Corning Glass Works, with attenuation low enough for communication purposes (about 20 dB/km) and at the same time GaAs semiconductor lasers were developed that were compact and therefore suitable for transmitting light through fiber optic cables for long distances.

The second generation of fiber-optic communication was developed for commercial use in the early 1980s, operated at 1.3μm and used InGaAsP semiconductor lasers. These early systems were initially limited by multimode fiber dispersion, and in 1981 the single-mode fiber was revealed to greatly improve system performance, however practical connectors capable of working with single mode fiber proved difficult to develop.

Third-generation fiber-optic systems operated at 1.55μm and had losses of about 0.2 dB/km. This development was spurred by the discovery of Indium gallium arsenide and the development of the Indium Gallium Arsenide photodiode by Pearsall.

The fourth generation of fiber-optic communication systems used optical amplification to reduce the need for repeaters and wavelength-division multiplexing to increase data capacity.

Advantages of using Fiber Optic Sensors-

- ✓ Extremely High bandwidth.
- ✓ Long Distance
- ✓ Resistance to Electromagnetic Interference:
- ✓ Safety
- ✓ Easy to Accommodate Increasing Bandwidth:
- ✓ Easy to use.
- ✓ Less in weight
- ✓ Instead of heavy traditional big instruments, fiber optic sensors can be up to few mm.

In the above paragraphs, we discuss the advantages of using Fiber Optic Sensors but it also brings with back draws as well. Few of the negatives about fiber optic sensor is given below-

- ✓ Attenuation & Dispersion:
- ✓ Need Specialised person to use the equipment made up of fiber optic sensor.

- ✓ Also, the price is more in comparison to traditional copper wires.

Application of Fiber Optic Sensors-

Fiber optic cables find many uses in a wide variety of industries and applications. In modern times, fiber optic sensors are used in various industries/ departments ranging from medical, communication and defence etc. Some uses of fiber optic cables include:

- ✓ Data Storage
- ✓ Medical Science
- ✓ Defence
- ✓ Telecommunication.
- ✓ Networking.
- ✓ Aviation Industry.

Here we are more inclined towards the use of fiber optic sensors in aviation industry. There is huge benefit of using fiber optic sensors in aviation/ aircraft industry over traditional copper-based instruments. The detailed discussion is given below.

Fiber Optic Sensors in Aviation Industry-

Today, fiber optic sensors in aviation are being used for numerous applications, including hard landing detection, hydraulic temperature, and pressure monitoring, fuel tank level monitoring, and surveillance of fuel management systems.

These sensors have been used to support tests on military and commercial aircraft that have demonstrated performance comparable to conventional electrical position sensors used for rudder, flap, and throttle position. The principal advantages of the fiber position sensors are immunity to electromagnetic interference and overall weight savings.

The two beautiful images of how fiber optic sensor bring revolution and change in the traditional behaviour of aviation industry specially aircraft management and construction and how it simplifies and changes this industry is shown in figure 3 and figure 4 below.

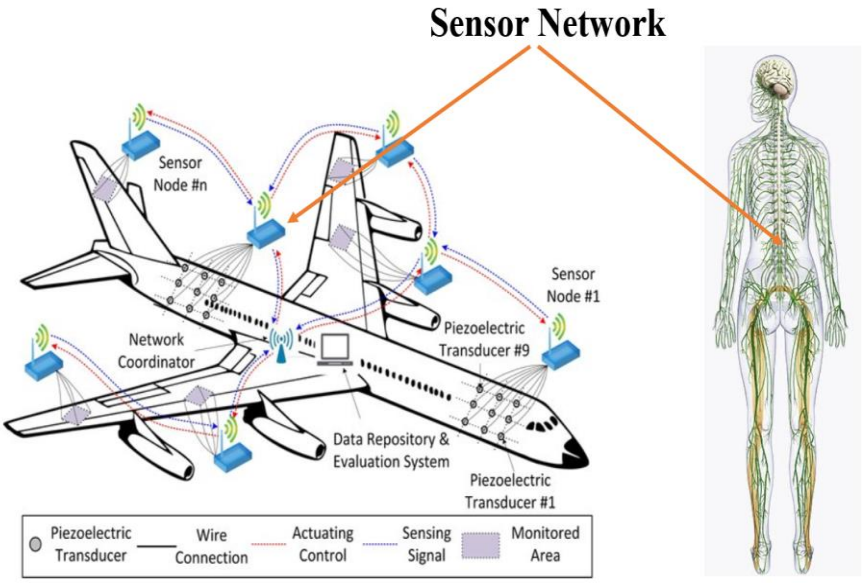

Fig. 3 SHM as an imitation of the human nervous system.

(Fu, H.; Sharif-Khodaei, Z.; Aliabadi, M.F. An energy-efficient cyber-physical system for wireless on-board aircraft structural health monitoring. *Mech. Syst. Signal Process.* **2019**, *128*, 352–368.)

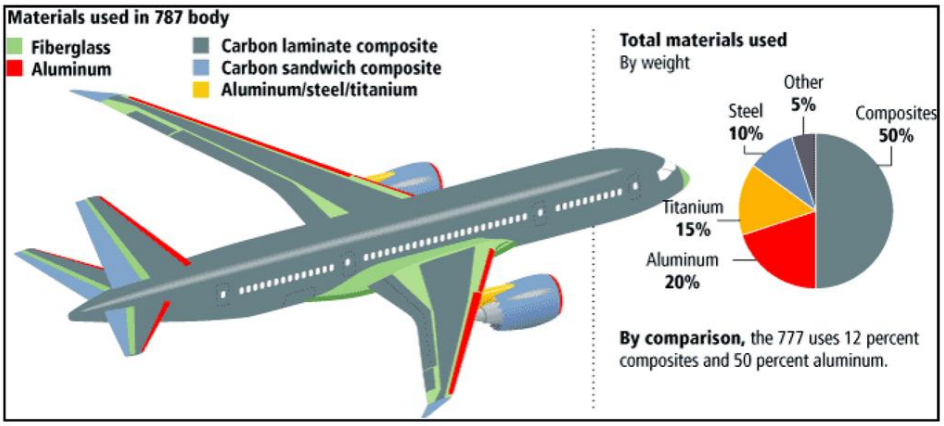

(**a**)

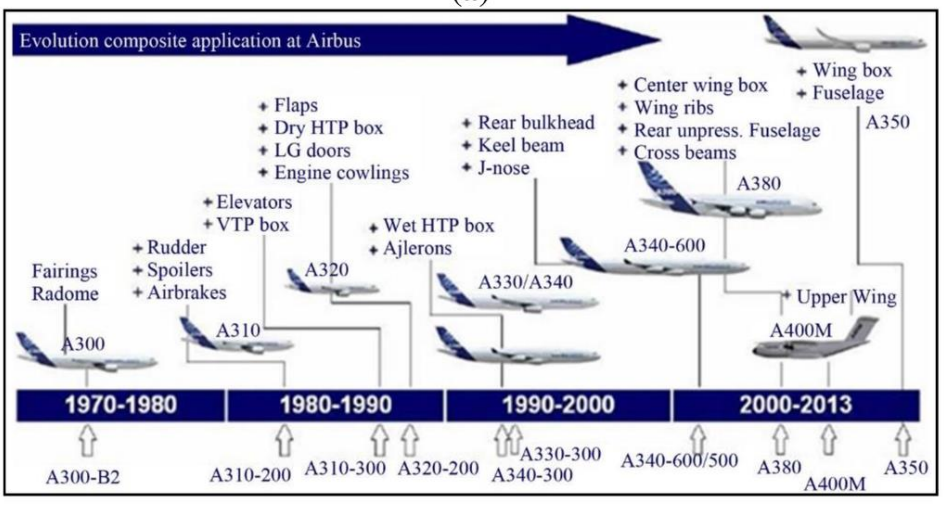

(**b**)

Fig. 4 (**a**) Use of composite materials in the Boeing 787 and (**b**) evolution of the use of composites in Airbus aircraft

(R. D. Sante, Fibre Optic Sensors for Structural Health Monitoring of Aircraft Composite Structures: Recent Advances and Applications, *Sensors* **2015**, *15*(8), 18666-18713; **https://doi.org/10.3390/s150818666)**

Fiber optic sensors for aerospace

- Structural health monitoring
- Distributed sensors
- Fiber Bragg gratings
- Long period gratings
- Spatial fibers
- Photonic crystal fibers
- Whispering gallery mode sensors
- Non liner sensors (Brillion, Raman)
- Chemical and gas sensors
- Ice accretion and ice crystals detection
- Magnetic and electromagnetic sensors

An optical fiber is a flexible, transparent, and cylindrical waveguide made of plastic or silica, with diameters slightly thicker than that of a human hair. Fibers can be classified into two categories based on the number of guided modes: single-mode and multimode fibers. Commonly, the single-mode fibers have a core diameter of 8–10 μm, and are developed to function in the short infrared region. While multimode fibers are manufactured with a core diameter in the range of 50 μm to hundreds of micrometres, and are used when high power is required to be transferred.

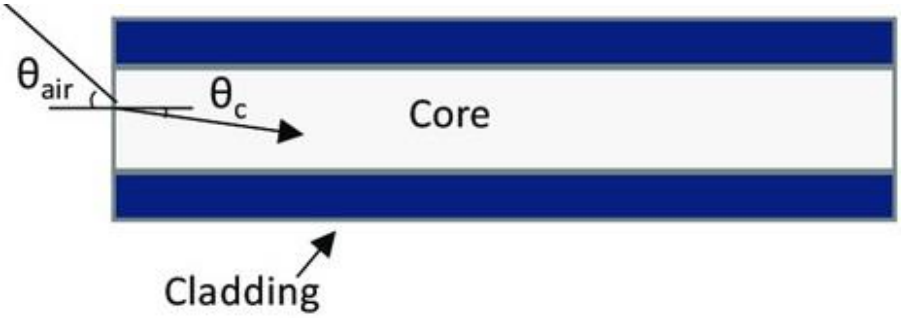

Fig. 4 Fiber Optic Sensors

Is there any safety concerned in the application of sensor in Aircraft?

There is no safety concerned of aircraft if we use fiber optic sensors. Fiber optic sensors are also inherently safer than conventional sensors. Hermetically coated glass is chemically inert, not susceptible to corrosion, and does not have potential for ground loops, electrical faults, sparking, or Joule heating. These sensors also are not negatively impacted like common aircraft avionics systems with reactions to Electro-Magnetic Interference (EMI) or Electro-Magnetic Pulses (EMP).

Use of sensors in Aviation Industry-

A significant step forward in aviation technology has been the use of sensors. They are used to measure, monitor, and analyse data from numerous sources, as well as reporting back any potential dangers to pilots and on-ground support facilities instantly. Sensors can monitor the structural health of the plane, and enhance operations through reducing fuel usage and calculating the shortest flight paths.

One part of the aviation sensors market is gaining significant traction, and that is fiber optic sensors. It has become a popular piece of equipment because it is considered to be an intrinsically safe component, with the ability to resist harsh environmental forces.

After 2000, the gradually matured optoelectronic elements and signal processing technologies provide researchers with how to apply various sensors, such as Fabry-Perot Interferometric (FPI) fiber optic sensors, FBG sensors, distributed fiber optic sensors, to different engineering application areas. Fiber optic sensor systems with very quick response are becoming available, with readout frequencies over 100 kHz, enabling the fiber optic sensors to operate as both static and dynamic loading sensors. This means that the fiber optic sensors enter into a practical stage. Following the development of optical fiber communication industry, the optical fiber sensing technologies become another major industry of optoelectronic technologies.

Benefits of Fiber Optic Sensors-

There is a huge benefit of using these sensors to measure and report data and also reduces the weight of the craft by replacing larger systems to fiber optic sensors, that makes it cost effective and providing data that helps flights become more fuel-efficient.

Way Forward-

The benefit of using fiber optic sensors over other alternatives is that they can be installed in a fraction of the time compared with their counterparts. Due to the nature of how fiber optics work, multiple sensors can be integrated within a single fiber, meaning that installation only requires one fiber to be attached to the craft and connected to the data acquisition equipment. With their vast applications in aviation, we can expect to see fiber optic sensors continuing to make noise in the industry, as we see them enabling the sector to reach significant safety and emission reduction goals.

References-

1. https://opsens-solutions.com/industries/defense-and-aerospace/fiber-optic-temperature-solution-emc-testing/
2. Zhu P, Xie X, Sun X, Sotoac MA (2019) Distributed modular temperature–strain sensor based on optical fiber embedded in laminated composites. Compos B Eng 168:267–273.
3. Yu H, Wang Y, Ma J, Zheng Z, Luo Z, Zheng Y (2018) Fabry-Perot interferometric high-temperature sensing up to 1200 ℃ based on a silica glass photonic crystal fiber. Sensors 18:273.
4. Yoshino T, Kurosawa K, Itoh K, Ose T (1982) Fiber–optic Fabry-Perot interferometer and its sensor applications. IEEE J Quantum Electron 4:626–665
5. Hartog AH (2017) An introduction to distributed optical fiber. Sensors 442.
6. https://aia.springeropen.com/articles/10.1186/s42774-020-00033-y
7. Nash PJ, Cranch GA, Hill DJ (2000) Large scale multiplexed fiber-optic arrays for geophysical applications. In: Proceedings of industrial sensing systems, vol 4202. International Society for Optics and Photonics, Boston, pp 55–65.
8. Qing, X.; Li, W.; Wang, Y.; Sun, H. Piezoelectric transducer-based structural health monitoring for aircraft applications. *Sensors* **2019**, *19*, 545.
9. Min, J.; Park, S.; Yun, C.-B.; Lee, C.-G.; Lee, C. Impedance-based structural health monitoring incorporating neural network technique for identification of damage type and severity. *Eng. Struct.* **2012**, *39*, 210–220.

10. Azimi, M.; Eslamlou, A.D.; Pekcan, G. Data-driven structural health monitoring and damage detection through deep learning: State-of-the-art review. *Sensors* **2020**, *20*, 2778.
11. Kralovec, C.; Schagerl, M. Review of structural health monitoring methods regarding a multi-sensor approach for damage assessment of metal and composite structures. *Sensors* **2020**, *20*, 826.
12. Udd, E. *Fiber Optic Smart Structures*; Wiley-Interscience: New York, NY, USA, 1995; Volume 12.
13. Speckmann, H.; Roesner, H. Structural health monitoring: A contribution to the intelligent aircraft structure. In Proceedings of the ECNDT 2006, Berlin, Germany, 25–29 September 2006.
14. Ou, J.; Li, H. Structural health monitoring in mainland China: Review and future trends. *Struct. Health Monit.* **2010**, *9*, 219–231.